PALEOCEANOGRAPHY, VOL. 4, NO. 4, PAGES 353-412, AUGUST 1989

PLEISTOCENE EVOLUTION: NORTHERN HEMISPHERE ICE SHEETS AND NORTH ATLANTIC OCEAN

W. F. Ruddiman,[1] M. E. Raymo,[1,2] D. G. Martinson,[1]
B. M. Clement,[3,4] and J. Backman [5]

Abstract. We analyze five high-resolution time series spanning the last 1.65 m.y.: benthic foraminiferal $\delta^{18}O$ and $\delta^{13}C$, percent $CaCO_3$, and estimated sea surface temperature (SST) at North Atlantic Deep Sea Drilling Project site 607 and percent $CaCO_3$ at site 609. Each record is a multicore composite verified for continuity by splicing among multiple holes. These climatic indices portray changes in northern hemisphere ice sheet size and in North Atlantic surface and deep circulation. By tuning obliquity and precession components in the $\delta^{18}O$ record to orbital variations, we have devised a time scale (TP607) for the entire Pleistocene that agrees in age with all K/Ar-dated magnetic reversals to within 1.5%. The Brunhes time scale is taken from Imbrie et al. [1984], except for differences near the stage 17/16 transition (0.70 to 0.64 Ma). All indicators show a similar evolution from the Matuyama to the Brunhes chrons: orbital eccentricity and precession responses increased in amplitude; those at orbital obliquity decreased. The change in dominance from obliquity to eccentricity occurred over several hundred thousand years, with fastest changes around 0.7 to 0.6 Ma. The coherent, in-phase responses of $\delta^{18}O$, $\delta^{13}C$, $CaCO_3$ and SST at these rhythms indicate that northern hemisphere ice volume changes have controlled most of the North Atlantic surface-ocean and deep-ocean responses for the last 1.6 m.y. The $\delta^{13}C$, percent $CaCO_3$, and SST records at site 607 also show prominent changes at low frequencies, including a prominent long-wavelength oscillation toward glacial conditions that is centered between 0.9 and 0.6 Ma. These changes appear to be associated neither with orbital forcing nor with changes in ice volume.

[1] Lamont-Doherty Geological Observatory, Columbia University, Palisades, New York.
[2] Now at Department of Geology, Monash University, Clayton, Victoria, Australia.
[3] Ocean Drilling Program, Texas A and M University, College Station, Texas.
[4] Now at Department of Geology, Florida International University, Miami, Florida.
[5] Department of Geology, University of Stockholm, Stockholm, Sweden.

Paper number 89PA00434.
0883-8305/89/89PA-00434$10.00

INTRODUCTION

During the later portion of the Brunhes Chron, high-latitude northern hemisphere climate was dominated by a quasi-periodic cycle of 100,000 years, close to periods of change in orbital eccentricity. This rhythm is registered in stable isotopic ($\delta^{18}O$) records that serve as proxies for global ice volume [Shackleton and Opdyke, 1973; Hays et al., 1976; Imbrie et al., 1984], in European and Chinese loess deposits [Kukla, 1970, 1987], and in other signals indicative of responses of the upper layers of the high-latitude North Atlantic Ocean [Ruddiman and McIntyre, 1981, 1984].

The strength of the 100,000-year rhythm has not, however, been constant through the Brunhes Chron. Imbrie [1985] found that it was weaker in amplitude by about half in $\delta^{18}O$ signals from the early part of the Brunhes Chron (prior to 0.4 Ma), and Ruddiman et al. [1986a] noted an analogous change in the surface temperature response of the North Atlantic Ocean. These differences suggest significant evolution of the climatic system within the Brunhes Chron.

Northern hemisphere climatic variations during the Matuyama Chron were very different. Records from hydraulic piston cores taken on Deep Sea Drilling Project (DSDP) leg 94 [Ruddiman et al., 1986b] support earlier suggestions [Shackleton and Opdyke, 1976; Pisias and Moore, 1981; Start and Prell, 1984] that the 41,000-year period of orbital

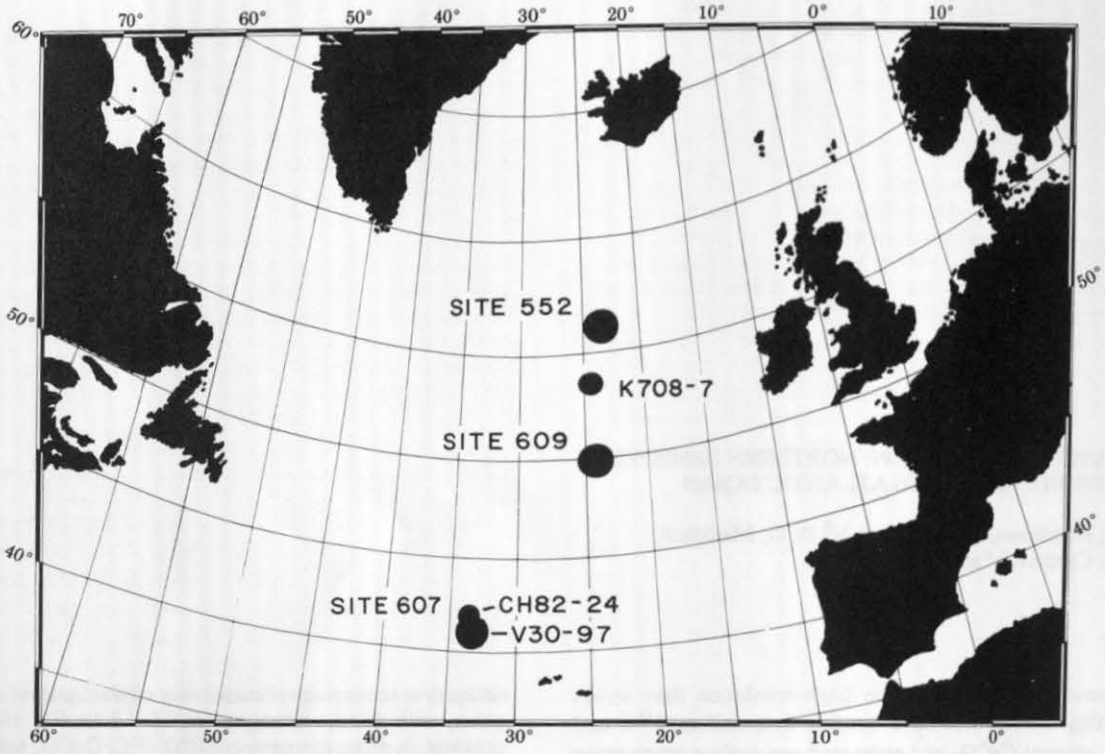

Fig. 1. Locations of DSDP sites and of nearby conventional piston cores. Core V30-97 almost directly overlays site 607.

obliquity was the primary rhythm of northern hemisphere climatic change during the Matuyama Chron, with variations at periods near 100,000 years generally much weaker and even absent altogether during some intervals in the leg 94 records. This conclusion was based both on $\delta^{18}O$ and other indicators known to be sensitive to northern hemisphere ice sheet size, such as estimated North Atlantic sea surface temperature (SST) and percent $CaCO_3$. This 41,000-year rhythm prevailed from the beginning of moderate-scale northern hemisphere glaciation near 2.6 to 2.4 Ma [Backman, 1979; Shackleton et al., 1984] through most of the Matuyama Chron [Ruddiman et al., 1986b]. By 0.9 Ma, a longer-period, higher-amplitude signal had begun to develop [Shackleton and Opdyke, 1976; Pisias and Moore, 1981; Prell, 1982], leading to the Brunhes 100,000-year fluctuations.

We focus on the transition between regimes. When did it occur? Was it abrupt or gradual? Did other periodicities briefly emerge?

CORE SELECTION

The data for this study consist of composite depth and time series from DSDP sites in the northern subtropical and subpolar North Atlantic Ocean (Figure 1; Table 1). We report detailed records of $\delta^{18}O$, $\delta^{13}C$, percent $CaCO_3$, and SST from the southernmost site (607), situated high on the upper western flank of the Mid-Atlantic Ridge. This site is located beneath the northern limb of the North Atlantic Drift flow in the subtropical gyre. It is also situated near piston cores V30-97 and CHN82-24-4, both of which contain detailed records of late Pleistocene climatic change. Site 609 is located on the eastern flank of the Mid-Atlantic Ridge, beneath the diffuse northeastward flow of the North Atlantic Drift in the eastern Atlantic.

Also reported in this study are correlations with records from site 552 (hole 552A), located on the lower flank of the southwestern slope of the Rockall Plateau. Site 552 is

TABLE 1. Locations and Depths of DSDP Sites and Piston Cores

	Latitude, N	Longitude, W	Depth, m
Site 607	41°00'	32°58'	3427
Core V30-97	41°00'	32°56'	3371
Core CHN82-24-4	41°43'	32°51'	3427
Site 609	49°53'	24°14'	3883
Site 552	56°03'	23°14'	2311
Core K708-7	53°56'	24°05'	3502

situated beneath the broad northeastward flow of the North Atlantic Drift, somewhat north of the location of piston core K708-7.

DATA ANALYSIS

For site 607, we present here 1.65-m.y. records of percent $CaCO_3$, benthic foraminiferal $\delta^{18}O$ and $\delta^{13}C$, census counts of four species of planktonic foraminifera (*Neogloboquadrina pachyderma* sinistral, *Globigerina bulloides*, *Globorotalia inflata*, and *Globigerinoides ruber*), and estimated sea surface temperature (SST). For site 609, we report a 1.65-m.y. record of percent $CaCO_3$ for comparison with that of site 607. Data for site 607 are listed in Tables A1 and A2 in the appendix, and 609 $CaCO_3$ values in Table A3. Data from a 1.2-m.y. record of the middle and late Pleistocene compiled from site 552 and piston core K708-7 have been reported by Ruddiman et al. [1986a].

High-resolution late Pleistocene records of $\delta^{18}O$ and $\delta^{13}C$ from cores V30-97 and CHN82-24-4 were used in place of the late Pleistocene section at site 607, which was not analyzed. Data for $\delta^{18}O$ and $\delta^{13}C$ from core V30-97 were listed by Mix and Fairbanks [1985], and data for core CHN82-24-4 by Boyle and Keigwin [1985]. Relative to site 607, core V30-97 is closer in location, but core CHN82-24-4 is closer in depth (Table 1). Relative to the long isotopic record at site 607 presented here, the record in V30-97 relies more heavily on the genus *Uvigerina*, whereas that in core CHN82-24-4 relies entirely on *Cibicidoides*. We created stacked isotopic records of $\delta^{18}O$ and $\delta^{13}C$ from both of these late Pleistocene piston cores for splicing to the site 607 record.

We correlated the two piston cores by mapping the $\delta^{18}O$ record of core CHN82-24-4 into that of core V30-97 in the time domain, using a time scale established by correlation of V30-97 to the $\delta^{18}O$ stack of Imbrie et al. [1984]. Next, we resampled the $\delta^{18}O$ record from each core at an interval of 3400 years and then stacked the two $\delta^{18}O$ signals. We chose the 3400-year interval to achieve a sampling density equal to that in the deeper record from site 607. The resampled values comprising the stacked $\delta^{18}O$ signal are listed in Table A4, adjusted to *Uvigerina*. The two $\delta^{18}O$ signals comprising this stack are very similar, except in isotopic stages 2, 4, and 6, where the V30-97 record is heavier than CHN82-24-4. The resampled values comprising the stacked $\delta^{13}C$ signal are also listed in Table A4, adjusted to *Cibicidoides*. We see no evidence in either paired or closely adjacent $\delta^{13}C$ analyses of the kind of species-specific offsets measured in other regions [Zahn et al., 1986]. Apparently, North Atlantic productivity did not reach high enough levels to trigger additional carbon isotopic disequilibrium in *Uvigerina*.

Because the bottom of core CHN82-24-4 ends in the upper part of isotopic stage 7, there is an interval between about 215,000 and 245,000 years B.P. through which the stacked record is based only on core V30-97. Over this interval, the V30-97 record was based on analyses of both *Uvigerina* and (adjusted) *Cibicidoides* [Mix and Fairbanks, 1985].

Table A5 contains census counts of planktonic foraminifera and SST estimates covering the last 250,000 years from core V30-97, and Table A6 contains $CaCO_3$ values. These were analyzed and reported by Ruddiman and McIntyre [1981, 1984], but were not previously published in tabular form. For the remainder of this paper, we refer to any records constructed by combining site 607 data with data from the two piston cores as the "site 607" record.

The average sample spacing for all analyses is 15 cm at site 607, equivalent to 3400 years. The spacing is 30 cm at site 609 (equivalent to 4100 years or less), except for $CaCO_3$ analyses at 15-cm intervals near core breaks. The original spacing for most analyses in cores V30-97 and CHN82-24-4 (before resampling) was 5 cm, equal to average intervals of 1000 and 1600 years, respectively. For $CaCO_3$, the original sample spacing in V30-97 was 2 cm, equivalent to 400 years.

All $CaCO_3$ values were determined by gasometric analyses of bulk sediment following techniques described by Hulsemann [1966]. The reproducibility of replicate analyses was 1-2%. The faunal counts and estimates of sea surface temperature follow the simplified North Atlantic counting requirements (four species and an "other" category) and the transfer function equation of Ruddiman and Esmay [1986], with standard errors of estimate for SST values of about 2°C.

All $\delta^{18}O$ and $\delta^{13}C$ analyses at site 607 (Table A1) were made using a Carousel-48 automatic carbonate preparation device attached to a Finnegan-MAT 251 mass spectrometer. Analytical precision for this machine on replicate standards was 0.10‰ for $\delta^{18}O$ and 0.05‰ for $\delta^{13}C$. Precision on replicate samples for this study was 0.2‰ for $\delta^{18}O$ and 0.1‰ for $\delta^{13}C$. Calibration to the PDB standard is via the NBS-16, NBS-17, NBS-19, and NBS-20 standards. Values of $\delta^{18}O$ and $\delta^{13}C$ for *Cibicidoides wuellerstorfi* and *Cibicidoides kullenbergi* are reported unadjusted in Table A1. In order to create a composite $\delta^{18}O$ record, we followed standard practice by adding 0.64‰ to analyses of *Cibicidoides* to make them comparable to *Uvigerina*, which appears to have deposited calcite in oxygen isotopic equilibrium with seawater. We also follow standard practice by adding 0.9‰ to $\delta^{13}C$ values measured on *Uvigerina* to bring them into equilibrium with *Cibicidoides*, which is in near equilibrium with seawater.

Ruddiman et al. [1986c] previously reported numerous site 607 $\delta^{18}O$ analyses run on a VG 903 mass spectrometer. In general, the VG 903 values for a given sample were considerably lighter than the MAT 251 values, with differences often in excess of 0.5‰ and sometimes in excess of 1.0‰. We were unable to determine the reason for this extremely poor reproducibility; all samples for both machines were prepared using standard (and identical) techniques, and all samples were run during an interval when standards on both machines appeared acceptable. Because the VG 903 data from site 607 were much noisier than the MAT 251 data, both in terms of analysis of duplicates and reproducibility of basic downcore trends, we discarded all VG data, repicked the discarded samples, and reran them on the MAT 251. The resulting $\delta^{18}O$ and $\delta^{13}C$ trends from site 607 have an acceptably low noise level.

COMPOSITE DEPTH SECTIONS

Analysis of time series from sequences of hydraulic piston cores are complicated by gaps in the record at breaks between successive cores caused by disturbances associated with the coring process. These gaps may range from a few centimeters to several meters in length. With coring of two or more holes at a site, it is possible to splice across these gaps by correlating into the offset hole and then back into the main hole. For sites 607 and 609, this was done onboard leg 94 based on visual examination of the $CaCO_3$ layering of North Atlantic sediments [Ruddiman et al., 1986d]. All shipboard correlations have subsequently been checked by $CaCO_3$ analyses and in some cases adjusted slightly.

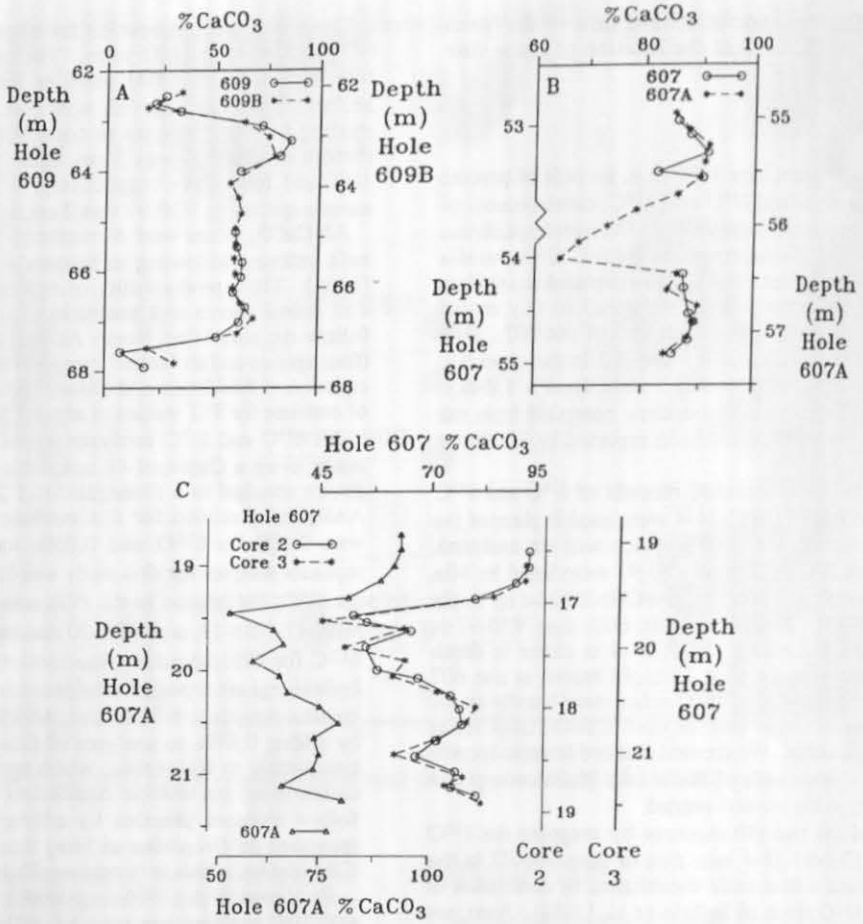

Fig. 2. Examples of between-hole splices and HPC-coring problems based on percent $CaCO_3$: (a) core splice from site 609, with negligible loss of $CaCO_3$ signal at hole 609 in the break between cores; (b) core splice from site 607, with full (41,000-year) $CaCO_3$ cycle lost at hole 607 in the break between cores; and (c) double-coring at site 607. The top of core 3 at hole 607 recored the same section already recovered in the bottom of core 2. The record from hole (607A) is also shown offset to left for comparison.

Examples are shown in Figure 2. In the example from site 609 (Figure 2a), little additional information is provided by splicing a short section of core 609A-8 into the gap between cores 609-7 and 609-8. In the example from site 607 (Figure 2b), however, splicing roughly 1 m of core 607A-7 into the gap between cores 607-6 and 607-7 adds a major (41,000-year) $CaCO_3$ fluctuation to the composite record. Another kind of coring problem is shown in Figure 2c: an interval spanning stages 11 and 12 was cored in the bottom of core 607-2 and then recored in the top of core 607-3, as proven by the overlay of $CaCO_3$ signals. Heaving and drifting of the ship apparently moved the bottom-hole assembly away from the center of the hole due to incomplete seating in the watery upper sediments.

Using these techniques, we have correlated across every core break in the entire Pleistocene record at site 609 and across all but one core break at site 607 (Tables 2 and 3). At site 607, we could not splice core 607A-4 into the break between cores 607-3 and 607-4, because core 607A-4 contained a slump. As a result, we joined the bottom of core 607-3 directly to the top of core 607-4. Correlations to other $\delta^{18}O$ records discussed later suggest that no significant thickness of sediment is missing across this core break.

The composite Pleistocene depth models at sites 607 and 609 (Tables 2 and 3; Figure 3) are based primarily on long sections in the main holes (607 and 609), joined by shorter sections in the offset holes (607A and 609B). Composite depth models are assembled at each site by assigning the sediment-water interface a depth of 0 m and incrementally adding the length of each subsequent spliced section down through the sediment column (Tables 2 and 3). The composite subbottom depths usually differ by less than 2 m from those obtained from standard DSDP depth-recording conventions. Composite subbottom depths of individual samples are listed in the appendix.

Because the $CaCO_3$ samples used to verify these splices were on average run at 15-cm intervals, most of the splices are accurate to within at least 15 cm, representing about 3500 years at site 607 and 2000 years at site 609. In most of the Pleistocene splices at these two sites, visual correlations of $CaCO_3$ layering can resolve the correlations to within about 5 to 10 cm, representing 2000 years or less.

Overlapped $CaCO_3$ records were also used to join the late Pleistocene piston core data to the earlier sections from the DSDP sites. Piston core V30-97 ends at the $\delta^{18}O$ stage 8/7

TABLE 2. Composite Depth Model for Site 607

Interval in Hole 607		Interval in Hole 607A	Composite Depth (m)
1-1-0		----	0
↓			
1-7-16	→	2-3-31	9.16
		↓	
2-1-55	←	2-4-15	10.50
↓			
2-7-24/ 3-2-78*			19.19
↓			
3-4-91/ 4-1-32†			22.32
↓			
4-7-24	→	5-4-105	31.24
		↓	
5-1-16	←	5-5-91	32.60
↓			
5-7-21	→	6-4-105	41.65
		↓	
6-1-16	←	6-5-105	43.15
↓			
6-7-9	→	7-4-135	52.08
		↓	
7-1-16	←	7-5-75	52.98
↓			
7-7-24	→	8-4-135	62.06
		↓	
8-1-5	←	8-5-15	62.36
↓			
8-7-5	→	9-4-58	71.36
		↓	
9-1-1	←	9-5-41	72.68

*Sequence cored in bottom of core 607-2 recored in top of 607-3.

†No splice attempted across this core break.

boundary at a depth of 9.16 m; this precisely matches the age and depth of the bottom of core 607-1 in the site 607 composite depth section (Table 2). Thus, core V30-97 was directly substituted for HPC core 607-1 in the composite depth section. Also, because we mapped the CHN82-24-4 $\delta^{18}O$ record into the V30-97 $\delta^{18}O$ record, the stacked $\delta^{18}O$ record from both cores could be directly substituted in the composite depth model. The complete Pleistocene $\delta^{18}O$ record at site 607 is shown plotted to composite depth in Figure 4. For the rest of this paper, all composite subbottom depths will be referred to simply as "depth" or "subbottom depth."

STRATIGRAPHY

DSDP leg 94 shipboard magnetic stratigraphy, supplemented by subsequent postcruise analyses, provides the primary stratigraphy. Initial shipboard determinations were made at average intervals of 1.5 m [Clement and Robinson, 1986]. Later analyses of some reversals at much closer intervals with continuous "U channel" sampling were reported by Clement and Kent [1986, 1987]. Additional work is included here.

The range of uncertainty in placement of magnetic reversals versus depth in each hole at sites 607 and 609 is listed in Table 4. With magnetic reversal measurements available from two holes at each site, it is possible to narrow the range of uncertainty in depth placement of most reversals by using

TABLE 3. Composite Depth Model for Site 609

Interval in Hole 609		Interval in Hole 609B	Composite Depth (m)
1–1–0			0
↓			
1–5–79	→	2–3–30	6.79
		↓	
2–1–31	←	2–4–91	8.90
↓			
2–7–1	→	3–3–1	17.60
		↓	
3–3–90	←	3–6–15	22.24
↓			
3–6–75*	→	4–2–1*	26.59
		↓	
4–3–1	←	4–5–61	31.68
↓			
4–6–1	→	5–2–91	36.18
		↓	
5–3–1	←	5–5–1	39.78
↓			
5–6–91	→	6–2–31	45.18
		↓	
6–1–31	←	6–3–61	46.98
↓			
6–7–51	→	7–2–121	56.18
		↓	
7–1–31	←	7–3–31	56.78
↓			
7–7–1	→	8–2–121	65.48
		↓	
8–1–61	←	8–3–61	66.38
↓			
8–6–91*	→	9–1–121*	74.18
		↓	
9–1–31	←	9–3–45	76.42
↓			
9–6–121	→	10–2–61	84.82
		↓	
10–1–61	←	10–3–1	85.72
↓			
10–6–61	→	11–2–0	93.22
		↓	
11–2–61	←	11–4–121	97.43
↓			
11–6–24*	→	12–2–1*	103.06
		↓	
12–1–11	←	12–3–1	104.56
↓			
12–6–61*	→	13–2–1*	112.56
		↓	
13–2–61	←	13–5–1	117.06

*Greater uncertainty in determining splice depths.

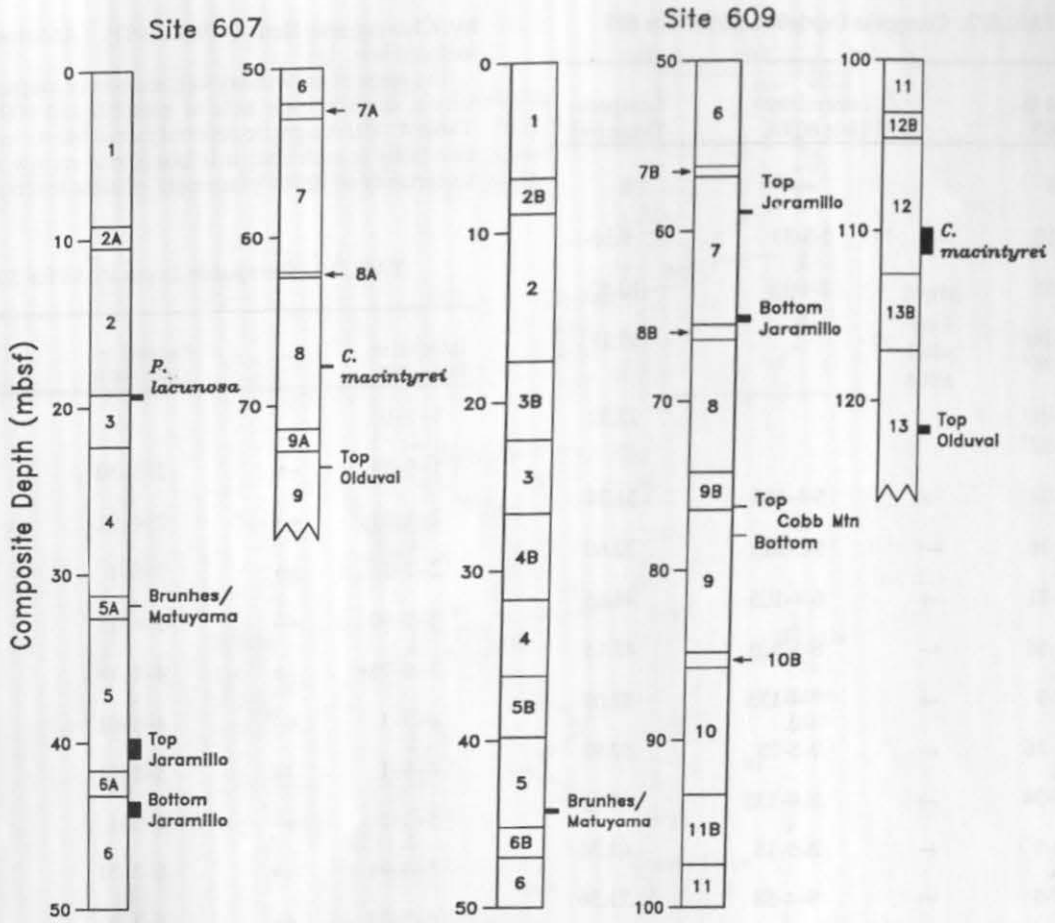

Fig. 3. Composite depth sections for sites 607 and 609, with sections from offset holes (607A, 609B) spliced into main holes (607, 609). Splices are based on $CaCO_3$ correlations (Figure 2), supplemented by visual correlations of layering from core photographs. The range of uncertainty of depths of magnetic reversals (and of last occurrences of *C. macintyrei* and *P. lacunosa*) is shown by solid bars to right of the composite depth columns.

between-hole correlations. This involves using the hole that spans the reversal and is included in the composite depth section (Tables 2 and 3; Figure 3) as a standard of reference into which the magnetic record from the other hole is projected by correlation. In all such cases, the between-hole correlations near the magnetic reversals were of very high quality, and the depths of the magnetic reversals could be transferred with an uncertainty of less than 10 cm (about 2000 years). The common depth overlap of the reversal as measured both in the main hole and in the offset hole (correlated into the main hole) then narrows the reversal depth range.

All composite depth ranges of magnetic reversals listed in Table 4 are shown in the composite site 607 and 609 depth sections in Figure 3. Also shown are the depth ranges of the *Pseudoemiliania lacunosa* and *Coccolithus macintyrei* datums.

TESTS OF TIME SCALE METHODOLOGY

The SPECMAP time scale for the Brunhes portion of the Pleistocene [Imbrie et al., 1984] was developed by identifying minima and maxima in a stacked composite of stable isotope ($\delta^{18}O$) records and linking these features to specific minima and maxima in orbital insolation forcing at the periods of obliquity (41,000 years) and precession (23,000 and 19,000 years). The $\delta^{18}O$ events were assigned lags behind the forcing based on assumed ice sheet physics: roughly 8000 years for events related to obliquity forcing, and 4000 to 5000 years for events related to precessional forcing. The resulting time scale produced a good match in amplitude modulation between orbital forcing and the $\delta^{18}O$ response for obliquity and an extraordinary match for precession [Imbrie et al., 1984].

Martinson et al. [1987] showed that a number of orbital tuning approaches yield effectively identical results in the late Pleistocene. This validates in a general way both the correlation to orbital insolation curves used by Imbrie et al. [1984], as well as the methods used later in this paper.

Here we apply the same methodology to the $\delta^{18}O$ record from site 607 to develop a time scale for the Matuyama portion of the Pleistocene, after initially testing several key assumptions. First, we verify that Ruddiman et al. [1986b] defined the correct match between $\delta^{18}O$ cycles and obliquity forcing in the Matuyama portion of the record, including the long interval unconstrained by magnetic reversal datums between about 1.1 and 1.66 Ma. Then we show that the

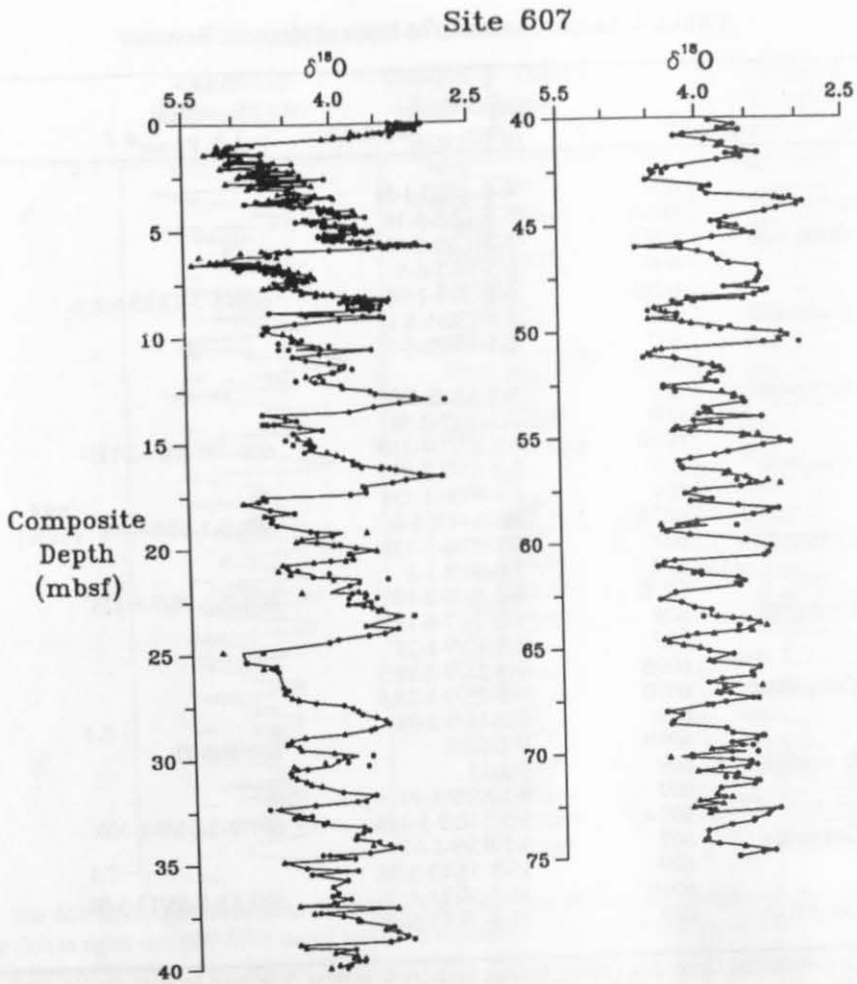

Fig. 4. Site 607 $\delta^{18}O$ record plotted to composite depth (record above 250,000 years based on cores V30-97 and CHN82-24-4). Individual analyses of *Cibicidoides* (circles) and *Uvigerina* (triangles) are shown.

precessional component of the Brunhes $\delta^{18}O$ record at site 607 is correlated to orbital forcing and provides a useful additional criterion for tuning at least the upper part of the Matuyama record.

Testing the Match of Obliquity Cycles

Using K/Ar-dated magnetic reversals for initial chronologic control, Ruddiman et al. [1986b] found that oscillations in $\delta^{18}O$, percent $CaCO_3$, and estimated SST at site 607 during the late Matuyama were concentrated at a period near that of orbital obliquity. These oscillations were used to tune the record by assigning each a 10,000-year lag behind a specific obliquity minimum or maximum.

These initial efforts depended solely on counting the number of tilt cycles in the interval between the upper Olduvai subchron boundary and the Brunhes-Matuyama reversal. Although constrained at several levels by other dated magnetic reversals, such an approach depends critically on neither skipping tilt cycles in the $\delta^{18}O$ record nor adding extra ones.

We can use the site 607 $\delta^{18}O$ record to test whether or not the amplitude variations of orbital obliquity and of the $\delta^{18}O$ response at the same period are sufficiently coherent to support or refute the Obliquity time scale match. We focus on the interval between 1.48 and 1.07 Ma, which contains a very pure obliquity signal evident in both untuned $\delta^{18}O$ records and in the Obliquity time scale (Figure 5). (Note that despite the addition of new $\delta^{18}O$ data, the original Obliquity time scale still captures the major 41,000-year $\delta^{18}O$ oscillations at site 607 clearly.)

We made three different correlations between the 10 orbital obliquity cycles within this 41,000-year interval and the 10 $\delta^{18}O$ events in the site 607 record over the same interval. One correlation followed the match used for the Obliquity time scale (as in Figure 5), and the other two matches were made by moving the $\delta^{18}O$ record up and down one obliquity cycle. In accord with Imbrie et al. [1984], we lagged the $\delta^{18}O$ signal 8000 years behind the 41,000-year obliquity forcing for each of the three proposed matches.

The match of $\delta^{18}O$ events with orbital obliquity used in the Obliquity time scale gave a slightly higher correlation than the

TABLE 4. Sample Constraints on Levels of Magnetic Reversals

Datum Level	Hole		Depth Range of Reversal*	Equivalent Depth Range+	Source of Data†
Brunhes/ Matuyama		607	4-6-140/5-1-54	—	C
		607A	5-5-12/5-5-14	—	C&K
	Composite	607A	5-5-12/5-5-14		
		609	5-5-98/5-6-5	—	C, C&R
		609B	6-1-50/6-1-70	609-5-5-130/5-6-1	C&K
	Composite	609	5-5-130/5-6-1		
Top of Jaramillo		607	5-5-130/5-6-97	—	C, C&R
		607A	?	—	
	Composite	607	5-5-130/5-6-97		
		609	7-2-50/7-2-98	—	C, C&R
		609B	7-4-85/7-4-110	609-7-2-85/7-2-115	C&K, C&R
	Composite	609	7-2-85/7-2-98		
Bottom of Jaramillo		607	6-1-97/6-1-138	—	C, C&R
		607A	6-5-144/6-6-0	607-6-1-53/6-1-68	C, C&R
	Composite	607	6-1-53/6-1-138		
		609	7-6-98/8-1-8	—	C, C&R
		609B	8-2-68/8-2-105	609-7-6-98/7-6-135	C&K
	Composite	609	7-6-98/7-6-135		
Top of Cobb Mountain		609	9-1-10/9-1-25	—	C&K
		609B	9-3-25/9-3-25.5		C&K
	Composite	609B	9-3-25/9-3-25.5		
Bottom of Cobb Mountain		609	9-2-18/9-2-98	—	C, C&R
		609B	9-4-50.5	609-9-2-33	C
	Composite	609	9-2-33		
Top of Olduvai		607	9-1-69/9-1-97	—	C, C&R
		607A	9-5-140/9-5-145	607-9-1-95/9-1-100	C, C&R
	Composite	607	9-1-95/9-1-97		
		609	13-5-55/13-5-98	—	C, C&R
		609B	14-1-50/14-1-95	609-13-5-55/13-5-98	C&K
	Composite	609	13-5-55/13-5-98		

*Depths shown in conventional Deep-Sea Drilling Project units: hole number, followed by core-section-depth in section (in cm).

+Depths of several magnetic reversals measured directly in offset hole and then transferred by $CaCO_3$ or visual correlations into the hole used as part of the composite depth sequence.

†C&R is Clement and Robinson [1986]; C&K, Clement and Kent [1986, 1987]; C, Clement (new work reported in this paper).

other two matches, but the difference was insignificant (Table 5). These results show that simple linear correlation at the obliquity rhythm alone at site 607 is not a highly diagnostic criterion for verifying a time scale.

Next, we tried using sedimentation rate changes as a criterion to test matches between orbital obliquity and site 607 $\delta^{18}O$ cycles. We first chose the same 10 $\delta^{18}O$/obliquity cycles from the previous test and calculated the correlation between the centimeter length of each half cycle and the Kiloyear duration of the corresponding orbital obliquity half cycle. We again used the match from the Obliquity time scale and other correlations with the orbital obliquity signal shifted up and down one cycle. The match from the Obliquity time scale produced the highest positive correlation coefficient (Table 5). We then extended the comparison to include all $\delta^{18}O$ stages from 1.07 Ma back to the top of the Olduvai subchron, and the Obliquity time scale again gave the best correlation (Table 5).

The Obliquity time scale thus appears to define the best $\delta^{18}O$/orbital match at the obliquity period for the long gap between magnetic reversal constraints at the top of the Olduvai subchron (about 1.66 Ma) and the Cobb Mountain event (K/Ar-dated at 1.1 Ma). The Obliquity time scale match in the Matuyama Chron younger than 1.1 Ma is anchored by K/Ar-dated constraints at the Brunhes/Matuyama boundary (0.73 Ma) and at the top and bottom of the Jaramillo subchron (0.90 and 0.97 Ma).

Testing Precessional Modulation of $\delta^{18}O$ at Site 607

Next we used the Brunhes $\delta^{18}O$ record from site 607 to test whether or not there is a reliable precessional cycle and whether or not it is modulated similarly to the SPECMAP $\delta^{18}O$ stack [Prell et al., 1986] and to the orbital forcing. If so, the precessional signal in the site 607 record should be a valid basis for additional tuning of the Obliquity time scale in the early Pleistocene.

We accept the shape of the SPECMAP $\delta^{18}O$ stack for the Brunhes as definitive, with one exception: the amplitude of isotopic event 18.4 at 0.721 Ma in the SPECMAP $\delta^{18}O$ stack

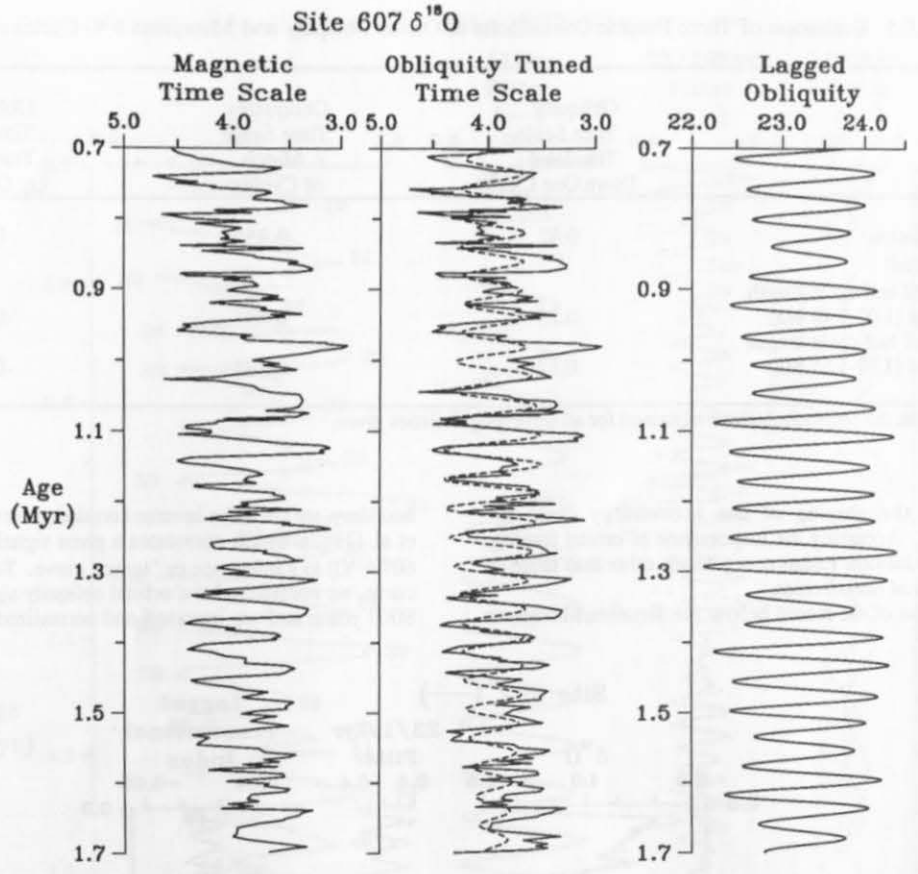

Fig. 5. Site 607 benthic foraminiferal $\delta^{18}O$ record through the Pleistocene portion of the Matuyama Chron, showing (left to right) site 607 $\delta^{18}O$ record plotted to magnetic reversal chronology, site 607 $\delta^{18}O$ record tuned to orbital tilt (using Obliquity time scale of Ruddiman et al., [1986b] with filtered obliquity signal (dashed line), and orbital obliquity lagged 10,000 years. Obliquity filters here (and hereafter) have a central frequency of 0.0247 cycles/kyr and bandwidth 0.0223-0.0271 cycles/kyr.

is substantially underrepresented compared to the $\delta^{18}O$ record from site 607 (Figure 6). Several high-resolution $\delta^{18}O$ records derived from both planktonic and benthic foraminifera resemble the site 607 version of event 18.4 more closely than they do the SPECMAP stack: see piston core V28-239 [Shackleton and Opdyke, 1976] and DSDP sites 502 [Prell, 1982], 504 [Shackleton and Hall, 1983], and 552A [Shackleton et al., 1984].

The correlation between the site 607 $\delta^{18}O$ record and the SPECMAP $\delta^{18}O$ stack (Figure 6) is 0.88. There are some dissimilarities within isotopic stage 14 near 0.55 to 0.475 Ma, a region of relatively low sedimentation rates at site 607 (1-2 cm/1000 years). Because these disagreements occur within core 607-3, they are not related to the unspliced core break between cores 607-3 and 607-4. That core break occurs within stage 15, which has the same structure in the site 607 record as in the SPECMAP stack (Figure 6).

The correlation between the filtered orbital components of these two $\delta^{18}O$ signals is very high, with a coherence-squared value of 0.95 for precession, 0.97 for tilt, and 0.95 for eccentricity. The coherence between the precessional component of $\delta^{18}O$ and the orbital precessional index is moderately high (0.87). In general, the amplitude modulation of the site 607 $\delta^{18}O$ record in the precessional band is similar both to the SPECMAP curve and to the orbital precessional index (Figure 6), except for offsets of the "envelope" of precessional amplitude at some intervals (e.g., stages 15-13, 0.6 to 0.5 Ma). For a single unsmoothed signal, the site 607 $\delta^{18}O$ record sufficiently resembles the orbital forcing to encourage use of the precessional $\delta^{18}O$ component as an additional criterion for tuning the Matuyama portion of the record.

TIME SCALE

In this section, we develop a time scale for the early and middle Pleistocene based on site 607 $\delta^{18}O$ data. First, we refine the Obliquity time scale in the Matuyama portion of the Pleistocene. Then, we reexamine the SPECMAP time scale for the Brunhes Chron and make adjustments in stages 17 and 16 from 0.70 to 0.64 Ma.

Matuyama Time Scale

Following the approach of Imbrie et al. [1984], we tune the $\delta^{18}O$ record to the direct forcing provided by orbital precession and obliquity (irradiation signals). Orbital eccentricity is not used as a target, but the consequences of tuning to tilt and

TABLE 5. Evaluation of Three Possible Correlations of Orbital Obliquity and Matuyama $\delta^{18}O$ Cycles at Site 607

	Obliquity Time Scale Translated Down One Cycle	Obliquity Time Scale Match of Cycles	Obliquity Time Scale Translated Up One Cycle
Signal correlation ($\delta^{18}O$/orbital)	0.82	0.85*	0.83
Correlation of half-cycle length vs duration (1.07-1.48 Ma)	0.25	0.43*	-0.44
Correlation of half-cycle length vs duration (1.07-1.65 Ma)	0.17	0.52*	-0.11

*Represents the best correlations obtained for all three possibilities given.

precession on the phasing of the eccentricity cycle are examined later. Accepting the importance of orbital forcing, we also try to minimize variance at periods other than those of the primary orbital periodicities.

For the portion of the record below the Brunhes/Matuyama boundary, we used the inverse correlation method of Martinson et al. [1982], which correlates a given signal (in this case site 607 $\delta^{18}O$) to a reference or "target" curve. To produce a target curve, we normalized the orbital obliquity signal and lagged it 8000 years, and we inverted and normalized the precessional

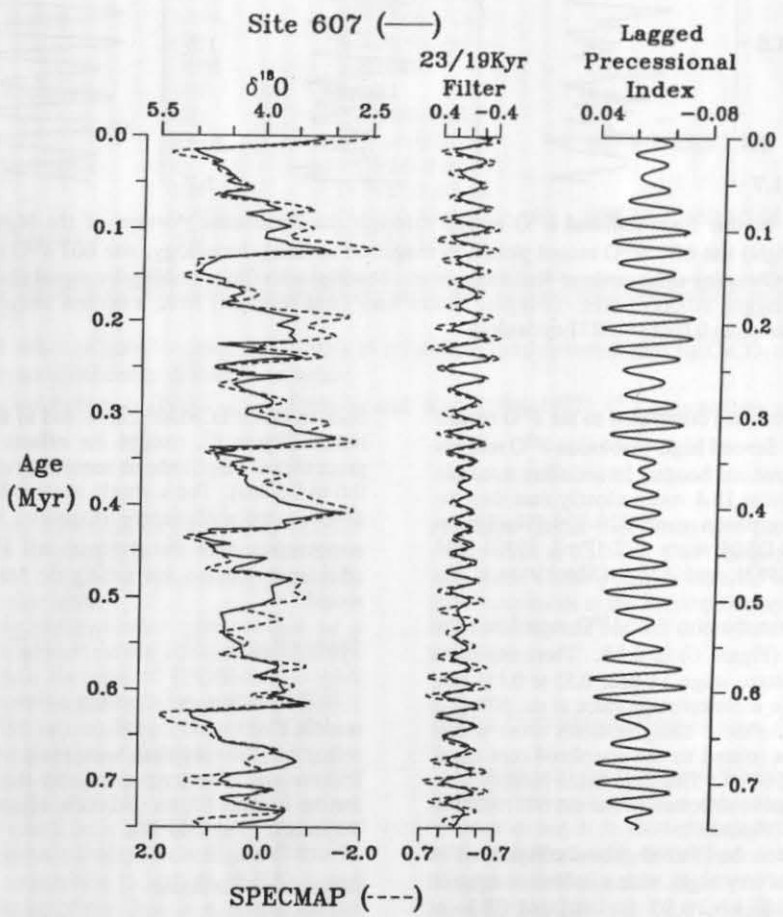

Fig. 6. Records of $\delta^{18}O$ for the Brunhes Chron: (left to right) site 607 $\delta^{18}O$ record (solid curve) overlaid on SPECMAP $\delta^{18}O$ stack (dashed curve) from Imbrie et al. [1984], filtered precession component of $\delta^{18}O$ signals from site 607 (solid curve) and SPECMAP (dashed curve), and lagged orbital precessional index. The precessional filter here (and hereafter) has a central frequency of 0.0477 cycles/kyr and bandwidth 0.0382-0.0573 cycles/kyr.

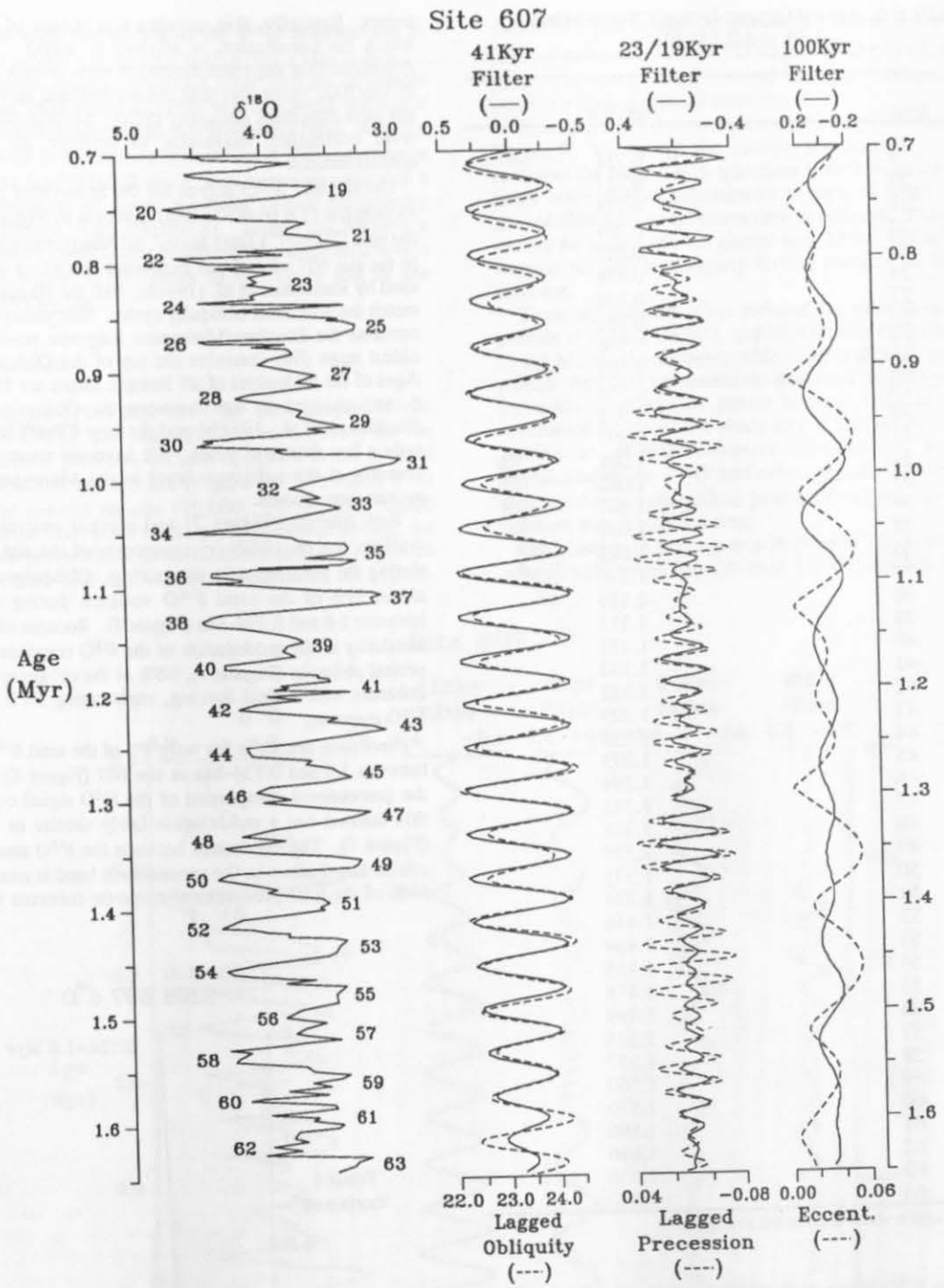

Fig. 7. Site 607 $\delta^{18}O$ data plotted to TP607 time scale for interval 1.65-0.734 Ma: (left to right) $\delta^{18}O$ data with numbered isotopic stages, filtered $\delta^{18}O$ obliquity signal (solid curve) versus lagged orbital obliquity (dashed curve), filtered $\delta^{18}O$ precessional signal (solid curve) versus lagged orbital precession (dashed curve), and filtered eccentricity signal (solid curve) versus orbital eccentricity (dashed curve). Filters have a central frequency at 41,000 years.

index curve and lagged it 5000 years. Both choices follow values derived in Imbrie et al. [1984]. We then combined these two orbital signals by adding one half the lagged and normalized precessional curve to the lagged and normalized tilt curve. This target curve (called T + 1/2P) was chosen to reflect the dominance of tilt in the $\delta^{18}O$ response but to also allow some tuning to precession. Sensitivity tests showed that this ratio (tilt/precession) could vary through a wide range of values with negligible effect on the results.

We then imposed tie lines in the correlation program at three

TABLE 6. Ages of Oxygen Isotopic Stages between 1.60 and 0.734 Ma

Stage	Age, Ma
19	0.734
20	0.751
21	0.775
22	0.799
23	0.819
24	0.838
25	0.859
26	0.881
27	0.906
28	0.922
29	0.946
30	0.965
31	0.985
32	1.007
33	1.022
34	1.047
35	1.068
36	1.088
37	1.110
38	1.130
39	1.153
40	1.173
41	1.192
42	1.212
43	1.229
44	1.254
45	1.273
46	1.294
47	1.313
48	1.335
49	1.359
50	1.371
51	1.394
52	1.416
53	1.434
54	1.455
55	1.478
56	1.499
57	1.514
58	1.537
59	1.560
60	1.576
61	1.596
62	1.616
63	1.636
64	1.662

Stages and events are shown in Figure 7.

levels in the $\delta^{18}O$ curve, each marking a K/Ar-dated magnetic reversal: the Brunhes/Matuyama boundary (0.73 Ma), the bottom of the Jaramillo subchron (0.97 Ma), and the top of the Olduvai subchron (1.66 Ma). With only this initial guidance, the inverse technique reproduced the same match of $\delta^{18}O$ cycles to orbital obliquity as previously determined by Ruddiman et al. [1986c].

As the inverse-correlation method tuned to progressively higher-frequency (precessional) components of the orbital target signal, subjective decisions arose as to what degree of distortion (stretching and compression) of the original record to accept. Basically, this amounts to a choice of the resolution which the correlation is allowed to attain. We accepted distortions that kept sedimentation rates within the range 2 to 10 cm/1000 years and that did not degrade obvious power in the more dominant obliquity cycles. Several shorter intervals were correlated manually to achieve all these goals simultaneously.

The site 607 $\delta^{18}O$ signal for the Matuyama portion of the Pleistocene (1.6 to 0.734 Ma) is shown in Figure 7 plotted to the new ("TP607") time scale. All Matuyama-age $\delta^{18}O$ stages in the site 607 record are numbered according to the scheme used by Ruddiman et al. [1986b], with the stages numbered to match the dominant obliquity cycles. The youngest stage (19) contains the Brunhes/Matuyama magnetic reversal, and the oldest stage (64) contains the top of the Olduvai subchron. Ages of the midpoints of all isotopic stages are listed in Table 6, and changes in age between the Obliquity time scale [Ruddiman et al., 1986b] and the new TP607 time scale are only a few thousand years. We have not attempted to name features at the substage level in the Matuyama; that will require more records.

Both filtering (Figure 7) and spectral analysis (Figure 8) confirm that the obliquity component of the site $\delta^{18}O$ signal during the Matuyama is very strong. Obliquity accounts for about 55% of the total $\delta^{18}O$ variance during the interval between 1.6 and 0.734 Ma (Figure 8). Because of the general similarity in the modulation of the $\delta^{18}O$ response and that of orbital obliquity (Figure 7), 96% of the obliquity response is coherent with orbital forcing, representing 53% of the total $\delta^{18}O$ response.

Precession accounts for only 8% of the total $\delta^{18}O$ response between 1.6 and 0.734 Ma at site 607 (Figure 8). However, the precessional component of the $\delta^{18}O$ signal over some of this interval has a modulation fairly similar to the forcing (Figure 7). The coherence between the $\delta^{18}O$ record and the orbital target curve in the precessional band is moderate, with 64% of the total precessional response coherent with orbital

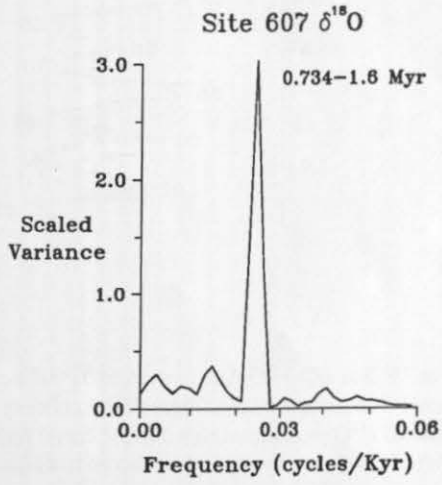

Fig. 8. Spectra of site 607 $\delta^{18}O$ record derived from TP607 time scale during interval 1.6-0.734 Ma. Spectral analyses here (and hereafter) followed the Blackman-Tukey technique with a Hamming window, 1/3 lag, resampling interval of 3400 years, and N = 217.

forcing. This adds another 5% to the $\delta^{18}O$ response that is coherent with orbital forcing after tuning, for a total of 60%.

No distinctive peak is observed near periods of orbital eccentricity at 94,000 and 125,000 years; instead, there is a broad minimum in power across this frequency band. Roughly 13% of the total $\delta^{18}O$ variance is associated with responses at periods longer than 100,000 years, with some suggestion of a small concentration of power near the orbital eccentricity period of 413,000 years (Figure 8). Some low-frequency contribution may result from nonstationarity associated with a drift toward higher $\delta^{18}O$ values in the upper part of the Matuyama $\delta^{18}O$ record.

Brunhes Time Scale

In merging the TP607 time scale for the Matuyama chron with the SPECMAP time scale [Imbrie et al., 1984] for the Brunhes, several problems became apparent in the interval between about 0.8 and 0.6 Ma (Figure 9). We found $\delta^{18}O$ responses at several periods (70,000, 54,000, and 30,000 years) different from those of the primary orbital forcing; for the latter two periodicities, these were the strongest responses within the entire 1.65 m.y. of the record. Also, the 41,000-year $\delta^{18}O$ signal weakened substantially across this interval, in part because interglacial $\delta^{18}O$ stage 17 in the SPECMAP time scale is centered on an interval for which obliquity forcing predicts a (lagged) glacial response.

These problems were reduced with the adjustments shown in Figure 9. We moved the isotopic transition that appears to represent the stage 17/16 transition from 0.66 to 0.68 Ma and made other smaller adjustments of parts of stage 16 and 17 toward older ages to accommodate this change. These changes moved the middle of interglacial stage 17 into the middle of an interval for which obliquity forcing predicts an interglacial response.

These adjustments also reduced the excessive power at periods of 70,000, 54,000, and 30,000 years in the interval 0.8 to 0.6 Ma to levels comparable to several other parts of the record. And they increased the amount of 41,000-year power, increased precessional power between 0.75 and 0.6 Ma, maintained the excellent phase lock of precession with orbital forcing, and slightly enhanced the agreement between the modulation of the $\delta^{18}O$ and orbital signals. These changes thus transformed anomalous power at three periods into power coherent with orbital forcing.

Our changes in part agree with those of Black et al. [1988], who also proposed that the stage 17/16 transition should date

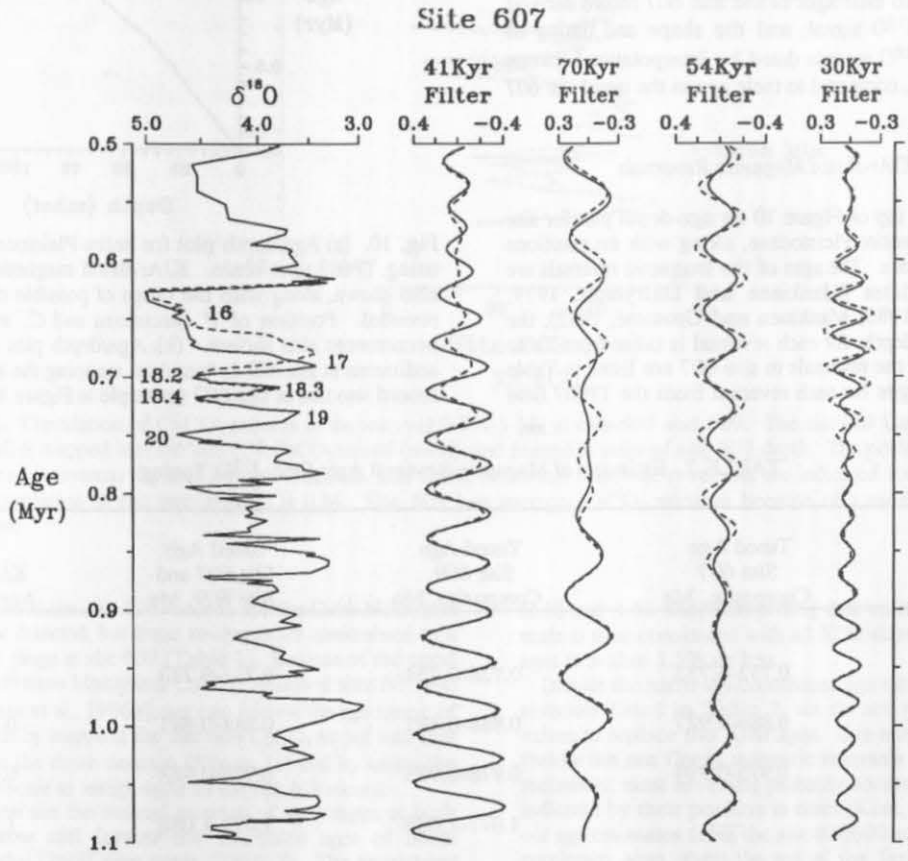

Fig. 9. Site 607 $\delta^{18}O$ data for interval 1.1-0.5 Ma plotted to two time scales. Data from the Matuyama Chron (>0.734 Ma) are plotted according to the TP607 time scale in both versions. Data from Brunhes Chron are plotted to SPECMAP time scale for the version in dashed lines and to adjusted SPECMAP time scale for the version in solid lines. Shown, from left to right, are the $\delta^{18}O$ record and filtered $\delta^{18}O$ signal at 41,000 years, 70,000 years, 54,000 years, and 30,000 years. SPECMAP data are resampled at a 2000-year time step.

some 15,000 years older than shown in the SPECMAP time scale of Imbrie et al [1984]. Below stage 17, however, our adjustments disagree with that of Black et al., who redated the high-amplitude oscillations of stage 18 (events 18.2, 18.3, and 18.4) to older levels, altering the SPECMAP time scale by compressing all of stage 18 and upper stage 19 against the lower limit of the Brunhes/Matuyama boundary. In contrast, our changes retain the SPECMAP time scale from event 18.2 through the Brunhes/Matuyama boundary; our adjustments all occur above the middle of event 18.2.

At this point, we do not suggest formalizing our adjustments as a new time scale. The reason for caution is that the single-peaked isotopic stage 17 in the site 607 record looks different from the double-peaked stage 17 in the SPECMAP composite and in several individual cores. It seems unwise to base a time scale revision on an atypical feature. Still, we recommend that close attention be paid in future efforts with stacked multicore composites to the likelihood that the stage 17/16 is older than estimated by SPECMAP.

EVALUATION OF TP607 TIME SCALE

We evaluate the TP607 time scale by comparison with two kinds of evidence: the ages of magnetic reversals from K/Ar dating, compared to their ages in the site 607 record derived from tuning the $\delta^{18}O$ signal; and the shape and timing of features in other $\delta^{18}O$ records dated by interpolation between magnetic reversals, compared to their age in the tuned site 607 $\delta^{18}O$ record.

Comparison With K/Ar-Dated Magnetic Reversals

We show at the top of Figure 10 an age-depth plot for site 607 spanning the entire Pleistocene, along with the positions of magnetic reversals. The ages of the magnetic reversals are based on K/Ar dates [Mankinen and Dalrymple, 1979; Mankinen et al., 1980; Mankinen and Grommé, 1982]; the range of possible depths for each reversal is taken from Table 4. Age ranges for the reversals in site 607 are listed in Table 7. The range of ages for each reversal from the TP607 time scale agrees closely with the K/Ar dates, particularly at the narrowly constrained Brunhes/Matuyama boundary and top of the Olduvai subchron.

The top and bottom of the Jaramillo subchron are not as

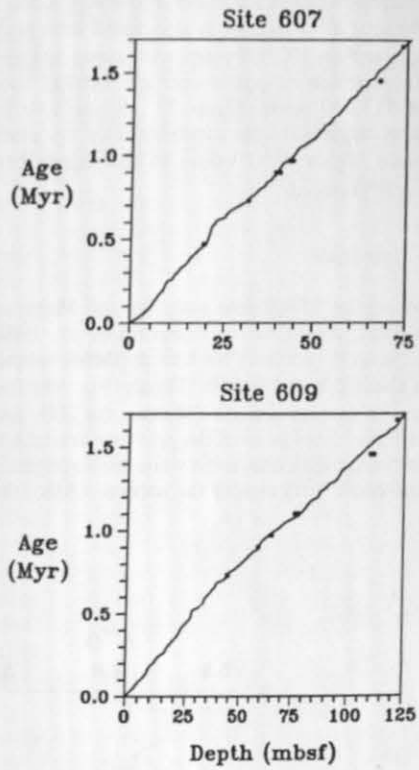

Fig. 10. (a) Age/depth plot for entire Pleistocene at site 607, using TP607 time scale. K/Ar-dated magnetic reversals are also shown, along with the range of possible depths for each reversal. Position of *P. lacunosa* and *C. macintyrei* last occurrences also shown. (b) Age/depth plot of Pleistocene sediments at site 609 is based on mapping the site 609 $CaCO_3$ record into that of site 607 (example in Figure 11).

TABLE 7. Estimates of Magnetic Reversal Ages From $\delta^{18}O$ Tuning

Reversal	Tuned Age Site 607 Composite, Ma	Tuned Age Site 609 Composite, Ma	Tuned Age Site 607 and Site 609, Ma	K/Ar Age, Ma
Brunhes/ Matuyama	0.732-0.733	0.728-0.734	0.732-0.733	0.73*
Top of Jaramillo	0.886-0.927	0.888-0.891	0.888-0.891	0.90
Bottom of Jaramillo	0.975-0.994	0.978-0.983	0.978-0.983	0.97
Cobb Mountain	-----	1.077-1.088	1.077-1.088	1.10
Top of Olduvai	1.653	1.630-1.638	1.630-1.653	1.66†

*Tuned estimate of Imbrie et al. [1984] is 0.734 Ma.

†Calculated by interpolating age of magnetic anomalies on seafloor relative to K/Ar-dated top and bottom of Matuyama Chron.

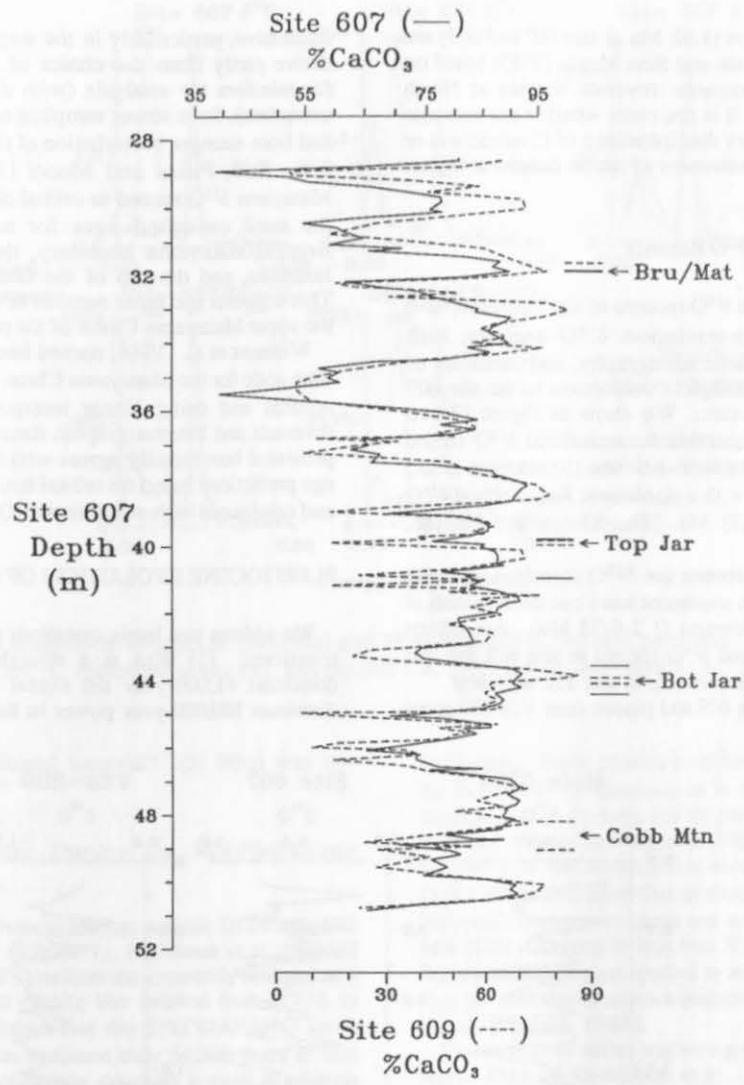

Fig. 11. Correlation of $CaCO_3$ records in the interval 0.7-1.1 Ma at sites 607 and 609. The site 609 $CaCO_3$ record (dashed) is mapped into the site 607 $CaCO_3$ record (solid) and plotted in units of site 607 depth. The positions of the Brunhes-Matuyama, top and bottom Jaramillo, and Cobb Mountain magnetic reversals are indicated for each site. The correlation of the two signals is 0.84. Site 609 has stronger $CaCO_3$ minima because of a more northerly location.

closely defined in the site 607 record, and the Cobb Mountain event was not detected, but these reversals are constrained to a narrow depth range at site 609 (Table 4). Because of the good correlations between Matuyama $CaCO_3$ records at sites 607 and 609 [Ruddiman et al., 1986b], we can narrow the age range of these reversals by mapping the site 609 $CaCO_3$ record into that of site 607 in the depth domain (Figure 11) and by using the site 607 time scale to assign ages to the site 609 record.

We can then use the mutual overlap of age ranges at both sites to narrow still further the estimated ages of these reversals in the TP607 time scale (Table 7). The agreement with the K/Ar estimates is within 1% for all reversals except the Cobb Mountain event. The estimate of 1.085 Ma for the Cobb Mountain event from the TP607 time scale differs with the mean value of 1.10 Ma from Mankinen and Grommé [1982] by only 1.5% and matches one of two age clusters (1.08 and 1.12 Ma) comprising that value. The TP607 time scale is thus consistent with all K/Ar-dated magnetic reversal ages to within 1.5% or less.

Despite the narrowly constrained age ranges for the magnetic reversals listed in Table 7, we do not propose using these values to replace the K/Ar ages. It is not clear at what depth (below the sea floor) magnetic reversals "lock in" to marine sediments; most reversals probably occurred later in time than indicated by their position in cores [Kent, 1973]. If, however, our age estimates from the site 607/609 records are viewed as maximum ages, then the top of the Jaramillo and Olduvai subchrons would have to be somewhat younger than the K/Ar ages.

The *P. lacunosa* extinction dates to 0.463 Ma in site 607, in good agreement with the age obtained previously [Thierstein et al., 1977; Imbrie et al., 1984]. Our estimates for the age of

the *C. macintyrei* extinction (1.52 Ma at site 607 and 609) are older than those of Backman and Shackleton [1983] based on interpolation between magnetic reversal datums at North Atlantic DSDP site 552. It is not clear whether our estimate dates an earlier evolutionary disappearance of *C. macintyrei* or reflects the time-transgressiveness of some datums at higher latitudes.

Comparison With Other $\delta^{18}O$ Records

Relatively few published $\delta^{18}O$ records of the Matuyama have the combination of high-resolution $\delta^{18}O$ analyses, high sedimentation rates, magnetic stratigraphy, and continuity of record necessary for meaningful comparison to the site 607 record and TP607 time scale. We show in Figure 12 two records: site 552, with a benthic foraminiferal $\delta^{18}O$ record spanning 1.2-0.73 Ma and 1.66-1.5 Ma [Shackleton et al., 1984] and core V28-239, with a planktonic foraminiferal $\delta^{18}O$ record spanning 1.66-0.73 Ma. [Shackleton and Opdyke, 1976].

The close agreement between the $\delta^{18}O$ signals at sites 607 and 552 indicates that both sequences have complete records of the upper part of the Matuyama (1.2-0.73 Ma). Age offsets between the orbitally tuned $\delta^{18}O$ record at site 607 and that interpolated from magnetic reversals at site 552 are minor.

Agreement between site 607 and piston core V28-239 is not impressive, particularly in the amplitude matches. This may derive partly from the choice of benthic versus planktonic foraminifera for analysis (with different local temperature overprints), from lower sampling resolution in core V28-239, and from stronger bioturbation of the $\delta^{18}O$ signal at core V28-239. Still, Pisias and Moore [1981] tuned the V28-239 Matuyama $\delta^{18}O$ record to orbital obliquity and derived nearly the same estimated ages for magnetic reversals at the Brunhes/Matuyama boundary, the top and bottom of the Jaramillo, and the top of the Olduvai as those in Table 7. This suggests the same number of 41,000-year oscillations in the upper Matuyama Chron of the two cores.

Williams et al. [1988] named isotopic stages and proposed a time scale for the Matuyama Chron based on four stacked $\delta^{18}O$ records and using linear interpolation between magnetic reversals and biostratigraphic datums. The TP607 time scale presented here broadly agrees with theirs, but we make explicit age predictions based on orbital tuning of a verifiably complete and continuous high-resolution $\delta^{18}O$ record.

PLEISTOCENE EVOLUTION OF CLIMATIC RESPONSES

We address two basic questions about the mid-Pleistocene transition: (1) Was it a straightforward shift from the dominant 41,000-year tilt signal of the Matuyama to the dominant 100,000-year power in the Brunhes, or did rhythms

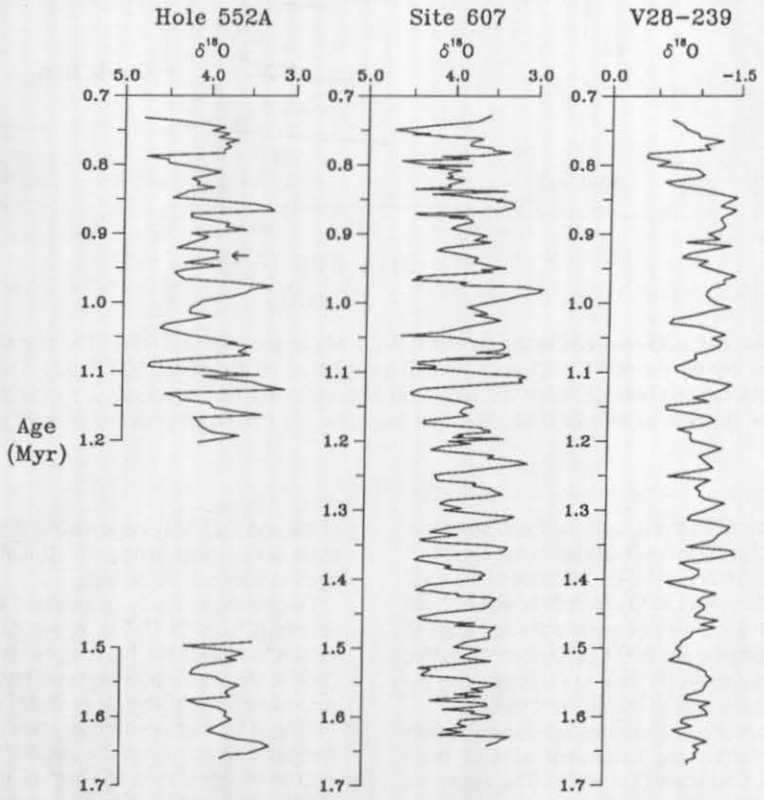

Fig. 12. Comparison of site 607 upper Matuyama $\delta^{18}O$ record plotted to TP607 time scale (center) with $\delta^{18}O$ records plotted to magnetic reversal chronology: North Atlantic site 552 (left) and western equatorial Pacific piston core V28-239 (right). The gap in the site 552 record is due to a disturbed core. The arrow marks the position of a core break in the record from site 552.

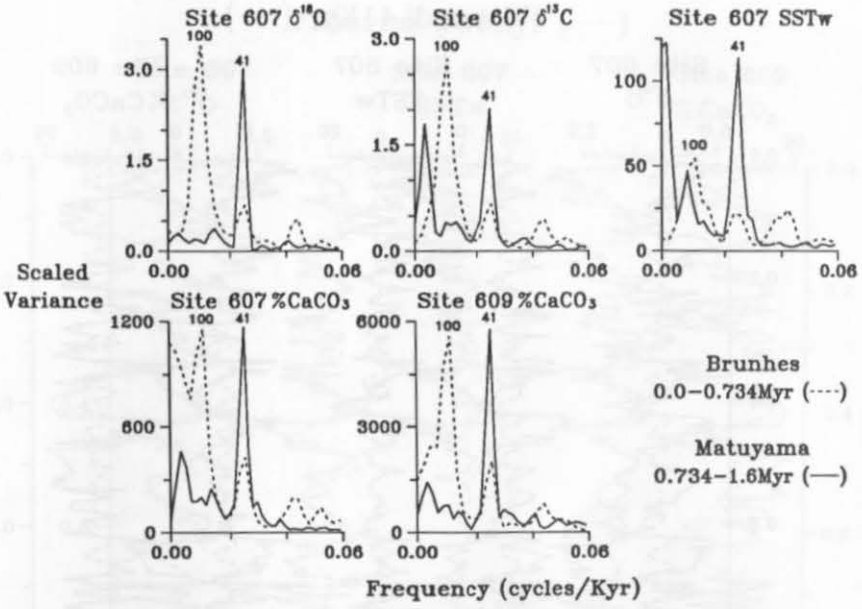

Fig. 13. Spectral analysis of Brunhes (0.734-0 Ma) and Matuyama (1.6-0.734 Ma) portions of the Pleistocene for five records: $\delta^{18}O$, $\delta^{13}C$, estimated winter SST, and percent $CaCO_3$ at site 607; and percent $CaCO_3$ at site 609.

emerge during a transitional interval? (2) What was the duration of the transition?

Anomalous Periodicities During the Mid-Pleistocene Transition

In a record compiled from northeast Atlantic DSDP site 552 and piston core K708-7 (Figure 1), Ruddiman et al. [1986a] detected a sequence of SST oscillations apparently centered at a rhythm of 54,000 years during the interval from 0.775 to 0.625 Ma. They also found that the SPECMAP $\delta^{18}O$ stack showed some increase in variance near 54,000 years at this time. Because orbital obliquity contains a small insolation forcing component at this period [Berger, 1978], they suggested that this SST signal could be an insolation-driven response amplified within the climate system. However, they cautioned that these oscillations could be an artifact of an incorrect time scale or of incorrect transfer of the SPECMAP time scale.

The results in Figure 9 demonstrate that a small but plausible adjustment to the SPECMAP time scale greatly reduced the amount of 54,000-year power (and 30,000-year and 70,000-year power) in the $\delta^{18}O$ record of site 607. Other tests (not shown) show that large concentrations of power at 54,000, 70,000, and 30,000 years in this same interval of the site 607 $CaCO_3$ and SST records were also substantially reduced by this change. As a result, there is no evidence of unusually strong periodic responses other than those at the primary orbital rhythms during the mid-Pleistocene transition.

Orbital Periodicities Through the Pleistocene

The central focus of this paper is the timing of the change in response at high latitudes of the northern hemisphere from 41,000-year Matuyama variations to 100,000-year Brunhes oscillations. Some studies have favored a rapid transition. On the basis of $\delta^{18}O$ fluctuations in core V28-239 (Figure 12), Shackleton and Opdyke [1976] placed the change at about 0.8 Ma, and Pisias and Moore [1981] suggested that strong 100,000-year fluctuations first occurred abruptly after 0.9 Ma. Prell [1982] concluded that an abrupt switch in "mode" of $\delta^{18}O$ variation (changes in mean and standard deviation) in DSDP hole 502B occurred in less than 50,000 years at about 0.9 Ma. Statistical techniques applied to several $\delta^{18}O$ records suggest that the mid-Pleistocene transition was an abrupt "jump" at 0.9 Ma [Maasch, 1988].

Evidence from other studies argues for a later, more gradual shift. Data of Ruddiman et al. [1986b] indicate near-total dominance of 41,000-year power at site 607 until very late in the Matuyama Chron, with much of the transition to 100,000-year power thus consigned to the Brunhes Chron. Imbrie [1985] found that 100,000-year power almost doubled from the interval 0.78-0.4 Ma to the interval 0.4-0 Ma. Ruddiman et al. [1986a] noted a similar doubling of 100,000-year power during the same time period in the composite northeast Atlantic SST record cited above.

With high-resolution $\delta^{18}O$ data at site 607 and a time scale spanning the entire Pleistocene, we can further address this problem. In addition, we can examine the shift in power in the other proxy indicators: $\delta^{13}C$, percent $CaCO_3$, and estimated SST at site 607 and percent $CaCO_3$ at site 609. Spectral analysis of these signals (Figure 13) shows the nearly total change in concentration of orbital power from the Matuyama Pleistocene (1.60 to 0.735 Ma) to the Brunhes (0.735 to 0 Ma).

We choose to present band-pass filtered versions of the records to portray most clearly the nature of the changes (Figures 14-18). Sensitivity tests show that filtering smooths very abrupt changes to some extent, but the fact that filtered signals can be directly overlaid on the original data at least permits direct visual evaluation of the success of the filtering

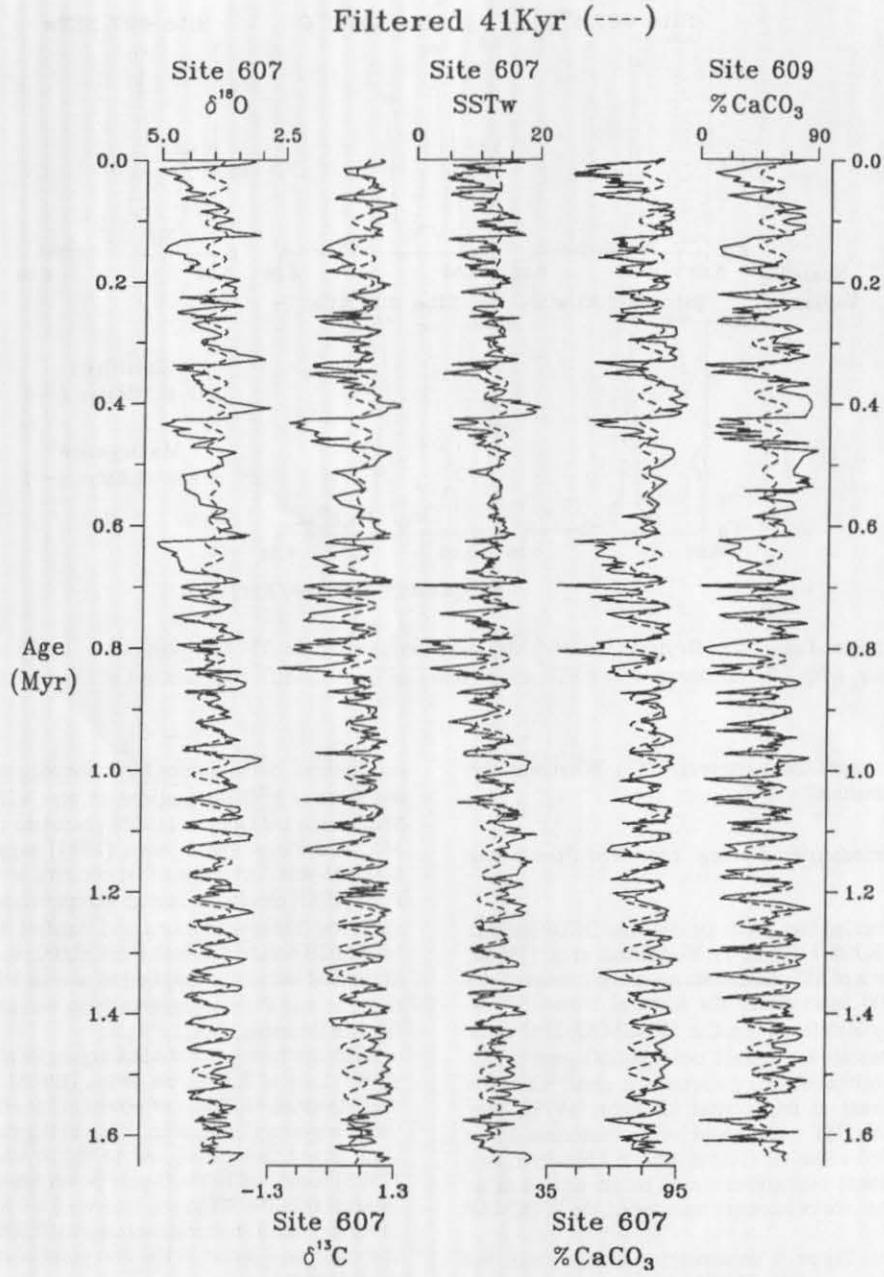

Fig. 14. Overlays of filtered 41,000-year signals (dashed line) on original records (solid line) of site 607 $\delta^{18}O$, $\delta^{13}C$, SST, and percent $CaCO_3$ and of site 609 percent $CaCO_3$ for the last 1.65 m.y.

process and thus the actual rates of change. In effect, the filtered records set an upper limit on the rates of change.

Obliquity. All five records filtered at the central frequency of orbital obliquity (Figure 14) show dominant 41,000-year power in the Matuyama Chron, giving way to weaker power in the Brunhes Chron. The $\delta^{18}O$-based time scale produces strong 41,000-year oscillations in all five records through the Matuyama portion of the Pleistocene, and all of these signals are in phase to within 10° (1100 years) or less (Table 8). The mid-Pleistocene decline in 41,000-year power varies among the records, beginning as early as 1.1 Ma in the $\delta^{18}O$ record and as late as 0.7 Ma in the $\delta^{13}C$ and $CaCO_3$ records. In all records, a minimum in variance is reached at 0.55 Ma, with subsequent reemergence of moderate power. In all five records, the 41,000-year signals are also in phase to within 20° (2200 years) or less during the Brunhes Chron (Table 8).

The 100,000-year ("eccentricity") power. The amplitude of the filtered 100,000-year signals for all five records increased markedly from the Matuyama to the Brunhes Chron (Figure 15). Shorter intervals of increased 100,000-year power are

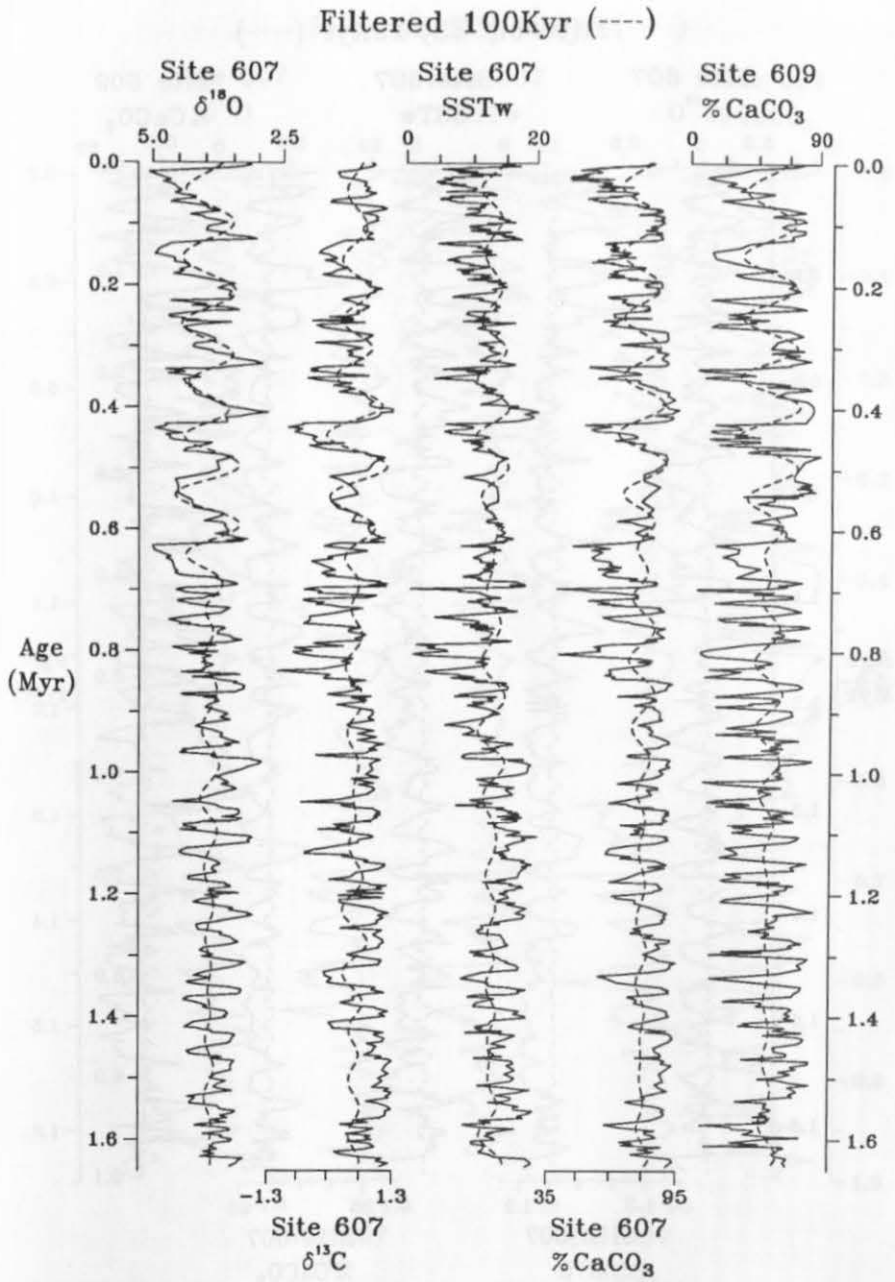

Fig. 15. Overlays of filtered 100,000-year signals (dashed line) on original records (solid line) of site 607 $\delta^{18}O$, $\delta^{13}C$, SST, and percent $CaCO_3$ and of site 609 percent $CaCO_3$ for the last 1.65 m.y. The eccentricity filter has a central frequency of 0.0103 cycles/kyr and bandwidth 0.008-0.0127 cycles/kyr.

evident during the Matuyama, but the timing of these intervals differs considerably among the various parameters, and comparisons of the filtered and original signals do not show the kind of convincing 100,000-year signal that developed during the Brunhes. The temporary increase in 100,000-year $\delta^{18}O$ variance near 1.0 Ma appears to be linked to a brief shift toward lighter isotopic values (stages 33 to 31), but this is opposite to the association of 100,000-year power with a trend toward heavier $\delta^{18}O$ values during the Brunhes. In general, there is remarkably little evidence in these records of significant 100,000-year power during most of the Matuyama Chron.

By 0.9 Ma, 100,000-year power in all five signals begins for the first time to approach or achieve a phase lock with orbital eccentricity (Figure 7). Although 100,000-year power remained weak, this phase lock suggests that the climate system had begun to develop the typical 100,000-year power of the Brunhes Chron. Records of $\delta^{18}O$ in some regions reached very heavy values in isotopic stage 22 (at 0.8 Ma), perhaps indicating greater increases in 100,000-year power in

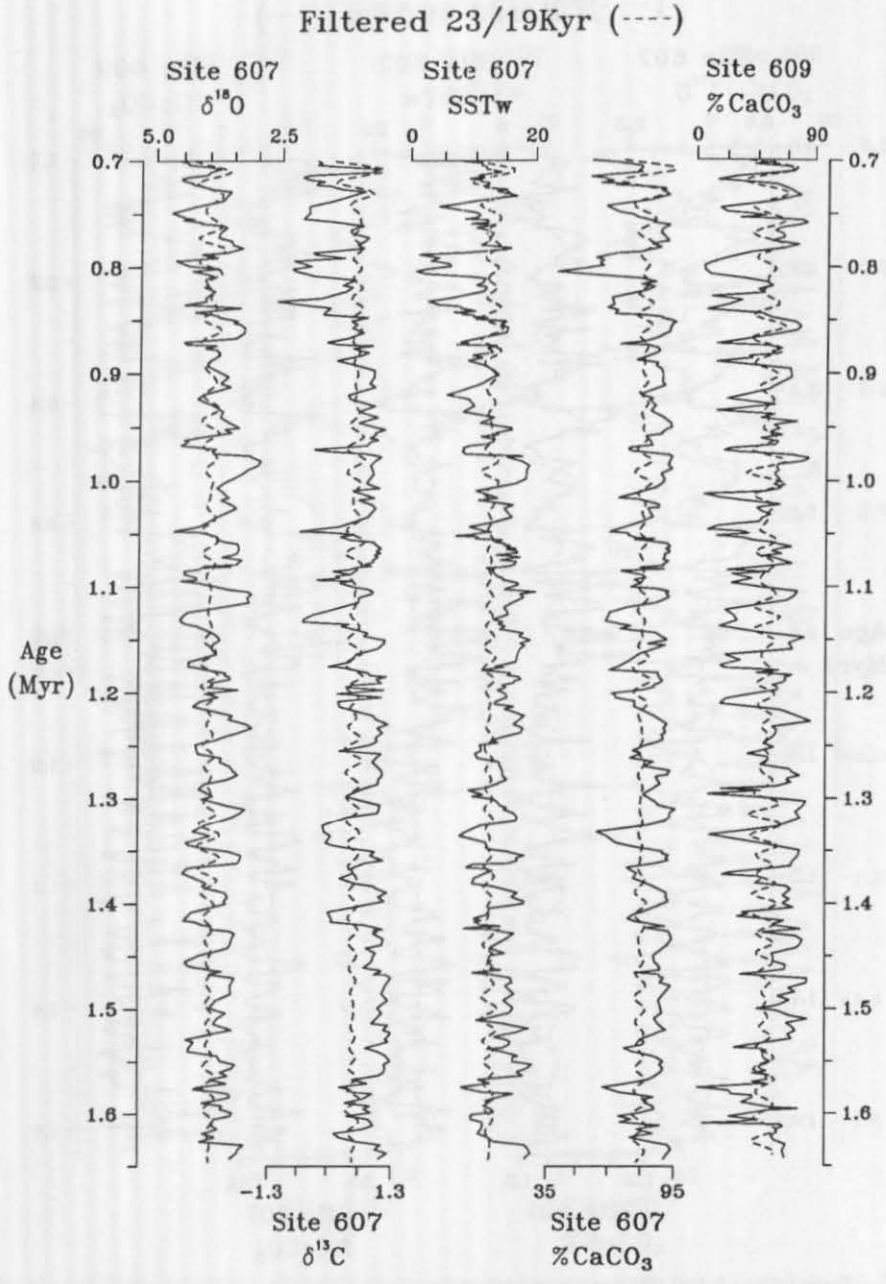

Fig. 16. Overlays of filtered 23,000/19,000-year signals (dashed line) on original records (solid line) of site 607 $\delta^{18}O$, $\delta^{13}C$, SST, and percent $CaCO_3$ and of site 609 percent $CaCO_3$ for the early Pleistocene (1.65-0.734 Ma).

those records, but North Atlantic sites 607 and 552 record a less extreme glaciation (Figure 12) and only moderate 100,000-year power.

Stronger and more convincing 100,000-year power emerged in the filtered signals (Figure 15) after 0.7 Ma (although less clearly in the SST record) and culminated in a very strong signal by 0.6 to 0.4 Ma. The increases in 100,000-year power are thus basically constrained between 0.9 and 0.4 Ma, with the fastest changes between 0.7 and 0.6 Ma. The 100,000-year components of the $\delta^{18}O$ and $\delta^{13}C$ signals are in phase to within 5° (1400 years) during the Brunhes Chron, whereas SST and $CaCO_3$ lag $\delta^{18}O$ by 14° (3900 years) to 34° (9400 years) at the 100,000-year rhythm (Table 8).

Precession. The filtered precessional responses in all five signals increase in amplitude from the Matuyama to the Brunhes Chron, with a very sharp increase between 0.8 and 0.7 Ma (Figures 16 and 17). The strongest precessional variations occur between 0.75 and 0.675 Ma, with oscillations of moderate strength during several intervals in the upper half of the Brunhes Chron. The SST signal also has a very strong 23,000-year signal after 0.2 Ma (Figure 17).

During the strong precessional responses after 0.9 Ma, the

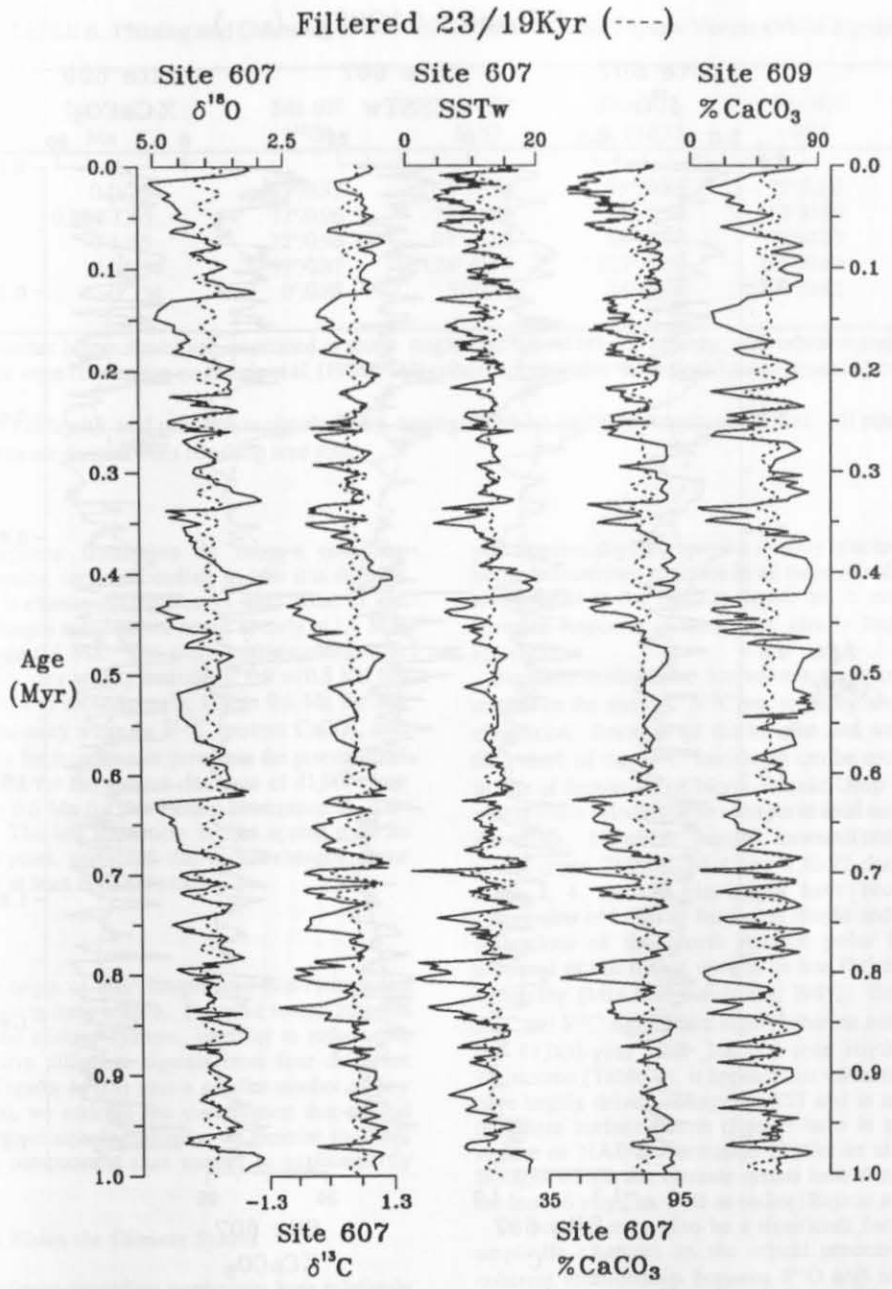

Fig. 17. Overlays of filtered 23,000/19,000-year signals (dashed line) on original records of site 607 $\delta^{18}O$, $\delta^{13}C$, SST, and percent $CaCO_3$ and of site 609 percent $CaCO_3$ for the late Pleistocene (1.0-0 Ma).

SST, $\delta^{13}C$, and $CaCO_3$ signals lag $\delta^{18}O$ by between 30° (2000 years) and 52° (3300 years), as shown in Table 8. Before 0.9 Ma, there are very few intervals in which these parameters have strong precessional responses in common, and coherences are generally low.

Low-Frequency Responses

All five signals show substantial concentrations of power at very low frequencies. In Figure 18, we show signals derived from a low-pass filter that extracts power at all periods longer than 120,000 years, which is the low-frequency limit of the 100,000-year filter. This long-wavelength power reflects several different trends in the data, all of which reflect a degree of nonstationarity.

Part of the low-frequency power reflects changes in the mean values of these signals toward more "glacial" conditions (heavier $\delta^{18}O$, lighter $\delta^{13}C$, lower $CaCO_3$, and colder SST). Although each record is somewhat different, the major part of this shift appears to be centered on 0.9 to 0.7 Ma, close to the level determined by Prell [1982] and Maasch [1988]. This is the most prominent low-frequency shift visible in the $\delta^{18}O$ record.

A second kind of low-frequency trend that is prominent in

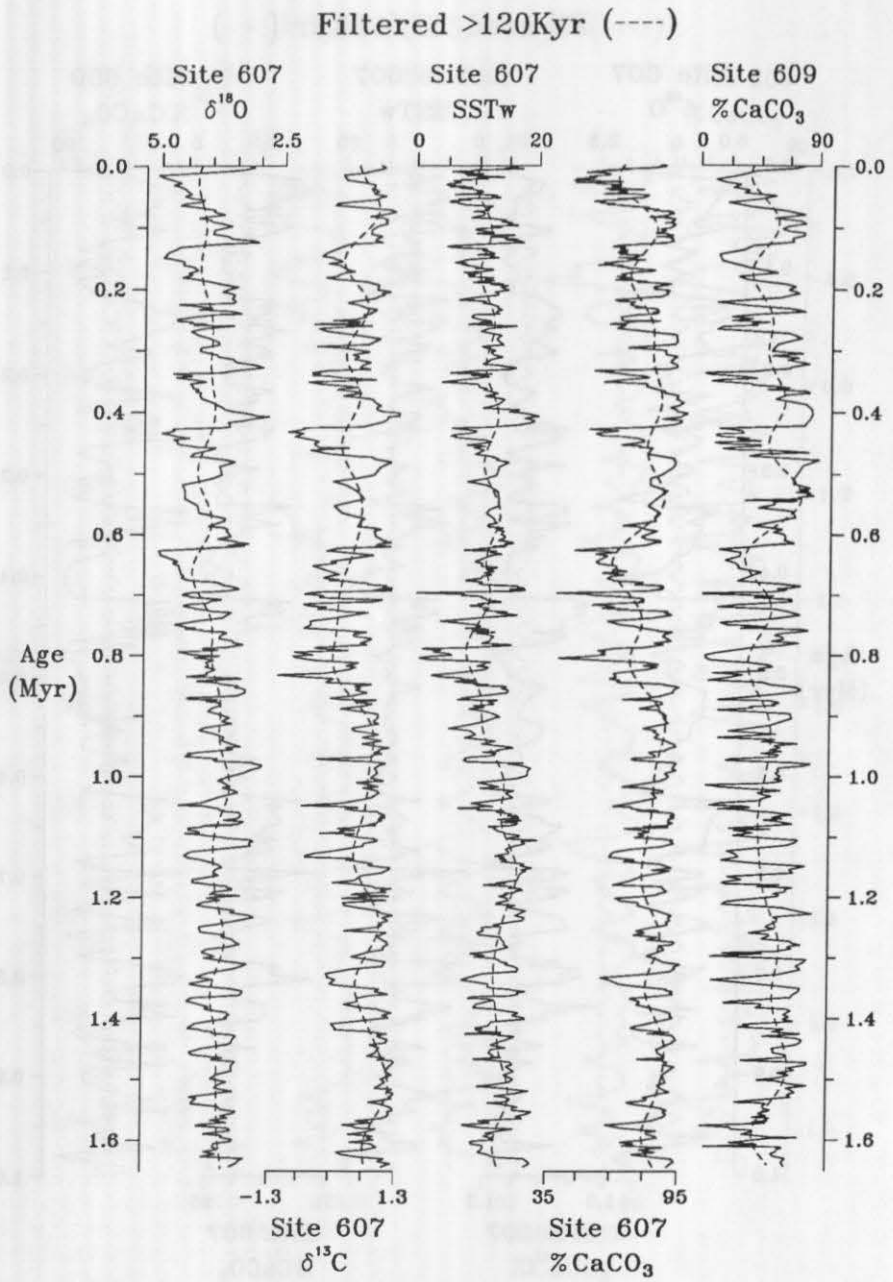

Fig. 18. Overlays of filtered low-frequency (>120,000-year) signals (dashed line) on original records (solid line) of site 607 $\delta^{18}O$, $\delta^{13}C$, SST, and percent $CaCO_3$ and of site 609 percent $CaCO_3$ for the last 1.65 m.y. The filter has a central frequency of 0.004 cycles/kyr and bandwidth 0-0.008 cycles/kyr.

the $\delta^{13}C$, percent $CaCO_3$, and SST records at site 607 is a distinctive interval between 0.9 and 0.6 Ma during which unusually high-amplitude variations occur at orbital periods and create the strongest glacial maxima during the entire Pleistocene. This pattern is different from most $\delta^{18}O$ curves, which register the largest fluctuations and strongest glaciations at and after 0.6 Ma, not in the middle Pleistocene.

Some records also show pseudoperiodic behavior at wavelengths of about 200,000 to 500,000 years (Figure 18), and these are not strongly concentrated at the 413,000-year period of orbital eccentricity (Figure 13). The $\delta^{13}C$ and percent $CaCO_3$ spectra have variance minima at 413,000 years, while SST and $\delta^{18}O$ spectra have small maxima (Figure 13).

Finally, the low-frequency oscillation toward warm SST values near 1.25-1.1 Ma is an artifact of the absence of the species *N. pachyderma* (sinistral-coiling), the polar end-member foraminifer [Ruddiman et al., 1986a, c]. It is unclear whether this reflects climatic change or evolutionary effects.

TABLE 8. Phasing and Coherence of Site 607 and 609 Climatic Signals Versus Orbital Signals

Orbital Signal	Interval, Ma	Site 607 $\delta^{18}O$*	Site 607 $\delta^{13}C$	Site 607 % $CaCO_3$	Site 607 SST	Site 609 % $CaCO_3$
Obliquity	0-0.734	73°/0.83	84°/0.86	93°/0.85	75°/0.60	94°/0.91
	0.734-1.65	72°/0.96	78°/0.87	71°/0.92	68°/0.90	70°/0.94
	0-1.65	72°/0.90	81°/0.92	80°/0.90	70°/0.83	80°/0.90
Precession	0-0.734	93°/0.87	128°/0.79	123°/0.69	145°/0.66	144°/0.65
Eccentricity	0-0.734	0°/0.88	5°/0.61	34°/0.60	14°/0.42	20°0.52

All phases (number before slash) are expressed as phase angle lags behind orbital forcing, with orbital signal phasing defined using the same convention as Imbrie et al. [1984]. All coherences (number after slash) are expressed as coherency squared.

*Phase of $\delta^{18}O$ obliquity and precession signals set by tuning to orbital forcing as explained in text. All other phases and all coherences are derived from resulting time scale.

The mid-Pleistocene transition is thus a complex phenomenon; its timing varies according to how it is defined and which record is examined (Figures 14-18). Some of the mid-Pleistocene changes noted above occur as early as 1.1 Ma, and others as late as 0.4 Ma. The most striking changes in different parameters vary widely in timing: 0.9 to 0.8 Ma for changes in the mean of most signals; 0.9 to 0.6 Ma for the distinctive low-frequency wave in $\delta^{13}C$, percent $CaCO_3$, and SST; 0.8 to 0.7 Ma for increases in power in the precessional band; 0.8 to 0.6 Ma for the fastest decrease of 41,000-year power; and 0.7 to 0.6 Ma for the fastest emergence of 100-000-year power. The full transition is thus spread over as much as 700,000 years, and even the fastest changes occur over an interval of at least 200,000 years.

DISCUSSION

We explore the origin of this complicated mid-Pleistocene evolution of climate in three stages. First, we review internal linkages within the climate system, in order to reduce the complexities in five different signals from four different climate proxies (Figures 14-18) into a smaller number of key variables. Second, we address the contribution that orbital forcing makes to these signals. Finally, we examine the low-frequency signal components that cannot be explained by orbital forcing.

Internal Linkages Within the Climate System

Several of the climate-recording parameters have relatively clear linkages within the climate system. Changes in northern hemisphere (particularly North American) ice volume dominate the $\delta^{18}O$ trends, and general circulation modeling experiments show that ice in North America affects North Atlantic SST and sea ice extent by altering surface winds over the ocean [Manabe and Broccoli, 1985; Broccoli and Manabe, 1987]. These ice sheet effects on the North Atlantic also impact the productivity of foraminifera and coccoliths in surface waters and thus the $CaCO_3$ content of the sediments, as does continental sediment rafted from the ice sheets to the ocean via icebergs [Ruddiman, 1977]. These proposed ice sheet/ocean linkages are all consistent with data summarized in Tables 8 and 9: the highly coherent, in-phase behavior of $\delta^{18}O$, SST, and percent $CaCO_3$ at the dominant 41,000-year Matuyama rhythm; the highly coherent, nearly in-phase responses at the dominant 100,000-year Brunhes rhythm; and the roughly synchronous transitions between these two regimes in all three signals. Dissolution is also a factor in the $CaCO_3$ signal, but it may involve more complex response patterns less clearly linked to ice sheet forcing.

Northern hemisphere ice volume also exerts a significant control on the site 607 $\delta^{13}C$ variations by altering deep-ocean circulation. Because of the location and water depth of site 607, much of the $\delta^{13}C$ variability can be ascribed to changes in rate of formation of North Atlantic Deep Water (NADW), with a lesser effect due to changes in total carbon inventory in the ocean. Negative benthic foraminiferal $\delta^{13}C$ values in piston cores CHN82-24-4 and V30-97 during the isotopic stage 2, 4, and 6 glaciations have been attributed to suppression of NADW formation [Boyle and Keigwin, 1985]. Migrations of the North Atlantic polar front have been proposed as the major control on late Pleistocene deepwater variability [Mix and Fairbanks, 1985]. Because the $\delta^{18}O$, SST, and $\delta^{13}C$ signals are highly coherent and in phase at both the 41,000-year and 100,000-year rhythms during the Pleistocene (Table 9), it appears that variations in ice volume have largely driven changes in SST and in sea ice extent and that these surface-ocean changes have in turn had a major impact on NADW formation [Keffer et al., 1988]. These linkages within the climate system have thus been strong for the last 1.6 m.y., as well as earlier [Raymo et al., this issue].

Ice volume may also be a significant factor in the lower-amplitude changes in the orbital precession band. The coherent relationship between $\delta^{18}O$ and orbital precession during the Brunhes Chron indicates that ice volume is an important component of the precessional frequencies in the $\delta^{18}O$ signal [Imbrie et al., 1984], and we have shown similar, but weaker, trends during the upper portion of the Matuyama (Figure 7).

The precessional band connections between the ice sheets and the ocean are not, however, as clear as those for obliquity and eccentricity. The 3000-year lag of SST (minima) behind $\delta^{18}O$ (maxima) suggests that other factors override the immediate response of the surface ocean to ice volume, and both $\delta^{13}C$ (minima) and $CaCO_3$ (minima) also show substantial lags behind $\delta^{18}O$ (Table 8). One possibility is meltwater from the ice sheets, which would have a particularly strong precessional signal that would lag ice volume by a maximum of 1/4 wavelength or 5000 to 6000 years

TABLE 9. Coherences Among Site 607 and Site 609 Climatic Signals

	Site 607 $\delta^{18}O$	Site 607 $\delta^{13}C$	Site 607 % $CaCO_3$	Site 607 SST	Site 609 % $CaCO_3$
Site 607 $\delta^{18}O$		0.99/0.90/0.84	0.96/0.90/0.77	0.96/0.86/0.80	0.95/0.81/0.73
Site 607 $\delta^{13}C$			0.98/0.88/0.91	0.94/0.86/0.64	0.97/0.85/0.92
Site 607 $CaCO_3$			0.94/0.94/0.59	0.98/0.97/0.90	
Site 607 SST					0.91/0.95/0.64
Site 609 % $CaCO_3$					

All coherences are expressed as coherency squared. For each pair of parameters, three coherence values are shown separated by slashes. The left-hand value is coherence at the 41,000-year period of orbital obliquity during the last 1.65 m.y. (Brunhes plus upper Matuyama). The center value is coherence at the 100,000-year period of orbital eccentricity during the last 0.734 m.y. (Brunhes). The right-hand value is coherence at the 23,000-year period of orbital precession during the last 0.734 m.y. (Brunhes).

[Ruddiman and McIntyre, 1981]. Another possibility is that low-latitude insolation (monsoonal) forcing in part controls this SST response, perhaps in combination with the ice sheets. This might occur via (1) a spin-up of the North Atlantic subtropical gyre due to increased anticyclonic subsidence of air over the oceans as mass compensation for increased upward monsoonal motion over land [Kutzback and Guetter, 1984] and (2) effects of monsoon-modulated Mediterranean outflow on North Atlantic salinity and, perhaps, SST [Rossignol-Strick, 1983].

We conclude that much of the climatic information at the orbital periodicities in the five Pleistocene records can be ascribed directly to insolation-driven changes in ice sheets, especially in North America, and their subsequent impact on the adjacent ocean. Other responses, including the change in dominance of orbital rhythms and the low-frequency responses in $\delta^{13}C$, percent $CaCO_3$, and SST, cannot be explained by this kind of linkage.

Role of Orbital Forcing

Because obliquity provides the strongest orbital forcing at high latitudes [Milankovitch, 1941; Berger, 1978], it is the rhythm most likely to control high-latitude ice sheets, assuming that other forcing exists to initiate glaciation [Ruddiman and Raymo, 1988]. Thus, perhaps the least surprising result of this study is the dominance of a 41,000-year response in the Matuyama Chron, as well as the coherent 41,000-year responses in other climatic indicators ($\delta^{13}C$, percent $CaCO_3$, and SST) that are heavily impacted by ice sheet changes.

The long-term trend of orbital obliquity (Figure 19) shows relatively high-amplitude fluctuations early in the Pleistocene, followed by a slow decline to low-amplitude variations between about 0.9 and 0.65 Ma, and then some reemergence of power in the late Pleistocene. Because this trend is similar to the mid-Pleistocene decrease in 41,000-year power in the $\delta^{18}O$ (and other) signals (Figure 14), some of the mid-Pleistocene shift in orbital dominance may be related to a linear response of the climate system to the weaker obliquity forcing.

Other factors, however, suggest that the climate system lost sensitivity to obliquity forcing during the middle and late Pleistocene. The amplitude minima in all five climatic records (Figure 14) occur somewhat later than the orbital forcing, around 0.6 to 0.5 Ma, although this may be partly an artifact of the slow sedimentation rates in that part of both the site 607 and 609 records (Figure 10). More diagnostically, no record shows a return of the 41,000-year variations to the amplitudes attained during the Matuyama, whereas the orbital forcing does regain full amplitude (Figure 19). The system thus appears to have become less sensitive to obliquity forcing during the mid-Pleistocene and Brunhes.

The development of the 100,000-year signal is more enigmatic. Imbrie et al. [1984] found that tuning to orbital obliquity and precession yielded a 100,000-year $\delta^{18}O$ signal that was both coherent and in phase with eccentricity forcing, suggesting a linear response of the climate system to orbital eccentricity. Direct insolation forcing at this period is, however, too weak to explain the dominant Brunhes response; this suggests internal amplification of this signal within the climate system.

The kind of internal amplification remains unclear. Hypotheses that rely on nonlinear responses to precession, such as faster ablation than accumulation [e.g., Imbrie and Imbrie, 1980], also predict a strong response at the 413,000-year eccentricity period. Although it is difficult to test for 413,000-year power in the relatively brief interval during which the 100,000-year signal has been strong, there is no clear indication of such a trend in the low-frequency filter (Figure 18). This argues against this class of hypotheses.

This points toward hypotheses involving resonant interactions within the climate system, such as ice/bedrock interactions [e.g., Peltier, 1982] or interactions between the ice sheets and the deep ocean, which may involve changes in CO_2 levels [e.g., Saltzman, 1987]. It is unlikely that either of these alternatives can, by itself, explain the change from a 41,000-year to a 100,000-year regime during the mid-Pleistocene. Some additional change (probably tectonic) needs to be imposed to trigger different behavior in the key components of the climate system.

The mid-Pleistocene increase in precessional response of the $\delta^{18}O$ and other signals (Figures 16 and 17) is not explained by long-term trends in orbital forcing (Figure 19). It may be

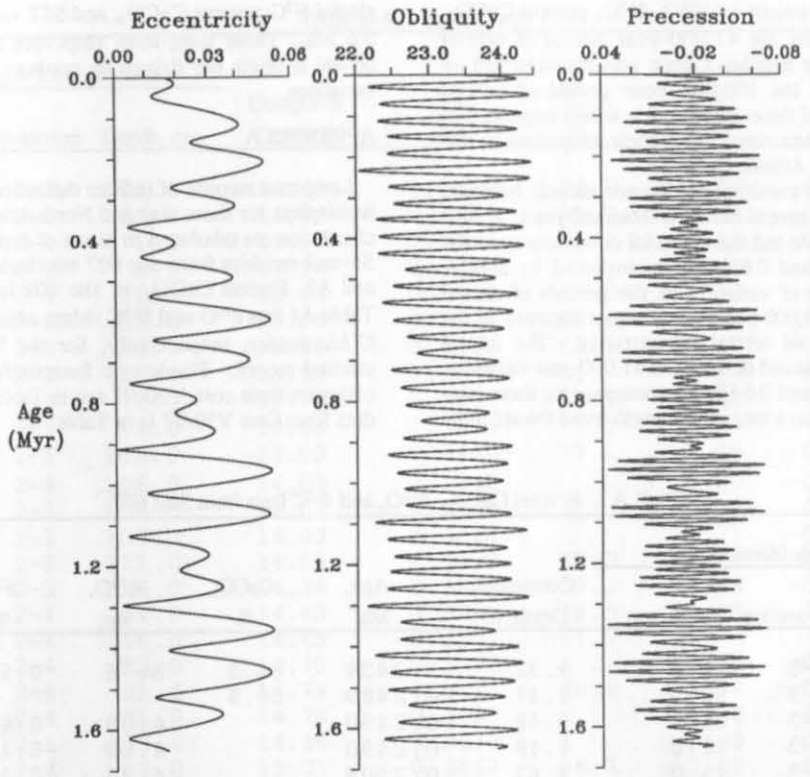

Fig. 19. Orbital eccentricity, obliquity, and precession (using the precessional index, e sin w) over the last 1.65 m.y. [from Berger, 1978].

linked to the onset of larger ice sheets, whose southern limits in North America and Europe must have extended farther into middle latitudes, and thus come under the influence of stronger precessional forcing [Ruddiman and McIntyre, 1981]. Or it might in some way reflect an increased sensitivity of ice sheets to precessional insolation heating of low- and mid-latitude land masses at latitudes south of the ice sheets [Kutzbach, 1981].

Non-orbital Climatic Change

Finally, there are components of these signals that are not explained by coherent responses to orbital forcing. We focus on the low-frequency components (Figure 18), but this category also includes that portion of signals concentrated at orbital periods but not coherent with the forcing. To some extent, these two categories are interrelated; for example, most of the low-frequency $\delta^{13}C$ and $CaCO_3$ signals during the Matuyama (Figure 18) appear to be due to changes in the amplitude of the glacial extremes of the 41,000-year oscillations. Thus, while the individual oscillations occur at orbital periods, part of the modulation of these oscillations is not explained by a linear model of orbital forcing.

To some extent, these signals may reflect imperfections in the climate monitors, raising the question of what portion of the signals is real. As noted earlier, the absence of the cold-water foraminifer *N. pachyderma* (sinistral) gives the SST curve a suspect warming trend between 1.25 and 1.1 Ma. For the $\delta^{18}O$ and $\delta^{13}C$ curves, the amplitude of a given glacial or interglacial oscillation depends critically on the presence of the analyzed species in abundances sufficient to avoid bioturbational dilution by individuals from adjoining levels.

The $CaCO_3$ curve, however, is less subject to such problems, and it is also in many ways very similar in appearance to the $\delta^{13}C$ curve (Figure 18). The fact that two such different monitors of the climate system experienced very similar changes supports the contention that this low-frequency signal is real, as does the more modest similarity to the SST signal, especially during the prominent shift toward more glacial values in the mid-Pleistocene (0.9-0.6 Ma).

As noted previously, the near absence of 413,000-year eccentricity power in these signals suggests that they are not orbital in origin. Because the site 607 $\delta^{18}O$ curve (like other $\delta^{18}O$ curves) shows little or no glacial long-wavelength anomaly in the mid-Pleistocene, the low-frequency $\delta^{13}C$, $CaCO_3$, and SST responses are probably not the result of ice sheet forcing. For this to be true, an anomalously large volume of ice in North America (needed to force the various North Atlantic responses) would have to be coincidentally offset by anomalously small volumes of ice elsewhere in the world, so that the $\delta^{18}O$ curve showed no long-wavelength anomaly between 0.9 and 0.6 Ma. This is unlikely.

The origin of these long-wavelength anomalies within certain parts of the climate system during the middle Pleistocene is uncertain. The fact that the most anomalous long-wavelength features in all three signals occur between 0.9 and 0.6 Ma during the mid-Pleistocene transition suggests that they may be in some way linked to the forcing that produced the transition in orbital power.

SUMMARY

The climatic response of the high latitudes of the northern hemisphere during the Matuyama Chron was characterized by

coherent, in-phase variations of $\delta^{18}O$, $\delta^{13}C$, percent $CaCO_3$, and SST dominated by the 41,000-year period of orbital obliquity. Most of the Brunhes Chron was characterized by similar variations at the 100,000-year period of orbital eccentricity. In each of these regimes, ice sheets responded to orbital forcing and then transferred their responses to the surface and deep North Atlantic Ocean.

The mid-Pleistocene transition in climatic records from site 607 was spread across several hundred thousand years. A shift toward higher-amplitude and more glacial conditions occurred mainly between 0.9 and 0.6 Ma, accompanied by a large increase in amplitude of variation at the periods of orbital precession (23,000/19,000 years) and some increase at the 100,000-year period of orbital eccentricity. The fastest increase in 100,000-year and decrease in 41,000-year variability occurred between 0.7 and 0.6 Ma. Accompanying these mid-Pleistocene changes was a long-wavelength trend toward more glacial $\delta^{13}C$, percent $CaCO_3$, and SST values between 0.9 and 0.6 Ma. These long-term responses appear to be neither orbital in origin nor driven by northern hemisphere ice sheet variations.

APPENDIX A

Long-term records of indices that reflect changes in northern hemisphere ice sheet size and North Atlantic surface and deep circulation are tabulated in terms of depth and estimated age. Several variables from site 607 are characterized in Tables A1 and A2. Percent $CaCO_3$ in site 609 is listed in Table A3. Table A4 lists $\delta^{18}O$ and $\delta^{13}C$ values adjusted to *Uvigerina* and *Cibicidoides*, respectively, for the V30-97/CHN82-24-4 stacked record. Planktonic foraminiferal counts and SST estimates from core V30-97 are in Table A5. Percent $CaCO_3$ data from Core V30-97 is in Table A6.

TABLE A1. Percent $CaCO_3$, $\delta^{18}O$, and $\delta^{13}C$ Data from Site 607

DSDP Sample Identification			Composite	Age,	$CaCO_3$,	$\delta^{18}O$,	$\delta^{13}C$,	Species
Hole	Core-section	Depth, cm	Depth, m	Ma*	%	‰	‰	Code†
607A	2-3	45.5	9.32	0.2454	66.3	3.76	0.62	C
607A	2-3	60.5	9.47	0.2489	66.9			
607A	2-3	61.0	9.48	0.2490		4.08	0.63	C
607A	2-3	61.0	9.48	0.2490		4.69	-0.75	U
607A	2-3	75.0	9.62	0.2508		4.70	-0.93	U
607A	2-3	75.5	9.63	0.2509	66.5			
607A	2-3	90.5	9.77	0.2520	83.7			
607A	2-3	91.0	9.78	0.2520		4.10	0.81	C
607A	2-3	91.0	9.78	0.2520		4.53	-0.70	U
607A	2-3	105.0	9.92	0.2530		4.44	-0.62	U
607A	2-3	105.5	9.93	0.2530	71.0			
607A	2-3	120.5	10.07	0.2541	69.9			
607A	2-3	121.0	10.08	0.2541		3.69	0.64	C
607A	2-3	121.0	10.08	0.2541		4.43	-0.53	U
607A	2-3	135.5	10.22	0.2551	69.4	3.94	0.65	C
607A	2-3	135.0	10.22	0.2551		4.37	-0.61	U
607A	2-4	0.5	10.38	0.2564	61.5	4.21	-0.92	U
607A	2-4	1.0	10.38	0.2564		3.39	-0.75	C
607	2-1	55.0	10.52	0.2585	68.6	3.94	0.71	C
607	2-1	55.0	10.52	0.2585		3.83	0.19	C
607	2-1	55.0	10.52	0.2585		3.48	0.08	C
607	2-1	61.0	10.59	0.2595		2.91	0.74	C
607	2-1	78.0	10.76	0.2637	64.7	3.50	-0.30	C
607	2-1	91.0	10.89	0.2684		3.79	-0.15	C
607	2-1	106.0	11.03	0.2745	90.8	3.65	0.44	C
607	2-1	121.0	11.18	0.2805		3.39	0.91	C
607	2-1	136.0	11.34	0.2861	91.2	3.22	0.77	C
607	2-2	1.0	11.48	0.2898	90.1	3.28	0.62	C
607	2-2	1.0	11.48	0.2898		3.13	0.73	C
607	2-2	16.0	11.63	0.2925	79.4	3.36	-0.32	C
607	2-2	16.0	11.63	0.2925		3.34	-0.33	C
607	2-2	31.0	11.78	0.2951	69.7	4.29	-0.75	U
607	2-2	31.0	11.78	0.2951		4.14	-0.79	U
607	2-2	53.0	12.01	0.2998	86.2	3.46	0.53	C
607	2-2	53.0	12.01	0.2998		3.76	0.55	C
607	2-2	61.0	12.09	0.3019	86.3	3.55	0.69	C
607	2-2	78.0	12.26	0.3064	86.2	3.26	0.36	C
607	2-2	91.0	12.38	0.3096	91.3	3.24	0.49	C
607	2-2	106.0	12.53	0.3139	89.4	2.93	0.39	C

TABLE A1. (continued)

DSDP Sample Identification			Composite	Age,	$CaCO_3$,	$\delta^{18}O$,	$\delta^{13}C$,	Species
Hole	Core-section	Depth, cm	Depth, m	Ma*	%	‰	‰	Code†
607	2-2	121.0	12.68	0.3187	88.2	2.87	0.72	C
607	2-2	136.0	12.84	0.3235	91.2	2.45	0.56	C
607	2-3	1.0	12.98	0.3276	91.1	2.13	0.35	C
607	2-3	1.0	12.98	0.3276		2.46	0.68	C
607	2-3	16.0	13.13	0.3301	88.3	2.60	0.71	C
607	2-3	31.0	13.28	0.3324	54.6	2.89	-0.12	C
607	2-3	53.0	13.51	0.3360	63.1	3.17	-0.43	C
607	2-3	61.0	13.59	0.3374	66.7	4.13	-0.27	C
607	2-3	78.0	13.76	0.3397	70.6	3.88	-0.43	C
607	2-3	91.0	13.88	0.3414	77.1			
607	2-3	106.0	14.03	0.3440	79.1	4.08	0.08	C
607	2-3	106.0	14.03	0.3440		4.00	-0.07	C
607	2-3	106.0	14.03	0.3440		4.12	0.09	C
607	2-3	106.0	14.03	0.3440		4.71	-0.44	U
607	2-3	121.0	14.18	0.3472	68.3	3.73	0.83	C
607	2-3	136.0	14.34	0.3506	59.2	3.48	-0.49	C
607	2-4	1.0	14.48	0.3541	78.5	3.80	-0.28	C
607	2-4	16.0	14.63	0.3577	77.7			
607	2-4	23.0	14.70	0.3593		4.39	-0.42	U
607	2-4	31.0	14.78	0.3613	80.8	3.88	0.09	C
607	2-4	31.0	14.78	0.3613		4.26	-0.59	U
607	2-4	39.0	14.86	0.3633		3.63	0.06	C
607	2-4	53.0	15.01	0.3668	86.1	3.80	0.20	C
607	2-4	53.0	15.01	0.3668		4.24	-0.28	U
607	2-4	61.0	15.09	0.3688	85.7	3.58	0.54	C
607	2-4	78.0	15.26	0.3734	91.9	3.59	0.24	C
607	2-4	78.0	15.26	0.3734		4.27	-0.77	U
607	2-4	91.0	15.38	0.3787	91.1	4.07	-0.21	U
607	2-4	91.0	15.38	0.3787		3.68	0.82	C
607	2-4	106.0	15.53	0.3855	94.5	3.96	-0.07	U
607	2-4	121.0	15.68	0.3892	92.3	3.88	0.02	U
607	2-4	136.0	15.84	0.3927	88.5	3.14	0.84	C
607	2-5	1.0	15.98	0.3960	91.0	3.77	-0.06	U
607	2-5	1.0	15.98	0.3960		3.08	0.85	C
607	2-5	16.0	16.14	0.3993	91.4	3.04	0.85	C
607	2-5	16.0	16.14	0.3993		2.81	1.08	C
607	2-5	23.0	16.20	0.4007		2.82	1.22	C
607	2-5	23.0	16.20	0.4007		2.72	1.24	C
607	2-5	31.0	16.28	0.4022	96.4	2.65	1.30	C
607	2-5	53.0	16.50	0.4061	93.7	2.40	1.29	C
607	2-5	61.0	16.58	0.4076	93.7	2.17	1.06	C
607	2-5	78.0	16.75	0.4111	85.0	2.54	1.05	C
607	2-5	91.0	16.89	0.4138	93.5	2.69	1.01	C
607	2-5	106.0	17.03	0.4167	93.5	3.03	0.93	C
607	2-5	121.0	17.18	0.4204	90.3	3.00	0.73	C
607	2-5	136.0	17.33	0.4237	80.4	2.99	0.56	C
607	2-5	143.0	17.40	0.4252		3.17	-0.61	C
607	2-6	1.0	17.48	0.4270	52.7	4.13	-0.56	C
607	2-6	7.5	17.55	0.4284	55.8			
607	2-6	16.0	17.64	0.4303	65.8	4.10	-0.76	C
607	2-6	23.0	17.70	0.4319		4.18	-0.92	C
607	2-6	31.0	17.78	0.4342	55.6	4.96	-1.49	U
607	2-6	53.0	18.00	0.4380	58.3			
607	2-6	61.0	18.08	0.4394	67.5	4.06	-0.77	C
607	2-6	78.0	18.25	0.4422	74.6	3.81	-0.58	C
607	2-6	91.0	18.39	0.4447	76.8	4.12	-0.42	C
607	2-6	106.0	18.53	0.4476	77.4	4.04	-0.28	C

TABLE A1. (continued)

DSDP Sample Identification			Composite	Age,	$CaCO_3$,	$\delta^{18}O$,	$\delta^{13}C$,	Species
Hole	Core-section	Depth, cm	Depth, m	Ma*	%	‰	‰	Code†
607	2-6	121.0	18.68	0.4505	71.6	4.05	-0.38	C
607	2-6	136.0	18.83	0.4526	67.2	3.99	-0.36	C
607	2-7	1.0	18.98	0.4546	75.9			
607	2-7	16.0	19.14	0.4566	75.1	3.63	-0.28	C
607	2-7	24.0	19.22	0.4576	81.0	3.63	0.00	U
607	3-2	78.0	19.22	0.4576		3.56	-0.29	C
607	3-2	91.0	19.34	0.4612	80.1	3.39	-0.45	C
607	3-2	106.0	19.49	0.4676	79.0	4.37	-0.98	U
607	3-2	119.0	19.63	0.4723		4.43	-0.31	U
607	3-2	121.0	19.65	0.4726	86.5	4.20	-0.15	U
607	3-2	136.0	19.80	0.4747	90.3	4.01	-0.05	U
607	3-2	136.0	19.80	0.4747		4.01	-0.09	U
607	3-2	136.0	19.80	0.4747		3.30	0.72	C
607	3-3	1.0	19.94	0.4768	90.2	3.76	-0.04	U
607	3-3	16.0	20.09	0.4807	91.0	3.52	0.24	U
607	3-3	31.0	20.24	0.4880	90.4	3.81	0.07	U
607	3-3	31.0	20.24	0.4880		3.20	0.92	C
607	3-3	53.0	20.47	0.5017	85.0	3.79	-0.10	U
607	3-3	61.0	20.55	0.5075	80.3	3.41	0.70	C
607	3-3	61.0	20.55	0.5075		3.88	-0.69	U
607	3-3	68.0	20.61	0.5121		4.24	-0.91	U
607	3-3	78.0	20.72	0.5180	80.1	4.58	-0.66	U
607	3-3	91.0	20.84	0.5277	87.6	4.53	-0.44	U
607	3-3	106.0	20.99	0.5411	82.8	3.78	0.74	C
607	3-3	106.0	20.99	0.5411		4.63	-0.43	U
607	3-3	121.0	21.15	0.5521	79.3	3.43	-0.07	C
607	3-3	121.0	21.15	0.5521		4.50	-0.79	U
607	3-3	136.0	21.30	0.5644	84.6	3.61	0.17	C
607	3-4	1.0	21.44	0.5735	82.1	2.76	0.83	C
607	3-4	16.0	21.59	0.5775	82.8	3.09	0.53	C
607	3-4	31.0	21.74	0.5803	77.3	3.20	0.53	C
607	3-4	53.0	21.97	0.5847	68.3			
607	3-4	61.0	22.05	0.5862	74.7	4.38	-0.48	U
607	3-4	61.0	22.05	0.5862		3.10	0.54	C
607	3-4	69.0	22.13	0.5887		3.17	0.68	C
607	3-4	69.0	22.13	0.5887		3.02	0.87	C
607	3-4	78.0	22.22	0.5914	78.8	3.02	0.94	C
607	3-4	91.0	22.34	0.5939	83.4	2.89	0.85	C
607	4-1	31.0	22.34	0.5939		3.21	0.77	C
607	4-1	53.0	22.55	0.6034	76.4	2.96	0.84	C
607	4-1	61.0	22.63	0.6074		3.22	0.94	C
607	4-1	62.5	22.64	0.6077	79.0			
607	4-1	70.0	22.72	0.6093		3.04	0.97	C
607	4-1	78.0	22.80	0.6103	84.4	2.95	1.04	C
607	4-1	91.0	22.93	0.6119		2.84	1.02	C
607	4-1	92.5	22.94	0.6121	85.0			
607	4-1	98.0	23.00	0.6128		2.88	1.14	C
607	4-1	106.0	23.08	0.6137	81.9			
607	4-1	121.0	23.23	0.6155		2.49	0.66	C
607	4-1	122.5	23.24	0.6156	80.5			
607	4-1	136.0	23.38	0.6163	79.3			
607	4-2	3.5	23.55	0.6172	78.9			
607	4-2	16.0	23.68	0.6180	77.7	3.02	0.85	C
607	4-2	31.0	23.83	0.6188		2.67	0.95	C
607	4-2	32.5	23.84	0.6189	73.9			
607	4-2	53.0	24.05	0.6201	72.7	2.81	1.13	C
607	4-2	61.0	24.13	0.6207		2.99	0.83	C

TABLE A1. (continued)

DSDP Sample Identification			Composite	Age,	$CaCO_3$,	$\delta^{18}O$,	$\delta^{13}C$,	Species
Hole	Core-section	Depth, cm	Depth, m	Ma*	%	‰	‰	Code†
607	4-2	62.5	24.14	0.6208	69.6			
607	4-2	78.0	24.30	0.6219	63.4	3.35	0.19	C
607	4-2	91.0	24.43	0.6229		3.44	0.08	C
607	4-2	92.5	24.44	0.6230	55.1			
607	4-2	106.0	24.58	0.6242	52.7			
607	4-2	122.5	24.74	0.6256	46.5			
607	4-2	136.0	24.88	0.6267	58.5	5.20	-1.18	U
607	4-2	136.0	24.88	0.6267		4.17	0.03	C
607	4-3	3.5	25.06	0.6298	65.0			
607	4-3	16.0	25.18	0.6320	56.0			
607	4-3	31.0	25.33	0.6346		4.34	0.80	C
607	4-3	32.5	25.34	0.6353	61.5			
607	4-3	53.0	25.55	0.6445	56.3	4.03	-0.04	C
607	4-3	61.0	25.63	0.6476		4.81	-0.66	U
607	4-3	61.0	25.63	0.6476		4.07	-0.10	C
607	4-3	63.5	25.65	0.6482	57.5			
607	4-3	78.0	25.80	0.6517	65.0	4.01	-0.39	C
607	4-3	93.5	25.95	0.6548	65.7			
607	4-3	106.0	26.08	0.6573	64.3			
607	4-3	122.5	26.24	0.6606	70.2			
607	4-3	136.0	26.38	0.6633	59.2			
607	4-4	1.0	26.53	0.6663		3.96	0.13	C
607	4-4	3.5	26.56	0.6667	69.1			
607	4-4	16.0	26.68	0.6691	63.1	3.91	-0.09	C
607	4-4	31.0	26.83	0.6719		3.95	-0.17	C
607	4-4	33.5	26.85	0.6723	61.3			
607	4-4	53.0	27.05	0.6750	63.7	4.51	-0.77	U
607	4-4	61.0	27.13	0.6758		4.44	-0.98	U
607	4-4	63.5	27.15	0.6760	64.2			
607	4-4	78.0	27.30	0.6774	70.3			
607	4-4	91.0	27.43	0.6788		3.29	0.43	C
607	4-4	92.5	27.44	0.6790	77.3			
607	4-4	106.0	27.58	0.6805	75.1	3.20	0.68	C
607	4-4	119.5	27.72	0.6822	73.7			
607	4-4	121.0	27.73	0.6824		3.14	0.69	C
607	4-4	136.0	27.88	0.6844	85.6	3.08	1.05	C
607	4-5	1.0	28.03	0.6864		2.92	0.98	C
607	4-5	3.5	28.06	0.6867	86.5			
607	4-5	16.0	28.18	0.6884	84.8	2.83	1.19	C
607	4-5	29.5	28.31	0.6899	86.1			
607	4-5	31.0	28.33	0.6900		2.78	0.92	C
607	4-5	53.0	28.55	0.6921	80.7	2.95	0.80	C
607	4-5	59.5	28.61	0.6927	80.7			
607	4-5	61.0	28.63	0.6928		3.00	1.17	C
607	4-5	78.0	28.80	0.6946	63.6	3.93	-1.11	U
607	4-5	89.5	28.91	0.6961	38.5			
607	4-5	91.0	28.93	0.6963		4.38	-1.31	U
607	4-5	106.0	29.08	0.6982	52.0	4.53	-1.45	U
607	4-5	120.5	29.22	0.7002	55.4			
607	4-5	121.0	29.23	0.7002		4.57	-1.11	U
607	4-5	121.0	29.23	0.7002		3.93	-0.29	C
607	4-5	136.0	29.38	0.7021	66.2	4.44	-1.07	U
607	4-6	1.0	29.53	0.7039		4.42	-1.16	U
607	4-6	3.5	29.55	0.7042	72.9			
607	4-6	16.0	29.68	0.7058	77.5	4.05	-0.63	U
607	4-6	29.5	29.81	0.7076	77.7			
607	4-6	31.0	29.83	0.7078		2.98	0.93	C

TABLE A1. (continued)

DSDP Sample Identification			Composite	Age,	$CaCO_3$,	$\delta^{18}O$,	$\delta^{13}C$,	Species
Hole	Core-section	Depth, cm	Depth, m	Ma*	%	‰	‰	Code†
607	4-6	53.0	30.05	0.7108	75.6	3.38	0.82	C
607	4-6	59.5	30.11	0.7116	77.8			
607	4-6	61.0	30.13	0.7118		4.16	-1.00	U
607	4-6	61.0	30.13	0.7118		3.26	0.86	C
607	4-6	78.0	30.30	0.7137	63.6	4.51	-1.47	U
607	4-6	78.0	30.30	0.7137		3.02	-0.27	C
607	4-6	91.0	30.43	0.7153		4.47	-1.27	U
607	4-6	91.0	30.43	0.7153		3.72	-0.77	C
607	4-6	92.5	30.44	0.7154	54.7			
607	4-6	106.0	30.58	0.7170	60.5	4.55	-1.40	U
607	4-6	119.5	30.72	0.7182	61.7			
607	4-6	121.0	30.73	0.7183		4.53	-1.27	U
607	4-6	136.0	30.88	0.7195	64.8	4.48	-1.01	U
607	4-7	1.0	31.03	0.7209		4.37	-1.14	U
607	4-7	5.5	31.07	0.7214	59.2			
607	4-7	16.0	31.18	0.7226	71.0	4.32	-1.19	U
607	4-7	24.0	31.26	0.7236	65.7	4.20	-0.91	U
607A	5-4	121.0	31.42	0.7254	81.7			
607A	5-4	135.0	31.56	0.7270	88.2	3.32	0.26	C
607A	5-5	1.0	31.72	0.7289	86.9	2.94	0.70	C
607A	5-5	15.0	31.86	0.7330	89.8			
607A	5-5	31.0	32.02	0.7377	81.8	3.16	-0.08	C
607A	5-5	31.0	32.02	0.7377		3.06	0.23	C
607A	5-5	45.0	32.16	0.7429	61.7	3.64	-0.43	C
607A	5-5	61.0	32.32	0.7488	67.4	4.14	-0.63	C
607A	5-5	61.0	32.32	0.7488		4.66	-1.10	U
607A	5-5	75.0	32.46	0.7512	73.7			
607	5-1	16.0	32.62	0.7538	75.9	3.83	-0.54	C
607	5-1	22.0	32.68	0.7545		3.68	-0.56	C
607	5-1	29.5	32.76	0.7554	79.1			
607	5-1	31.0	32.77	0.7556		3.88	-0.25	C
607	5-1	53.0	32.99	0.7581	84.3	3.52	0.25	C
607	5-1	61.0	33.07	0.7590	83.7	3.55	0.34	C
607	5-1	61.5	33.08	0.7590	83.7			
607	5-1	78.0	33.24	0.7609	90.1	3.10	0.67	C
607	5-1	89.5	33.35	0.7623	89.2			
607	5-1	93.0	33.39	0.7627		3.03	0.55	C
607	5-1	106.0	33.52	0.7649	86.8	3.10	0.41	C
607	5-1	117.5	33.63	0.7676	86.3			
607	5-1	119.0	33.65	0.7679	86.0	3.17	0.43	C
607	5-1	136.0	33.82	0.7719		3.19	0.77	C
607	5-1	138.5	33.84	0.7725	88.2			
607	5-2	1.0	33.97	0.7755		2.92	0.69	C
607	5-2	3.5	33.99	0.7760	89.7			
607	5-2	16.0	34.12	0.7789	82.4	3.63	-0.29	U
607	5-2	16.0	34.12	0.7789		2.80	0.48	C
607	5-2	30.5	34.26	0.7819	86.5			
607	5-2	31.0	34.27	0.7820		2.69	0.68	C
607	5-2	53.0	34.49	0.7862	77.4	3.03	-0.34	C
607	5-2	58.5	34.54	0.7873	66.7			
607	5-2	61.0	34.57	0.7878		3.58	-0.39	C
607	5-2	78.0	34.74	0.7912	57.3	3.21	0.31	C
607	5-2	89.5	34.85	0.7935	60.7			
607	5-2	91.0	34.87	0.7938		4.64	-1.65	U
607	5-2	106.0	35.02	0.7963	58.8			
607	5-2	119.5	35.15	0.7986	60.8			
607	5-2	121.0	35.17	0.7988		3.76	-0.37	C
607	5-2	136.0	35.32	0.8012	51.8			

TABLE A1. (continued)

DSDP Sample Identification			Composite	Age,	$CaCO_3$,	$\delta^{18}O$,	$\delta^{13}C$,	Species
Hole	Core-section	Depth, cm	Depth, m	Ma*	%	‰	‰	Code†
607	5-3	1.0	35.47	0.8035		3.70	-0.71	C
607	5-3	3.5	35.49	0.8039	39.4			
607	5-3	16.0	35.62	0.8058	49.1			
607	5-3	29.5	35.76	0.8078	59.1			
607	5-3	31.0	35.77	0.8080		3.29	-0.31	C
607	5-3	53.0	35.99	0.8106	76.6			
607	5-3	58.5	36.04	0.8113	79.1			
607	5-3	61.0	36.07	0.8116	79.1	3.46	0.51	C
607	5-3	78.0	36.24	0.8142	84.3			
607	5-3	92.5	36.38	0.8165	77.6			
607	5-3	93.0	36.39	0.8166		3.40	0.27	C
607	5-3	106.0	36.52	0.8187	83.8	3.47	0.46	C
607	5-3	119.5	36.65	0.8223	80.2			
607	5-3	121.0	36.67	0.8227		3.26	0.33	C
607	5-3	136.0	36.82	0.8290	64.6	3.45	-0.16	C
607	5-3	143.0	36.89	0.8320		3.42	-1.12	C
607	5-4	1.0	36.97	0.8352		4.48	-1.47	U
607	5-4	3.5	36.99	0.8357	65.6			
607	5-4	16.0	37.12	0.8382	62.7			
607	5-4	29.5	37.26	0.8409	67.4			
607	5-4	37.0	37.33	0.8424		3.61	0.05	C
607	5-4	37.0	37.33	0.8424		4.32	-1.10	U
607	5-4	53.0	37.49	0.8443	66.0	3.35	-0.12	C
607	5-4	59.0	37.55	0.8450	73.3			
607	5-4	59.5	37.56	0.8451	76.4			
607	5-4	68.0	37.64	0.8461		3.18	0.38	C
607	5-4	78.0	37.74	0.8473	86.9	3.18	0.79	C
607	5-4	78.0	37.74	0.8473		3.15	0.76	C
607	5-4	89.5	37.85	0.8487	87.4			
607	5-4	106.0	38.02	0.8507	91.5	2.78	0.45	C
607	5-4	119.5	38.15	0.8523	93.3			
607	5-4	121.0	38.17	0.8525		2.87	0.49	C
607	5-4	122.5	38.18	0.8526	93.2			
607	5-4	131.0	38.27	0.8537	92.2	2.74	0.57	C
607	5-5	3.0	38.49	0.8570	91.1	2.64	0.46	C
607	5-5	16.0	38.62	0.8615	90.6	2.57	0.54	C
607	5-5	16.0	38.62	0.8615		2.73	0.84	C
607	5-5	29.0	38.75	0.8671	85.3	2.82	0.37	C
607	5-5	37.0	38.83	0.8705	79.7	4.48	-0.93	U
607	5-5	53.0	38.99	0.8727	68.8	4.42	-0.70	U
607	5-5	61.0	39.07	0.8738	81.1	3.21	0.87	C
607	5-5	78.0	39.24	0.8762	85.3	4.09	-0.42	U
607	5-5	91.0	39.37	0.8781	86.3	3.84	-0.32	U
607	5-5	106.0	39.52	0.8802	86.1	3.74	-0.17	U
607	5-5	106.0	39.52	0.8802		3.24	0.85	C
607	5-5	119.0	39.65	0.8828	83.1	3.18	0.54	C
607	5-5	119.0	39.65	0.8828		3.11	0.80	C
607	5-5	136.0	39.82	0.8876	76.2	4.04	-0.68	U
607	5-5	136.0	39.82	0.8876		3.27	0.14	C
607	5-5	144.5	39.90	0.8903	85.5			
607	5-6	1.0	39.97	0.8924		3.31	0.51	C
607	5-6	1.0	39.97	0.8924		4.14	-0.27	U
607	5-6	3.5	39.99	0.8931	84.8			
607	5-6	16.0	40.12	0.8967	87.4	3.23	0.91	C
607	5-6	29.5	40.25	0.9009	87.9			
607	5-6	36.0	40.32	0.9029		2.97	0.91	C
607	5-6	53.0	40.49	0.9092	87.9	3.13	0.82	C

TABLE A1. (continued)

DSDP Sample Identification			Composite	Age,	$CaCO_3$,	$\delta^{18}O$,	$\delta^{13}C$,	Species
Hole	Core-section	Depth, cm	Depth, m	Ma*	%	‰	‰	Code†
607	5-6	58.5	40.54	0.9115	89.1			
607	5-6	61.0	40.57	0.9126		2.92	0.93	C
607	5-6	78.0	40.74	0.9198	77.9	3.48	0.40	C
607	5-6	88.0	40.84	0.9237	83.9	3.58	0.44	C
607	5-6	90.5	40.86	0.9246	82.1			
607	5-6	106.0	41.02	0.9301	84.9	3.26	0.93	C
607	5-6	120.5	41.17	0.9352	82.8	3.08	0.61	C
607	5-6	136.0	41.32	0.9406	87.9	3.77	0.09	U
607	5-7	1.0	41.47	0.9457		2.95	0.61	C
607	5-7	3.5	41.49	0.9465	91.7			
607	5-7	16.0	41.62	0.9505	92.0	2.74	0.99	C
607	5-7	21.0	41.67	0.9520	89.9	3.04	1.13	C
607A	6-4	121.0	41.83	0.9552	88.0	2.90	0.94	C
607A	6-4	135.0	41.97	0.9568	87.6	3.13	0.95	C
607A	6-5	1.0	42.13	0.9585	80.8			
607A	6-5	15.0	42.26	0.9601	80.9	3.74	0.83	C
607A	6-5	15.0	42.26	0.9601		3.49	0.84	C
607A	6-5	21.0	42.33	0.9607		3.64	0.95	C
607A	6-5	31.0	42.42	0.9618	82.2	3.82	1.00	C
607A	6-5	45.0	42.56	0.9634	82.8	3.80	0.91	C
607A	6-5	45.0	42.56	0.9634		3.69	0.78	C
607A	6-5	61.0	42.72	0.9653	83.2			
607A	6-5	75.0	42.86	0.9670	83.7	3.87	0.78	C
607A	6-5	91.0	43.02	0.9688	74.0			
607	6-1	16.0	43.17	0.9705	72.9			
607	6-1	32.5	43.33	0.9724	74.7			
607	6-1	53.0	43.54	0.9747	85.2	3.24	0.76	C
607	6-1	63.5	43.65	0.9759	90.8			
607	6-1	70.0	43.71	0.9766		3.22	0.08	U
607	6-1	70.0	43.71	0.9766		2.42	1.03	C
607	6-1	78.0	43.79	0.9777	92.4	2.53	1.08	C
607	6-1	78.0	43.79	0.9777		3.12	0.14	U
607	6-1	92.5	43.93	0.9817	91.4			
607	6-1	106.0	44.07	0.9855	90.8			
607	6-1	118.5	44.19	0.9889	92.3			
607	6-1	136.0	44.37	0.9937	87.6			
607	6-2	4.5	44.56	0.9988	89.2			
607	6-2	16.0	44.67	1.0020	88.4	3.05	0.77	C
607	6-2	30.5	44.81	1.0066	85.4			
607	6-2	39.0	44.90	1.0090		3.11	0.50	C
607	6-2	53.0	45.04	1.0159	68.8	3.59	0.03	U
607	6-2	55.5	45.06	1.0166	72.7			
607	6-2	59.5	45.10	1.0176	77.9			
607	6-2	78.0	45.29	1.0224	86.8			
607	6-2	87.5	45.38	1.0253	86.7			
607	6-2	89.0	45.40	1.0258	81.8			
607	6-2	106.0	45.57	1.0342	84.1	3.19	0.80	C
607	6-2	120.5	45.72	1.0385	79.3			
607	6-2	136.0	45.87	1.0430	72.5	3.51	0.04	C
607	6-2	136.0	45.87	1.0430		3.55	0.45	C
607	6-3	1.0	46.02	1.0474		3.99	-0.60	C
607	6-3	4.5	46.06	1.0480	64.9			
607	6-3	8.0	46.09	1.0485		3.51	0.09	C
607	6-3	16.0	46.17	1.0495	73.3			
607	6-3	23.0	46.24	1.0504		3.34	0.54	C
607	6-3	30.5	46.31	1.0514	73.1			
607	6-3	40.0	46.41	1.0526		3.19	0.27	C

TABLE A1. (continued)

DSDP Sample Identification			Composite	Age,	$CaCO_3$,	$\delta^{18}O$,	$\delta^{13}C$,	Species
Hole	Core-section	Depth, cm	Depth, m	Ma*	%	‰	‰	Code†
607	6-3	53.0	46.54	1.0543	77.2			
607	6-3	59.5	46.60	1.0551	85.1			
607	6-3	63.0	46.64	1.0556	75.7	3.14	0.46	C
607	6-3	78.0	46.79	1.0575	83.7	3.67	0.02	U
607	6-3	90.5	46.91	1.0591	90.4			
607	6-3	91.0	46.92	1.0592		2.76	0.94	C
607	6-3	106.0	47.07	1.0609	91.4			
607	6-3	119.5	47.20	1.0625	91.9			
607	6-3	129.0	47.30	1.0636		2.73	1.07	C
607	6-3	136.0	47.37	1.0644	89.9			
607	6-4	1.0	47.52	1.0663		2.75	0.97	C
607	6-4	4.5	47.56	1.0667	91.9			
607	6-4	16.0	47.67	1.0679	91.4	2.77	1.06	C
607	6-4	29.0	47.80	1.0696	89.2	2.85	0.94	C
607	6-4	30.5	47.81	1.0699	89.8			
607	6-4	40.0	47.91	1.0717		3.08	1.01	C
607	6-4	53.0	48.04	1.0744	89.0	2.67	0.91	C
607	6-4	60.5	48.11	1.0760	91.1			
607	6-4	61.0	48.12	1.0761		2.72	0.92	C
607	6-4	78.0	48.29	1.0788	89.2	2.79	0.74	C
607	6-4	90.5	48.41	1.0801	88.7			
607	6-4	91.0	48.42	1.0801		3.45	0.89	C
607	6-4	95.0	48.46	1.0806		2.90	0.74	C
607	6-4	106.0	48.57	1.0817	78.6	3.60	0.69	C
607	6-4	106.0	48.57	1.0817		4.03	-0.49	U
607	6-4	119.0	48.70	1.0831	83.4	4.16	-0.43	U
607	6-4	121.5	48.72	1.0834	89.3	4.19	-0.43	U
607	6-4	135.5	48.86	1.0849	70.1			
607	6-4	136.0	48.87	1.0849		4.43	-0.77	U
607	6-5	1.0	49.02	1.0881		3.86	0.61	C
607	6-5	1.0	49.02	1.0881		4.36	-0.54	U
607	6-5	3.5	49.04	1.0887	79.1			
607	6-5	8.0	49.09	1.0897		4.31	-0.73	U
607	6-5	16.0	49.17	1.0914	81.3	3.57	0.26	C
607	6-5	30.5	49.31	1.0932	76.0			
607	6-5	31.0	49.32	1.0933		3.58	-0.21	C
607	6-5	38.0	49.39	1.0942		4.50	-0.42	U
607	6-5	53.0	49.54	1.0964	78.8	4.15	-0.63	U
607	6-5	59.5	49.60	1.0973	77.8			
607	6-5	61.0	49.62	1.0976		4.06	-0.53	U
607	6-5	78.0	49.79	1.1002	74.6	3.88	-0.24	U
607	6-5	78.0	49.79	1.1002		3.03	0.46	C
607	6-5	90.5	49.91	1.1021	86.3			
607	6-5	91.0	49.92	1.1022		3.12	0.91	C
607	6-5	91.0	49.92	1.1022		2.81	0.75	C
607	6-5	106.0	50.07	1.1045	91.3	2.54	0.92	C
607	6-5	120.5	50.22	1.1067	90.3	2.47	0.88	C
607	6-5	136.0	50.37	1.1099	91.7	2.56	0.64	C
607	6-6	1.0	50.52	1.1145		2.71	0.47	C
607	6-6	1.0	50.52	1.1145		2.34	0.80	C
607	6-6	3.5	50.54	1.1153	86.0			
607	6-6	16.0	50.67	1.1192	73.1			
607	6-6	31.0	50.82	1.1238		4.36	-0.99	U
607	6-6	31.5	50.83	1.1240	65.1			
607	6-6	38.0	50.89	1.1260		4.43	-1.20	U
607	6-6	53.0	51.04	1.1305	63.6	4.51	-1.41	U
607	6-6	59.5	51.10	1.1323	63.5			

TABLE A1. (continued)

DSDP Sample Identification			Composite	Age,	$CaCO_3$,	$\delta^{18}O$,	$\delta^{13}C$,	Species
Hole	Core-section	Depth, cm	Depth, m	Ma*	%	‰	‰	Code†
607	6-6	61.0	51.12	1.1327		4.48	-1.41	U
607	6-6	70.0	51.21	1.1348		4.24	-0.67	U
607	6-6	70.0	51.21	1.1348		3.92	0.67	C
607	6-6	78.0	51.29	1.1367	74.7	3.58	0.30	C
607	6-6	89.5	51.40	1.1394	69.8			
607	6-6	106.0	51.57	1.1432	85.7	3.96	-0.06	U
607	6-6	106.0	51.57	1.1432		3.85	-0.09	U
607	6-6	119.0	51.70	1.1462	87.9	3.83	-0.32	U
607	6-6	119.0	51.70	1.1462		3.14	0.89	C
607	6-6	136.0	51.87	1.1499	90.9	3.11	1.16	C
607	6-7	1.0	52.02	1.1531		3.24	1.14	C
607	6-7	3.5	52.04	1.1537	82.3			
607	6-7	9.0	52.10	1.1548	90.1			
607A	7-5	1.0	52.25	1.1582	85.9	3.28	1.01	C
607A	7-5	15.0	52.40	1.1632	78.6	3.18	0.60	C
607A	7-5	30.0	52.54	1.1705	73.4	3.71	0.48	C
607A	7-5	41.0	52.65	1.1748		3.71	0.04	C
607A	7-5	45.0	52.69	1.1755	68.5	3.60	0.28	C
607A	7-5	60.0	52.84	1.1782	65.0	3.59	0.41	C
607A	7-5	60.0	52.84	1.1782		3.76	-0.12	U
607	7-1	16.0	52.99	1.1809	87.0	3.64	-0.07	U
607	7-1	29.0	53.13	1.1832	87.2	3.65	-0.02	U
607	7-1	53.0	53.36	1.1870	88.1	2.90	0.99	C
607	7-1	61.0	53.44	1.1881	89.0			
607	7-1	78.0	53.61	1.1905	88.0	3.30	1.10	C
607	7-1	91.0	53.74	1.1924	85.3	3.88	-0.39	U
607	7-1	106.0	53.90	1.1945	85.1	4.00	-0.48	U
607	7-1	121.0	54.04	1.1969	80.5	2.74	1.15	C
607	7-1	136.0	54.19	1.2004	66.0			
607	7-1	136.5	54.20	1.2005	67.2			
607	7-2	1.0	54.34	1.2039		3.14	1.10	C
607	7-2	3.5	54.37	1.2045	68.3			
607	7-2	16.0	54.49	1.2077	76.7	3.58	0.23	C
607	7-2	16.0	54.49	1.2077		4.04	-0.62	U
607	7-2	31.0	54.65	1.2124	76.4	4.26	-0.63	U
607	7-2	37.0	54.70	1.2148		4.09	-0.46	U
607	7-2	53.0	54.86	1.2212	85.2	3.42	-0.08	U
607	7-2	53.0	54.86	1.2212		2.92	1.06	C
607	7-2	63.0	54.97	1.2248		3.57	0.10	U
607	7-2	78.0	55.11	1.2292	91.1			
607	7-2	91.0	55.24	1.2329	89.6			
607	7-2	106.0	55.40	1.2373	90.5	2.73	1.13	C
607	7-2	121.0	55.54	1.2397	88.8			
607	7-2	136.0	55.69	1.2421	89.5	3.07	0.99	C
607	7-3	1.0	55.84	1.2445	89.3	3.20	1.02	C
607	7-3	16.0	55.99	1.2468	86.2	3.45	0.98	C
607	7-3	29.0	56.13	1.2489	82.1	3.57	0.87	C
607	7-3	53.0	56.36	1.2543	75.8	3.55	0.27	C
607	7-3	63.0	56.47	1.2571	79.7	3.53	1.10	C
607	7-3	78.0	56.61	1.2612	74.7	3.71	0.10	U
607	7-3	91.0	56.74	1.2648	85.3	3.75	0.03	U
607	7-3	106.0	56.90	1.2689	80.6	3.54	0.12	U
607	7-3	121.0	57.04	1.2730	92.6	2.99	1.11	C
607	7-3	121.0	57.04	1.2730		3.33	0.20	U
607	7-3	136.0	57.19	1.2772	91.5	2.80	1.14	C
607	7-3	136.0	57.19	1.2772		3.51	0.25	U

TABLE A1. (continued)

DSDP Sample Identification			Composite	Age,	$CaCO_3$,	$\delta^{18}O$,	$\delta^{13}C$,	Species
Hole	Core-section	Depth, cm	Depth, m	Ma*	%	‰	‰	Code†
607	7-3	136.0	57.19	1.2772		3.20	0.19	U
607	7-4	1.0	57.34	1.2786	86.3	2.95	1.05	C
607	7-4	16.0	57.49	1.2857	88.3	3.41	1.04	C
607	7-4	29.0	57.63	1.2894	85.6			
607	7-4	33.0	57.66	1.2905		3.51	0.72	C
607	7-4	53.0	57.86	1.2958	80.5			
607	7-4	59.0	57.92	1.2975	82.1	3.24	0.42	C
607	7-4	69.0	58.02	1.3001		3.46	0.61	C
607	7-4	78.0	58.11	1.3024	86.0			
607	7-4	91.0	58.24	1.3058	87.7	2.98	1.09	C
607	7-4	106.0	58.40	1.3097	95.0	2.59	1.06	C
607	7-4	121.0	58.54	1.3135	92.5	2.69	1.03	C
607	7-4	136.0	58.69	1.3172	92.7	2.84	0.46	C
607	7-5	1.0	58.84	1.3213	90.8			
607	7-5	16.0	58.99	1.3254	82.6	4.04	-0.97	U
607	7-5	30.0	59.13	1.3314	59.8	3.48	0.01	C
607	7-5	30.0	59.13	1.3314		4.40	-0.98	U
607	7-5	37.0	59.20	1.3355	64.1	3.00	0.24	C
607	7-5	37.0	59.20	1.3355		4.23	-0.94	U
607	7-5	53.0	59.36	1.3420	68.3	4.38	-0.90	U
607	7-5	61.0	59.44	1.3439	72.4	4.34	-0.80	U
607	7-5	78.0	59.61	1.3468	79.3	4.11	-0.46	U
607	7-5	91.0	59.74	1.3485	84.3			
607	7-5	106.0	59.90	1.3504	89.5	2.92	0.98	C
607	7-5	121.0	60.04	1.3523	89.5			
607	7-5	136.0	60.19	1.3543	92.1	2.67	0.89	C
607	7-6	1.0	60.34	1.3566	91.0			
607	7-6	16.0	60.49	1.3590	92.2	2.70	1.15	C
607	7-6	31.0	60.65	1.3616	86.5	2.74	0.77	C
607	7-6	53.0	60.86	1.3653	73.5	3.63	0.57	C
607	7-6	61.0	60.94	1.3667	74.5	3.73	0.53	C
607	7-6	78.0	61.11	1.3711	77.9	3.80	0.56	C
607	7-6	91.0	61.24	1.3756	76.4	3.58	0.29	C
607	7-6	106.0	61.40	1.3807	82.5	3.36	0.60	C
607	7-6	114.0	61.47	1.3832		3.44	0.96	C
607	7-6	121.0	61.54	1.3852	87.4	3.36	1.01	C
607	7-6	136.0	61.69	1.3893	91.3	3.00	1.22	C
607	7-7	1.0	61.84	1.3935	91.1	2.94	1.05	C
607	7-7	16.0	61.99	1.3976	92.2	3.02	1.17	C
607	7-7	24.0	62.07	1.3998	89.9	2.98	0.94	C
607A	8-5	1.0	62.23	1.4040	84.7			
607	8-1	5.0	62.38	1.4078	80.4	3.63	0.04	C
607	8-1	16.0	62.48	1.4104	76.3			
607	8-1	31.0	62.63	1.4140	74.0			
607	8-1	38.0	62.70	1.4157		3.78	0.13	C
607	8-1	53.0	62.85	1.4172	78.2	3.57	0.10	C
607	8-1	61.0	62.93	1.4181	82.1			
607	8-1	78.0	63.10	1.4199	86.8	3.44	0.76	C
607	8-1	89.0	63.22	1.4212	90.8	3.27	0.88	C
607	8-1	106.0	63.38	1.4228	81.6			
607	8-1	121.0	63.53	1.4242	86.4	3.85	0.23	U
607	8-1	121.0	63.53	1.4242		3.35	1.16	C
607	8-1	129.0	63.61	1.4251		3.70	0.06	U
607	8-1	136.0	63.68	1.4260	92.1	3.54	0.14	U
607	8-2	3.0	63.85	1.4281	92.9	3.44	0.05	U
607	8-2	16.0	63.98	1.4335	93.7	3.00	1.20	C
607	8-2	16.0	63.98	1.4335		3.37	0.20	U

TABLE A1. (continued)

DSDP Sample Identification			Composite	Age,	$CaCO_3$,	$\delta^{18}O$,	$\delta^{13}C$,	Species
Hole	Core-section	Depth, cm	Depth, m	Ma*	%	‰	‰	Code†
607	8-2	29.0	64.11	1.4391	91.9	2.89	1.12	C
607	8-2	38.0	64.21	1.4421		3.52	-0.19	U
607	8-2	38.0	64.21	1.4421		3.65	0.01	U
607	8-2	53.0	64.35	1.4470	87.1	3.42	1.09	C
607	8-2	53.0	64.35	1.4470		3.89	0.02	U
607	8-2	61.0	64.43	1.4495	85.6	4.16	0.06	U
607	8-2	78.0	64.60	1.4552	86.2	4.39	0.02	U
607	8-2	91.0	64.74	1.4587	88.0	4.34	-0.08	U
607	8-2	106.0	64.89	1.4606	88.7	4.20	-0.14	U
607	8-2	119.0	65.01	1.4615	88.2	4.03	-0.04	U
607	8-2	136.0	65.18	1.4628	88.8	3.30	1.07	C
607	8-3	1.0	65.33	1.4639	84.2	3.06	1.11	C
607	8-3	16.0	65.49	1.4654	77.0			
607	8-3	31.0	65.64	1.4669	88.2	3.94	0.07	U
607	8-3	38.0	65.71	1.4677		3.26	1.22	C
607	8-3	53.0	65.85	1.4693	88.7			
607	8-3	63.0	65.96	1.4704	90.4	2.81	1.30	C
607	8-3	78.0	66.10	1.4746	88.6			
607	8-3	89.0	66.21	1.4778	93.3	2.89	1.19	C
607	8-3	106.0	66.39	1.4857	90.3	2.88	1.12	C
607	8-3	119.0	66.51	1.4917	88.1	3.18	1.24	C
607	8-3	136.0	66.68	1.4988	89.0	3.31	1.04	C
607	8-4	1.0	66.83	1.5038	89.5	3.16	1.20	C
607	8-4	1.0	66.83	1.5038		3.43	0.13	U
607	8-4	16.0	66.99	1.5088	86.2	3.15	1.02	C
607	8-4	31.0	67.14	1.5136	87.7	3.87	0.02	U
607	8-4	37.0	67.19	1.5153		3.20	1.29	C
607	8-4	37.0	67.19	1.5153		3.10	1.21	C
607	8-4	53.0	67.35	1.5181	90.2			
607	8-4	61.0	67.43	1.5196	91.6	2.83	1.14	C
607	8-4	61.0	67.43	1.5196		2.89	1.17	C
607	8-4	78.0	67.60	1.5222	87.7	3.15	1.30	C
607	8-4	91.0	67.74	1.5241	85.7	3.33	1.32	C
607	8-4	91.0	67.74	1.5241		3.28	1.23	C
607	8-4	106.0	67.89	1.5264	82.6			
607	8-4	121.0	68.03	1.5287	79.8	3.74	1.19	C
607	8-4	136.0	68.18	1.5309	81.7	3.59	1.25	C
607	8-5	1.0	68.33	1.5338	80.8			
607	8-5	16.0	68.49	1.5367	72.6	3.68	0.80	C
607	8-5	31.0	68.64	1.5398	76.0	3.70	1.04	C
607	8-5	53.0	68.85	1.5444	85.5	3.15	1.21	C
607	8-5	61.0	68.93	1.5461	87.6			
607	8-5	76.0	69.08	1.5493		3.09	1.29	C
607	8-5	78.0	69.10	1.5497	90.3			
607	8-5	91.0	69.24	1.5525	88.6	2.78	1.20	C
607	8-5	91.0	69.24	1.5525		2.80	1.08	C
607	8-5	91.0	69.24	1.5525		2.78	1.24	C
607	8-5	106.0	69.39	1.5560	90.2	2.86	1.19	C
607	8-5	121.0	69.53	1.5597	89.3	3.10	1.17	C
607	8-5	136.0	69.68	1.5634	87.0	2.90	1.18	C
607	8-5	136.0	69.68	1.5634		3.00	0.94	C
607	8-6	1.0	69.83	1.5671	83.7	3.94	-0.35	U
607	8-6	16.0	69.99	1.5707	74.0	3.10	0.98	C
607	8-6	16.0	69.99	1.5707		2.85	0.69	C
607	8-6	29.0	70.11	1.5739		3.50	0.29	C
607	8-6	29.5	70.12	1.5740	63.1			
607	8-6	37.0	70.19	1.5759		4.13	-0.51	U

TABLE A1. (continued)

DSDP Sample Identification			Composite	Age,	$CaCO_3$,	$\delta^{18}O$,	$\delta^{13}C$,	Species
Hole	Core-section	Depth, cm	Depth, m	Ma*	%	‰	‰	Code†
607	8-6	37.0	70.19	1.5759		4.36	-0.30	U
607	8-6	53.0	70.35	1.5790	70.4	3.10	0.56	C
607	8-6	61.0	70.43	1.5806	75.5	2.92	0.94	C
607	8-6	78.0	70.60	1.5838	86.0	2.86	0.90	C
607	8-6	78.0	70.60	1.5838		3.58	-0.15	U
607	8-6	89.0	70.71	1.5860	81.3	3.21	0.74	C
607	8-6	89.0	70.71	1.5860		3.60	-0.21	U
607	8-6	106.0	70.89	1.5892	82.0	4.08	-0.50	U
607	8-6	121.0	71.03	1.5921	85.5	3.05	0.89	C
607	8-6	136.0	71.18	1.5950	86.4	3.07	0.63	C
607	8-6	136.0	71.18	1.5950		3.71	-0.26	U
607	8-6	136.0	71.18	1.5950		3.17	1.03	C
607	8-7	1.0	71.33	1.5979	81.2			
607	8-7	5.0	71.38	1.5987	80.4	2.87	0.96	C
607	8-7	5.0	71.38	1.5987		2.84	0.86	C
607A	9-4	75.0	71.54	1.6020	70.1			
607A	9-4	91.0	71.71	1.6051	76.1	3.22	0.86	C
607A	9-4	105.0	71.85	1.6078	70.7			
607A	9-4	121.0	72.00	1.6108	88.8	3.90	0.06	U
607A	9-4	135.0	72.14	1.6144	78.5	3.18	0.71	C
607A	9-4	135.0	72.14	1.6144		3.75	-0.10	U
607A	9-5	1.0	72.31	1.6185	85.7	4.07	-0.73	U
607A	9-5	15.0	72.44	1.6223	75.3	3.84	-0.63	U
607A	9-5	30.0	72.60	1.6264	84.4	4.13	-0.28	U
607	9-1	1.0	72.71	1.6295	92.6			
607	9-1	16.0	72.85	1.6338	93.8	2.73	0.99	C
607	9-1	31.0	73.00	1.6375		2.76	1.23	C
607	9-1	53.0	73.22	1.6426	90.7	2.90	1.07	C

* Ages based on TP607 time scale.

† C, *Cibicidoides*; U, *Uvigerina*. Isotope data not corrected for species offsets.

TABLE A2. Percentages of Species Used in Transfer Function F13x5, and Summer and Winter Temperature Estimates for Site 607

DSDP Sample Identification										
Hole	Core-section	Depth, cm	Composite Depth, m	Age, Ma*	Species 1	Species 2	Species 3	Species 4	SSTs, °C	SSTw, °C
607A	2-3	45.0	9.32	0.2453	3.1	24.3	10.7	9.0	14.8	8.8
607A	2-3	61.0	9.48	0.2490	3.3	22.8	5.8	12.0	15.9	10.2
607A	2-3	75.0	9.62	0.2508	1.9	14.3	3.5	12.1	17.9	11.8
607A	2-3	91.0	9.78	0.2520	0.5	13.8	0.8	12.3	17.8	12.1
607A	2-3	105.0	9.92	0.2530	1.6	19.7	4.7	6.6	16.0	10.5
607A	2-3	121.0	10.08	0.2541	3.0	17.4	11.4	8.7	16.3	10.0
607A	2-3	135.0	10.22	0.2551	5.8	19.5	4.2	4.7	18.5	12.3
607A	2-4	1.0	10.38	0.2564	1.2	16.4	18.7	9.0	14.4	8.3
607	2-1	55.0	10.52	0.2585	4.0	15.0	7.2	7.6	18.0	11.6
607	2-1	61.0	10.59	0.2595	8.8	10.7	1.7	28.3	23.9	16.4
607	2-1	78.0	10.76	0.2637	1.9	14.2	4.7	9.4	17.7	11.6
607	2-1	91.0	10.89	0.2684	2.2	21.1	4.4	15.6	15.9	10.4
607	2-1	106.0	11.03	0.2745	2.7	9.7	0.3	18.2	20.5	13.8
607	2-1	121.0	11.18	0.2805	3.0	12.2	2.7	21.6	19.7	13.0
607	2-1	136.0	11.34	0.2861	4.0	13.2	1.8	23.5	20.3	13.6
607	2-2	1.0	11.48	0.2898	6.2	13.1	1.4	13.1	20.6	14.2

TABLE A2. (continued)

DSDP Sample Identification										
Hole	Core-section	Depth, cm	Composite Depth, m	Age, Ma*	Species 1	Species 2	Species 3	Species 4	SSTs, °C	SSTw, °C
607	2-2	16.0	11.63	0.2925	2.2	15.5	8.5	9.6	16.9	10.6
607	2-2	31.0	11.78	0.2951	4.4	14.6	10.2	13.5	17.8	11.2
607	2-2	53.0	12.01	0.2998	2.5	11.3	2.6	21.1	19.7	12.9
607	2-2	61.0	12.09	0.3019	1.1	13.5	2.2	11.3	18.0	12.0
607	2-2	78.0	12.26	0.3064	4.1	17.4	2.2	16.5	18.5	12.6
607	2-2	91.0	12.38	0.3096	4.3	8.7	2.3	18.3	21.1	14.0
607	2-2	106.0	12.53	0.3139	2.8	16.0	2.8	16.5	18.1	12.1
607	2-2	121.0	12.68	0.3187	2.1	19.5	1.7	9.6	16.7	11.4
607	2-2	128.0	12.76	0.3209	2.0	18.9	5.1	9.5	16.4	10.7
607	2-2	136.0	12.84	0.3235	2.2	8.0	2.5	21.4	20.6	13.4
607	2-3	1.0	12.98	0.3276	10.5	8.4	1.7	19.6	23.6	16.4
607	2-3	16.0	13.13	0.3301	10.0	10.4	5.2	20.4	22.4	15.2
607	2-3	31.0	13.28	0.3324	3.0	16.9	13.9	8.6	15.9	9.6
607	2-3	53.0	13.51	0.3360	1.4	30.9	20.7	7.9	11.7	5.4
607	2-3	61.0	13.59	0.3374	1.2	8.3	4.7	22.4	19.9	12.3
607	2-3	78.0	13.76	0.3397	1.6	23.5	8.7	9.1	14.3	8.7
607	2-3	91.0	13.88	0.3414	1.2	10.8	4.8	15.2	18.5	11.8
607	2-3	106.0	14.03	0.3440	1.1	13.9	10.1	8.2	16.6	10.2
607	2-3	121.0	14.18	0.3472	0.7	32.2	7.3	5.0	11.9	7.0
607	2-3	136.0	14.34	0.3506	0.0	39.9	16.1	0.5	10.2	4.1
607	2-4	1.0	14.48	0.3541	0.4	15.4	9.4	5.6	16.0	9.9
607	2-4	16.0	14.63	0.3577	1.3	19.9	5.0	9.3	15.7	10.2
607	2-4	23.0	14.70	0.3593	2.1	22.4	4.2	8.8	15.6	10.2
607	2-4	31.0	14.78	0.3613	2.4	14.0	5.9	11.9	17.9	11.5
607	2-4	39.0	14.86	0.3633	2.3	13.4	9.2	10.7	17.4	10.8
607	2-4	53.0	15.01	0.3668	3.1	13.5	4.1	12.6	18.6	12.3
607	2-4	61.0	15.09	0.3688	3.9	10.2	3.3	14.0	20.1	13.3
607	2-4	78.0	15.26	0.3734	2.2	10.3	9.6	16.8	18.4	11.2
607	2-4	91.0	15.38	0.3787	5.7	7.9	3.9	22.1	22.0	14.4
607	2-4	106.0	15.53	0.3855	2.8	9.9	1.2	18.5	20.3	13.6
607	2-4	121.0	15.68	0.3892	2.6	14.5	1.5	17.5	18.7	12.6
607	2-4	136.0	15.84	0.3927	2.4	11.6	10.4	19.0	18.0	10.8
607	2-5	1.0	15.98	0.3960	5.1	6.6	1.1	39.6	25.5	16.9
607	2-5	16.0	16.14	0.3993	5.6	12.6	2.7	32.9	22.6	15.2
607	2-5	23.0	16.20	0.4007	11.7	10.6	4.2	29.9	24.8	17.1
607	2-5	31.0	16.28	0.4022	12.5	7.7	0.3	27.9	25.9	18.3
607	2-5	53.0	16.50	0.4061	22.2	8.9	0.6	24.2	26.8	20.2
607	2-5	61.0	16.58	0.4076	16.6	6.7	1.1	25.8	26.3	19.1
607	2-5	68.0	16.65	0.4090	14.6	8.9	1.4	21.0	24.8	17.8
607	2-5	78.0	16.75	0.4111	17.2	8.3	1.0	22.1	25.6	18.7
607	2-5	91.0	16.89	0.4138	24.6	7.2	0.6	15.3	25.6	19.5
607	2-5	106.0	17.03	0.4167	19.4	18.7	0.4	18.3	26.6	18.9
607	2-5	121.0	17.18	0.4204	11.9	21.1	1.4	24.2	23.6	16.7
607	2-5	136.0	17.33	0.4237	6.5	10.7	14.3	20.2	18.9	11.8
607	2-5	143.0	17.40	0.4252	1.0	7.3	49.7	4.9	10.4	5.8
607	2-6	16.0	17.64	0.4303	1.9	19.0	10.3	28.7	16.4	9.8
607	2-6	23.0	17.70	0.4319	1.8	19.6	7.8	11.1	15.6	9.7
607	2-6	31.0	17.78	0.4342	1.0	13.9	18.4	17.1	15.0	8.4
607	2-6	40.0	17.88	0.4358	1.0	21.6	27.7	9.9	11.8	6.3
607	2-6	53.0	18.00	0.4380	0.0	17.3	41.8	5.2	10.3	5.6
607	2-6	61.0	18.08	0.4394	0.9	25.9	16.4	8.6	12.3	6.5
607	2-6	68.0	18.15	0.4405	1.1	25.6	19.3	9.6	12.1	6.3
607	2-6	78.0	18.25	0.4422	1.1	19.9	13.4	19.6	14.2	8.1
607	2-6	91.0	18.39	0.4447	1.1	13.4	6.7	28.6	18.4	11.2
607	2-6	106.0	18.53	0.4476	2.1	10.1	5.1	20.3	19.4	12.3
607	2-6	121.0	18.68	0.4505	2.3	15.6	9.9	11.4	16.6	10.3
607	2-6	136.0	18.83	0.4526	0.8	14.3	19.2	12.0	14.6	8.2

TABLE A2. (continued)

DSDP Sample Identification										
Hole	Core-section	Depth, cm	Composite Depth, m	Age, Ma*	Species 1	Species 2	Species 3	Species 4	SSTs, °C	SSTw, °C
607	2-7	1.0	18.98	0.4546	2.2	14.3	6.9	25.1	18.3	11.3
607	2-7	16.0	19.14	0.4566	1.2	15.1	12.9	12.2	15.7	9.3
607	2-7	24.0	19.22	0.4576	0.0	19.0	4.8	11.2	15.2	9.8
607	3-2	91.0	19.34	0.4612	3.1	8.7	13.0	12.4	18.3	11.1
607	3-2	106.0	19.49	0.4676	0.7	8.1	16.1	16.5	17.2	9.6
607	3-2	119.0	19.63	0.4723	6.3	10.5	8.6	8.2	19.7	12.8
607	3-2	121.0	19.65	0.4726	2.5	10.2	4.9	13.0	19.2	12.4
607	3-2	136.0	19.80	0.4747	4.1	9.0	4.5	23.2	21.0	13.5
607	3-3	1.0	19.94	0.4768	3.3	12.7	2.0	17.1	19.5	13.1
607	3-3	16.0	20.09	0.4807	6.8	8.6	1.1	18.4	22.3	15.2
607	3-3	31.0	20.24	0.4880	3.5	10.6	1.6	16.3	20.2	13.6
607	3-3	53.0	20.47	0.5017	5.0	14.4	2.7	12.1	19.5	13.2
607	3-3	61.0	20.55	0.5075	4.9	16.2	9.2	13.7	17.8	11.3
607	3-3	68.0	20.61	0.5121	1.4	13.8	19.7	15.2	14.9	8.4
607	3-3	78.0	20.72	0.5180	2.5	8.7	9.4	23.9	19.7	11.6
607	3-3	91.0	20.84	0.5277	4.0	14.4	1.4	21.6	19.8	13.4
607	3-3	106.0	20.99	0.5411	4.2	10.0	3.3	20.3	20.7	13.6
607	3-3	121.0	21.15	0.5521	2.4	8.8	2.1	25.5	21.0	13.6
607	3-3	128.0	21.22	0.5578	2.2	13.6	4.0	17.9	18.4	12.0
607	3-3	136.0	21.30	0.5644	0.7	13.2	3.7	20.7	18.0	11.5
607	3-4	1.0	21.44	0.5735	3.5	9.6	5.4	22.1	20.3	12.9
607	3-4	16.0	21.59	0.5775	3.3	11.6	3.3	13.1	19.4	12.9
607	3-4	31.0	21.74	0.5803	7.6	13.2	6.6	12.8	20.1	13.4
607	3-4	42.0	21.85	0.5825	5.8	9.6	12.9	8.3	18.8	12.0
607	3-4	53.0	21.97	0.5847	7.7	17.7	12.6	16.1	18.3	11.7
607	3-4	61.0	22.05	0.5862	2.8	14.2	4.5	14.2	18.3	11.9
607	3-4	69.0	22.13	0.5887	7.6	12.6	2.7	13.6	21.1	14.4
607	3-4	78.0	22.22	0.5914	4.5	12.0	3.4	12.4	19.8	13.2
607	3-4	91.0	22.34	0.5939	8.9	18.5	0.6	9.2	20.8	14.5
607	4-1	43.0	22.45	0.5988	4.5	9.6	1.6	14.1	20.8	14.0
607	4-1	53.0	22.55	0.6034	7.5	13.5	0.0	8.6	21.1	14.8
607	4-1	61.0	22.63	0.6074	4.6	9.9	1.3	10.2	20.6	14.1
607	4-1	70.0	22.72	0.6093	5.2	14.7	1.4	10.1	19.6	13.5
607	4-1	78.0	22.80	0.6103	6.7	10.9	1.2	11.9	21.3	14.6
607	4-1	91.0	22.93	0.6119	9.7	13.4	0.9	4.0	21.9	15.3
607	4-1	98.0	23.00	0.6128	11.3	12.7	1.3	9.0	22.5	15.8
607	4-1	106.0	23.08	0.6137	12.1	12.1	1.2	9.0	22.9	16.1
607	4-1	111.0	23.13	0.6143	12.4	13.6	2.9	9.1	22.5	15.6
607	4-1	121.0	23.23	0.6155	8.9	11.0	4.2	10.1	21.4	14.6
607	4-1	136.0	23.38	0.6163	9.9	13.2	3.6	11.2	21.5	14.8
607	4-2	1.0	23.53	0.6172	12.5	12.5	5.9	12.5	22.0	15.1
607	4-2	16.0	23.68	0.6180	9.8	17.5	5.8	12.7	20.5	13.8
607	4-2	23.0	23.75	0.6184	11.6	13.5	7.6	15.3	21.3	14.5
607	4-2	31.0	23.83	0.6188	8.3	14.2	10.5	12.5	19.3	12.6
607	4-2	42.0	23.94	0.6195	11.4	13.9	5.7	13.0	21.6	14.7
607	4-2	53.0	24.05	0.6201	9.7	13.0	8.8	12.7	20.4	13.6
607	4-2	61.0	24.13	0.6207	7.9	15.1	9.2	11.0	19.3	12.6
607	4-2	78.0	24.30	0.6219	5.3	14.4	10.1	13.6	18.3	11.6
607	4-2	91.0	24.43	0.6229	4.8	11.9	18.2	10.8	16.9	10.5
607	4-2	106.0	24.58	0.6242	2.3	14.1	11.5	16.9	16.9	10.2
607	4-2	121.0	24.73	0.6254	1.8	17.1	20.0	24.7	14.8	7.9
607	4-2	136.0	24.88	0.6267	3.7	15.9	3.4	30.2	19.9	13.3
607	4-3	1.0	25.03	0.6293	0.7	15.2	2.8	31.1	18.4	12.1
607	4-3	16.0	25.18	0.6320	3.3	18.5	2.7	35.8	19.8	14.1
607	4-3	31.0	25.33	0.6346	1.9	14.7	4.5	30.9	19.1	12.3
607	4-3	53.0	25.55	0.6445	1.1	21.0	5.5	16.9	15.1	9.7
607	4-3	61.0	25.63	0.6476	2.1	13.9	7.8	20.2	17.7	10.9

TABLE A2. (continued)

DSDP Sample Identification										
Hole	Core-section	Depth, cm	Composite Depth, m	Age, Ma*	Species 1	Species 2	Species 3	Species 4	SSTs, °C	SSTw, °C
607	4-3	78.0	25.80	0.6517	1.0	16.7	6.2	27.9	17.1	10.7
607	4-3	91.0	25.93	0.6543	1.3	12.9	4.8	40.2	20.8	13.4
607	4-3	106.0	26.08	0.6573	2.4	20.0	4.8	29.0	17.3	11.5
607	4-3	121.0	26.23	0.6603	4.7	20.5	2.5	25.2	18.6	12.9
607	4-3	136.0	26.38	0.6633	2.7	14.2	7.5	20.7	18.0	11.2
607	4-4	1.0	26.53	0.6663	4.3	6.4	9.8	21.3	20.6	12.5
607	4-4	16.0	26.68	0.6691	1.5	7.5	12.3	16.4	18.5	10.8
607	4-4	31.0	26.83	0.6719	1.8	7.5	12.6	12.9	18.3	10.9
607	4-4	53.0	27.05	0.6750	2.2	18.2	16.0	21.2	15.0	8.5
607	4-4	61.0	27.13	0.6758	2.2	9.3	28.5	16.1	14.4	8.2
607	4-4	78.0	27.30	0.6774	3.6	13.0	15.1	17.2	17.0	10.2
607	4-4	91.0	27.43	0.6788	4.8	16.1	10.6	11.9	17.5	11.0
607	4-4	106.0	27.58	0.6805	3.3	8.1	19.5	7.2	17.1	10.3
607	4-4	121.0	27.73	0.6824	4.9	17.9	8.5	13.5	17.6	11.2
607	4-4	136.0	27.88	0.6844	11.7	17.5	0.4	23.0	23.6	16.8
607	4-5	1.0	28.03	0.6864	17.5	11.7	4.4	13.9	23.6	16.9
607	4-5	16.0	28.18	0.6884	14.9	11.7	0.0	19.2	24.8	18.0
607	4-5	31.0	28.33	0.6900	11.1	16.9	2.0	16.9	22.2	15.5
607	4-5	42.0	28.44	0.6911	20.4	11.8	1.1	10.5	25.2	18.2
607	4-5	53.0	28.55	0.6921	17.2	12.8	0.9	10.3	24.5	17.5
607	4-5	61.0	28.63	0.6928	15.1	11.1	2.7	17.1	24.0	17.1
607	4-5	78.0	28.80	0.6946	5.3	14.7	37.9	12.6	12.5	8.0
607	4-5	91.0	28.93	0.6963	0.0	4.7	72.4	11.5	6.7	0.4
607	4-5	106.0	29.08	0.6982	2.3	7.4	26.1	27.6	16.5	8.0
607	4-5	121.0	29.23	0.7002	0.9	8.9	27.0	21.7	14.8	7.5
607	4-5	136.0	29.38	0.7021	2.2	9.5	12.0	29.5	19.5	10.9
607	4-6	1.0	29.53	0.7039	1.4	9.8	10.3	24.6	18.7	10.8
607	4-6	16.0	29.68	0.7058	2.4	15.6	4.6	18.7	17.8	11.6
607	4-6	31.0	29.83	0.7078	4.3	18.1	5.7	8.2	17.7	11.6
607	4-6	53.0	30.05	0.7108	8.3	13.3	4.1	12.7	20.9	14.1
607	4-6	61.0	30.13	0.7118	4.1	13.5	3.8	16.2	19.3	12.8
607	4-6	78.0	30.30	0.7137	4.2	15.2	14.2	17.7	16.9	10.3
607	4-6	91.0	30.43	0.7153	2.6	9.6	10.7	20.2	18.8	11.2
607	4-6	106.0	30.58	0.7170	2.5	14.4	19.5	14.4	15.2	8.9
607	4-6	121.0	30.73	0.7183	0.3	6.8	10.5	18.3	18.7	10.8
607	4-6	136.0	30.88	0.7195	0.6	13.5	7.4	26.4	17.7	10.6
607	4-7	1.0	31.03	0.7209	1.5	7.9	6.2	16.4	19.4	12.1
607	4-7	16.0	31.18	0.7226	3.1	9.3	11.1	34.9	21.1	12.0
607	4-7	24.0	31.26	0.7236	3.4	16.7	8.2	23.4	17.8	11.1
607A	5-4	121.0	31.42	0.7254	3.4	15.0	6.1	16.0	18.1	11.6
607A	5-4	135.0	31.56	0.7270	9.4	14.3	4.3	23.7	22.2	15.1
607A	5-5	1.0	31.72	0.7289	3.3	12.3	2.7	26.2	20.4	13.4
607A	5-5	15.0	31.86	0.7330	12.4	9.7	2.7	22.1	24.0	16.8
607A	5-5	30.0	32.01	0.7374	7.8	15.3	25.1	9.7	15.7	10.5
607A	5-5	45.0	32.16	0.7429	1.3	11.9	54.3	8.8	9.1	4.1
607A	5-5	61.0	32.32	0.7488	1.6	7.2	15.3	31.6	19.7	10.2
607A	5-5	75.0	32.46	0.7512	2.2	10.6	11.7	16.0	17.8	10.7
607	5-1	16.0	32.62	0.7538	1.5	13.6	12.1	22.4	16.9	9.8
607	5-1	22.0	32.68	0.7545	2.4	24.4	11.7	16.2	14.1	8.2
607	5-1	31.0	32.77	0.7556	2.5	13.2	5.1	12.4	18.3	11.9
607	5-1	53.0	32.99	0.7581	5.7	10.9	12.0	20.3	19.2	12.0
607	5-1	61.0	33.07	0.7590	3.4	16.7	17.3	16.1	15.5	9.2
607	5-1	78.0	33.24	0.7609	3.3	12.0	4.3	27.7	20.3	13.1
607	5-1	93.0	33.39	0.7627	3.8	9.5	21.0	12.1	16.5	10.0
607	5-1	106.0	33.52	0.7649	5.9	10.2	13.8	11.5	18.6	11.7
607	5-1	119.0	33.65	0.7679	7.1	14.9	7.5	18.8	19.8	12.9
607	5-1	136.0	33.82	0.7719	5.8	16.0	6.1	14.1	18.9	12.4
607	5-2	1.0	33.97	0.7755	7.0	13.3	11.1	9.2	18.9	12.2

TABLE A2. (continued)

DSDP Sample Identification										
Hole	Core-section	Depth, cm	Composite Depth, m	Age, Ma*	Species 1	Species 2	Species 3	Species 4	SSTs, °C	SSTw, °C
607	5-2	16.0	34.12	0.7789	4.4	14.5	11.6	11.3	17.5	10.9
607	5-2	31.0	34.27	0.7820	11.2	8.4	3.7	15.9	23.0	15.9
607	5-2	37.0	34.33	0.7831	13.0	10.9	8.3	14.2	21.6	14.9
607	5-2	46.0	34.42	0.7848	8.5	8.8	24.4	7.9	16.5	11.3
607	5-2	53.0	34.49	0.7862	4.0	12.6	35.6	9.8	12.7	8.2
607	5-2	61.0	34.57	0.7878	0.4	3.3	75.9	3.3	7.1	1.3
607	5-2	78.0	34.74	0.7912	1.5	5.5	49.1	16.8	10.1	4.2
607	5-2	91.0	34.87	0.7938	0.3	4.1	50.7	19.5	9.7	3.0
607	5-2	107.0	35.03	0.7965	0.4	10.8	39.2	16.2	11.1	5.6
607	5-2	121.0	35.17	0.7988	1.8	11.6	45.1	9.4	10.5	6.0
607	5-2	136.0	35.32	0.8012	0.6	5.4	59.5	11.4	8.3	2.7
607	5-3	1.0	35.47	0.8035	0.0	4.8	82.9	0.6	6.8	0.9
607	5-3	18.0	35.64	0.8061	0.6	4.0	60.3	12.9	8.2	2.3
607	5-3	31.0	35.77	0.8080	0.7	6.8	30.0	19.8	14.4	7.3
607	5-3	37.0	35.83	0.8087	2.2	6.2	23.7	15.3	16.4	9.2
607	5-3	53.0	35.99	0.8106	1.6	8.8	4.5	14.6	19.4	12.4
607	5-3	61.0	36.07	0.8116	2.2	9.9	8.7	20.4	18.9	11.4
607	5-3	78.0	36.24	0.8142	2.2	8.7	9.9	19.2	19.0	11.3
607	5-3	93.0	36.39	0.8166	2.6	7.1	19.4	9.7	17.2	10.1
607	5-3	106.0	36.52	0.8187	1.9	9.6	6.4	9.2	18.8	12.0
607	5-3	121.0	36.67	0.8227	5.2	11.9	13.3	14.1	18.1	11.3
607	5-3	136.0	36.82	0.8290	1.9	6.9	49.1	7.2	10.4	5.9
607	5-3	143.0	36.89	0.8320	0.0	4.9	61.9	8.1	8.1	2.7
607	5-4	1.0	36.97	0.8352	0.0	1.7	44.9	21.1	11.7	4.2
607	5-4	9.0	37.05	0.8368	0.0	3.4	28.4	19.8	15.8	7.6
607	5-4	16.0	37.12	0.8382	0.6	7.0	31.9	13.1	13.8	7.5
607	5-4	31.0	37.27	0.8412	3.6	6.4	21.0	20.2	17.5	10.0
607	5-4	37.0	37.33	0.8424	3.0	10.1	39.8	16.9	11.7	6.5
607	5-4	46.0	37.42	0.8435	4.2	16.6	29.0	10.3	13.7	8.6
607	5-4	53.0	37.49	0.8443	3.8	8.2	38.6	11.4	12.4	7.8
607	5-4	59.0	37.55	0.8450	6.3	8.9	30.0	15.1	14.6	9.6
607	5-4	68.0	37.64	0.8461	3.3	10.3	20.0	13.6	16.4	9.8
607	5-4	73.0	37.69	0.8467	5.3	19.8	17.2	11.2	15.9	9.6
607	5-4	78.0	37.74	0.8473	4.7	10.3	10.0	15.3	19.1	12.0
607	5-4	91.0	37.87	0.8489	2.5	8.8	17.5	16.6	17.3	10.0
607	5-4	106.0	38.02	0.8507	7.8	6.6	3.6	17.7	22.5	15.1
607	5-4	121.0	38.17	0.8525	7.6	10.9	1.8	12.0	21.5	14.8
607	5-4	131.0	38.27	0.8537	6.1	11.6	2.6	19.0	21.1	14.2
607	5-5	3.0	38.49	0.8570	12.3	14.1	4.6	16.3	22.3	15.4
607	5-5	16.0	38.62	0.8615	13.1	11.4	7.3	15.2	22.0	15.2
607	5-5	29.0	38.75	0.8671	8.6	22.4	23.4	14.5	17.1	10.4
607	5-5	37.0	38.83	0.8705	2.5	19.9	28.4	4.3	13.1	7.6
607	5-5	46.0	38.92	0.8717	3.8	9.0	28.3	14.7	14.7	9.0
607	5-5	53.0	38.99	0.8727	0.9	9.1	38.4	8.4	12.0	7.0
607	5-5	61.0	39.07	0.8738	7.8	16.7	3.7	10.7	20.0	13.6
607	5-5	78.0	39.24	0.8762	1.8	13.1	3.5	14.9	18.3	12.0
607	5-5	91.0	39.37	0.8781	5.4	14.0	6.0	18.7	19.5	12.7
607	5-5	106.0	39.52	0.8802	5.2	12.6	4.8	11.3	19.6	13.0
607	5-5	119.0	39.65	0.8828	2.3	13.8	16.4	6.4	16.0	9.6
607	5-5	127.0	39.73	0.8851	6.1	11.2	15.1	12.5	18.1	11.4
607	5-5	136.0	39.82	0.8876	1.8	10.7	22.7	8.7	15.3	8.9
607	5-6	1.0	39.97	0.8924	3.3	3.3	13.9	16.2	19.9	11.7
607	5-6	16.0	40.12	0.8967	2.6	6.7	5.4	26.6	21.4	13.1
607	5-6	31.0	40.27	0.9013	5.9	9.4	3.8	15.7	21.1	14.0
607	5-6	36.0	40.32	0.9029	5.5	11.0	5.8	15.0	20.1	13.1
607	5-6	53.0	40.49	0.9092	2.9	13.1	8.7	20.2	18.2	11.2
607	5-6	61.0	40.57	0.9126	3.9	10.5	25.8	5.8	15.3	9.5

TABLE A2. (continued)

DSDP Sample Identification			Composite	Age,	Species	Species	Species	Species	SSTs,	SSTw,
Hole	Core-section	Depth, cm	Depth, m	Ma*	1	2	3	4	°C	°C
607	5-6	78.0	40.74	0.9198	1.4	8.1	50.7	5.5	10.1	5.6
607	5-6	88.0	40.84	0.9237	6.0	9.1	34.9	11.0	13.4	9.1
607	5-6	106.0	41.02	0.9301	6.3	8.5	28.8	11.0	15.0	10.0
607	5-6	121.0	41.17	0.9354	5.5	6.1	39.9	11.7	12.4	8.2
607	5-6	136.0	41.32	0.9406	8.5	11.8	9.9	18.7	20.3	13.3
607	5-7	1.0	41.47	0.9457	5.8	8.8	18.8	15.4	17.7	11.0
607	5-7	16.0	41.62	0.9505	12.3	8.3	4.3	17.4	23.2	16.1
607	5-7	21.0	41.67	0.9520	13.8	12.4	3.2	12.9	23.1	16.2
607A	6-4	121.0	41.83	0.9552	9.5	17.3	7.1	14.8	20.3	13.5
607A	6-4	135.0	41.97	0.9568	8.4	10.6	6.8	17.9	21.1	14.0
607A	6-5	1.0	42.13	0.9585	5.9	11.1	16.5	11.3	17.7	11.2
607A	6-5	15.0	42.26	0.9601	3.8	15.6	3.5	6.8	18.4	12.4
607A	6-5	21.0	42.33	0.9607	6.4	14.7	3.0	10.4	19.9	13.5
607A	6-5	31.0	42.42	0.9618	6.4	12.6	5.3	10.8	20.0	13.3
607A	6-5	45.0	42.56	0.9634	4.0	11.0	4.3	19.9	20.1	13.1
607A	6-5	61.0	42.72	0.9653	3.4	11.6	6.4	19.5	19.2	12.2
607A	6-5	75.0	42.86	0.9670	3.6	12.9	22.5	15.6	15.3	9.2
607A	6-5	91.0	43.02	0.9688	3.6	10.0	32.5	14.3	13.5	8.3
607	6-1	16.0	43.17	0.9705	4.4	10.3	36.3	10.6	12.8	8.4
607	6-1	31.0	43.32	0.9722	3.1	14.5	29.0	13.4	13.4	8.1
607	6-1	53.0	43.54	0.9747	3.3	11.2	32.0	8.2	13.6	8.6
607	6-1	61.0	43.62	0.9756	1.5	12.5	4.9	6.1	18.0	11.8
607	6-1	70.0	43.71	0.9766	14.1	10.6	0.5	22.3	25.0	18.0
607	6-1	78.0	43.79	0.9777	9.6	13.3	1.1	14.8	22.1	15.4
607	6-1	91.0	43.92	0.9813	17.7	4.8	2.3	12.9	24.7	17.9
607	6-1	106.0	44.07	0.9855	21.4	7.4	0.0	14.4	25.8	19.2
607	6-1	121.0	44.22	0.9896	22.3	5.0	1.7	9.0	25.1	18.7
607	6-1	136.0	44.37	0.9937	20.8	8.1	0.0	7.8	25.5	18.7
607	6-2	1.0	44.52	0.9979	22.9	9.1	3.1	18.6	24.8	18.6
607	6-2	16.0	44.67	1.0020	14.5	16.5	1.2	17.3	24.0	17.0
607	6-2	31.0	44.82	1.0067	10.3	10.3	16.1	19.7	19.2	12.8
607	6-2	39.0	44.90	1.0090	8.5	17.3	26.6	14.6	15.7	10.4
607	6-2	53.0	45.04	1.0159	5.6	9.4	4.9	22.3	21.3	13.9
607	6-2	61.0	45.12	1.0180	6.8	4.5	23.4	20.1	17.6	10.8
607	6-2	78.0	45.29	1.0224	12.1	11.8	2.4	20.5	23.5	16.5
607	6-2	89.0	45.40	1.0258	12.7	12.6	6.5	10.9	21.8	15.0
607	6-2	106.0	45.57	1.0342	13.3	10.4	2.9	10.7	23.1	16.3
607	6-2	121.0	45.72	1.0386	7.1	10.2	8.1	18.3	20.6	13.4
607	6-2	136.0	45.87	1.0430	4.0	11.2	24.5	14.9	15.3	9.3
607	6-3	1.0	46.02	1.0474	1.9	5.3	9.7	30.5	21.4	12.0
607	6-3	4.0	46.05	1.0479	4.7	6.8	9.4	28.8	21.7	13.0
607	6-3	8.0	46.09	1.0485	3.4	6.8	11.5	28.3	20.7	11.9
607	6-3	16.0	46.17	1.0495	2.5	5.5	16.8	23.4	19.0	10.4
607	6-3	23.0	46.24	1.0504	5.2	9.5	23.6	25.9	17.1	9.6
607	6-3	31.0	46.32	1.0514	2.9	5.2	39.8	14.6	12.4	7.1
607	6-3	40.0	46.41	1.0526	6.3	10.1	20.6	18.6	17.2	10.7
607	6-3	53.0	46.54	1.0543	4.7	9.4	20.3	15.2	16.9	10.3
607	6-3	63.0	46.64	1.0556	9.5	8.4	10.2	31.9	23.3	14.8
607	6-3	78.0	46.79	1.0575	8.5	7.7	10.7	15.6	20.6	13.5
607	6-3	91.0	46.92	1.0592	11.6	6.8	7.1	15.3	22.3	15.2
607	6-3	101.0	47.02	1.0603	13.6	11.6	7.9	8.3	21.7	15.0
607	6-3	103.0	47.04	1.0606	16.6	12.8	7.3	6.2	22.5	15.7
607	6-3	106.0	47.07	1.0609	14.2	9.1	4.7	10.7	23.0	16.1
607	6-3	121.0	47.22	1.0627	11.7	11.4	3.9	8.8	22.3	15.4
607	6-3	129.0	47.30	1.0636	18.3	14.3	2.7	9.1	24.3	17.1
607	6-3	136.0	47.37	1.0644	12.8	14.1	4.2	11.2	22.3	15.4
607	6-4	1.0	47.52	1.0663	18.4	10.2	3.0	6.3	24.2	17.3

TABLE A2. (continued)

DSDP Sample Identification										
Hole	Core-section	Depth, cm	Composite Depth, m	Age, Ma*	Species 1	Species 2	Species 3	Species 4	SSTs, °C	SSTw, °C
607	6-4	16.0	47.67	1.0679	15.5	14.5	0.3	13.2	24.2	17.3
607	6-4	29.0	47.80	1.0696	11.3	14.1	10.8	17.2	20.5	13.8
607	6-4	40.0	47.91	1.0717	20.1	15.0	0.8	2.8	25.4	17.8
607	6-4	53.0	48.04	1.0744	9.1	17.8	2.2	14.1	20.9	14.4
607	6-4	61.0	48.12	1.0761	17.1	11.6	2.6	10.7	24.0	17.1
607	6-4	78.0	48.29	1.0788	15.4	15.1	0.6	6.8	23.9	16.8
607	6-4	91.0	48.42	1.0801	14.4	10.8	4.9	4.2	22.8	15.9
607	6-4	95.0	48.46	1.0806	14.9	13.3	6.5	4.9	22.4	15.4
607	6-4	106.0	48.57	1.0817	6.4	7.3	14.9	4.7	19.1	12.2
607	6-4	121.0	48.72	1.0833	5.9	6.8	7.4	13.9	20.9	13.5
607	6-4	136.0	48.87	1.0849	6.0	5.3	10.3	12.6	20.6	13.1
607	6-5	1.0	49.02	1.0881	5.5	3.4	7.9	7.6	21.2	13.7
607	6-5	8.0	49.09	1.0897	4.2	7.7	4.5	26.8	21.9	13.9
607	6-5	16.0	49.17	1.0914	8.0	8.7	3.1	13.9	22.0	14.9
607	6-5	18.0	49.19	1.0916	8.9	8.6	5.1	16.8	22.0	14.8
607	6-5	31.0	49.32	1.0933	5.9	6.7	2.6	23.4	22.8	15.0
607	6-5	38.0	49.39	1.0942	10.3	10.7	0.7	10.3	22.7	15.9
607	6-5	53.0	49.54	1.0964	13.5	5.3	2.3	22.0	24.9	17.5
607	6-5	60.0	49.61	1.0974	11.8	8.9	1.0	23.6	24.6	17.3
607	6-5	61.0	49.62	1.0976	13.7	4.3	2.2	20.5	25.0	17.5
607	6-5	78.0	49.79	1.1002	8.4	7.2	0.0	16.4	23.2	16.1
607	6-5	91.0	49.92	1.1022	7.2	7.6	2.0	16.1	22.3	15.2
607	6-5	106.0	50.07	1.1045	22.1	13.1	0.0	23.2	27.4	20.4
607	6-5	121.0	50.22	1.1068	14.8	11.7	0.8	19.1	24.6	17.7
607	6-5	136.0	50.37	1.1099	18.7	14.0	0.3	15.7	25.4	18.4
607	6-6	1.0	50.52	1.1145	10.2	10.2	0.7	21.1	23.6	16.5
607	6-6	16.0	50.67	1.1192	7.0	10.4	1.2	19.5	22.0	15.1
607	6-6	31.0	50.82	1.1238	5.6	4.0	1.6	26.7	24.0	15.7
607	6-6	38.0	50.89	1.1260	8.5	9.7	0.3	13.9	22.5	15.7
607	6-6	53.0	51.04	1.1305	0.9	7.2	1.2	16.2	20.2	13.3
607	6-6	61.0	51.12	1.1327	1.4	2.8	0.0	31.2	23.6	15.0
607	6-6	70.0	51.21	1.1348	3.5	8.9	0.7	16.1	20.8	14.1
607	6-6	78.0	51.29	1.1367	5.8	7.2	0.3	18.6	22.4	15.3
607	6-6	91.0	51.42	1.1397	6.5	6.2	4.9	15.4	21.8	14.4
607	6-6	106.0	51.57	1.1432	16.9	7.1	0.3	15.4	25.2	18.3
607	6-6	119.0	51.70	1.1462	10.6	8.8	0.3	27.3	25.0	17.6
607	6-6	136.0	51.87	1.1499	21.8	16.1	0.4	18.8	27.0	19.5
607	6-7	1.0	52.02	1.1531	15.3	11.7	0.3	17.3	24.7	17.8
607	6-7	9.0	52.10	1.1548	14.2	11.9	1.6	29.0	26.0	18.6
607A	7-5	1.0	52.25	1.1582	12.4	14.2	0.7	27.0	24.8	17.8
607A	7-5	15.0	52.40	1.1632	11.2	7.0	1.0	25.1	25.0	17.4
607A	7-5	30.0	52.54	1.1705	9.2	9.2	0.0	27.7	24.5	17.1
607A	7-5	41.0	52.65	1.1748	3.3	14.0	0.7	26.0	20.1	13.7
607A	7-5	45.0	52.69	1.1755	5.8	11.6	0.0	24.3	22.0	15.2
607A	7-5	60.0	52.84	1.1782	1.4	19.1	0.8	16.3	16.6	11.5
607	7-1	16.0	52.99	1.1809	10.0	10.3	0.7	18.9	23.3	16.3
607	7-1	29.0	53.13	1.1832	7.5	14.2	1.1	28.1	22.5	15.7
607	7-1	37.0	53.20	1.1845	12.6	12.1	0.0	22.7	24.5	17.6
607	7-1	53.0	53.36	1.1870	15.6	10.1	0.0	16.7	24.9	18.0
607	7-1	61.0	53.44	1.1881	15.6	12.6	1.7	11.6	23.9	17.0
607	7-1	78.0	53.61	1.1905	12.7	11.3	0.0	8.0	23.4	16.7
607	7-1	91.0	53.74	1.1924	5.7	13.0	0.4	24.0	21.5	14.9
607	7-1	106.0	53.90	1.1945	7.0	13.4	0.0	24.3	22.1	15.5
607	7-1	121.0	54.04	1.1969	6.5	16.4	0.3	15.0	20.2	14.1
607	7-1	136.0	54.19	1.2004	7.3	10.1	0.6	19.0	22.3	15.4
607	7-2	1.0	54.34	1.2039	10.2	10.2	1.2	0.3	22.5	15.7
607	7-2	16.0	54.49	1.2077	2.5	10.1	1.2	28.7	21.2	13.9

TABLE A2. (continued)

DSDP Sample Identification										
Hole	Core-section	Depth, cm	Composite Depth, m	Age, Ma*	Species 1	Species 2	Species 3	Species 4	SSTs, °C	SSTw, °C
607	7-2	24.0	54.57	1.2102	2.7	12.2	1.0	25.8	20.3	13.6
607	7-2	31.0	54.65	1.2124	5.0	9.2	0.4	38.3	24.5	16.8
607	7-2	37.0	54.70	1.2148	6.4	11.6	1.5	27.1	22.4	15.3
607	7-2	53.0	54.86	1.2212	19.4	7.7	0.7	14.3	25.3	18.6
607	7-2	63.0	54.97	1.2248	16.4	9.4	1.0	14.0	24.6	17.8
607	7-2	78.0	55.11	1.2292	13.1	10.5	1.3	15.6	23.7	16.8
607	7-2	91.0	55.24	1.2329	18.3	8.3	0.7	14.6	25.2	18.4
607	7-2	106.0	55.40	1.2373	19.8	10.7	1.5	9.9	24.9	18.0
607	7-2	121.0	55.54	1.2397	6.7	8.1	1.4	31.6	24.2	16.2
607	7-2	136.0	55.69	1.2421	7.8	15.0	0.6	13.8	21.0	14.7
607	7-3	1.0	55.84	1.2445	4.9	12.7	3.6	11.6	19.7	13.2
607	7-3	16.0	55.99	1.2468	8.2	10.5	5.1	15.2	21.3	14.3
607	7-3	29.0	56.13	1.2489	2.7	7.8	12.2	17.2	18.8	11.2
607	7-3	37.0	56.20	1.2507	3.6	7.7	13.1	14.2	18.8	11.4
607	7-3	53.0	56.36	1.2543	6.1	4.0	20.2	9.8	18.4	11.5
607	7-3	63.0	56.47	1.2571	3.7	7.1	18.3	19.5	18.1	10.5
607	7-3	78.0	56.61	1.2612	4.5	8.6	16.3	21.1	18.5	10.9
607	7-3	91.0	56.74	1.2648	2.7	6.5	0.4	22.1	21.7	14.4
607	7-3	106.0	56.90	1.2689	7.1	14.7	0.9	18.7	21.0	14.6
607	7-3	121.0	57.04	1.2730	10.2	19.0	0.3	11.2	21.5	15.0
607	7-3	136.0	57.19	1.2772	6.9	12.9	1.4	23.8	21.8	15.0
607	7-4	1.0	57.34	1.2815	10.6	12.3	1.4	12.3	22.5	15.7
607	7-4	16.0	57.49	1.2857	6.8	12.8	4.1	19.6	20.9	14.0
607	7-4	29.0	57.63	1.2894	6.2	13.1	9.9	9.1	18.9	12.2
607	7-4	37.0	57.70	1.2916	1.6	12.3	16.8	8.5	16.0	9.4
607	7-4	53.0	57.86	1.2958	7.1	11.8	14.5	16.8	18.6	11.8
607	7-4	59.0	57.92	1.2975	4.6	19.7	12.4	15.9	16.4	10.0
607	7-4	69.0	58.02	1.3001	5.3	15.2	5.3	28.8	20.5	13.5
607	7-4	78.0	58.11	1.3024	8.7	14.5	5.5	20.4	21.1	14.1
607	7-4	91.0	58.24	1.3058	4.7	8.3	0.7	16.0	21.4	14.6
607	7-4	100.0	58.33	1.3082	11.0	15.2	3.1	21.4	22.7	15.7
607	7-4	106.0	58.40	1.3097	10.0	15.2	1.6	14.8	21.9	15.2
607	7-4	121.0	58.54	1.3135	12.6	12.0	0.5	16.6	23.7	16.8
607	7-4	136.0	58.69	1.3172	15.3	8.4	1.1	10.2	24.3	17.4
607	7-5	1.0	58.84	1.3213	15.6	12.0	2.7	18.3	24.1	17.2
607	7-5	16.0	58.99	1.3254	4.4	11.3	11.6	20.4	18.8	11.5
607	7-5	30.0	59.13	1.3314	2.8	15.3	17.9	15.3	15.4	9.1
607	7-5	37.0	59.20	1.3355	1.1	14.2	19.5	23.8	15.2	8.0
607	7-5	53.0	59.36	1.3420	3.1	8.7	9.0	31.3	21.1	12.3
607	7-5	61.0	59.44	1.3439	3.4	7.5	9.1	27.5	20.9	12.4
607	7-5	78.0	59.61	1.3468	2.1	12.5	3.9	23.8	19.2	12.3
607	7-5	91.0	59.74	1.3485	1.5	6.6	3.8	25.3	21.0	13.1
607	7-5	106.0	59.90	1.3504	8.2	12.0	1.3	25.1	22.9	15.8
607	7-5	121.0	60.04	1.3523	14.4	15.2	1.1	17.0	24.0	17.0
607	7-5	136.0	60.19	1.3543	18.8	11.4	0.0	14.8	25.4	18.6
607	7-6	1.0	60.34	1.3566	12.2	9.3	1.4	22.9	24.4	17.2
607	7-6	16.0	60.49	1.3590	17.8	10.0	3.1	15.2	24.2	17.5
607	7-6	31.0	60.65	1.3616	12.5	10.3	4.5	18.6	23.0	16.0
607	7-6	37.0	60.70	1.3626	2.7	9.9	16.0	19.4	17.5	10.1
607	7-6	53.0	60.86	1.3653	2.7	13.9	19.6	13.5	15.4	9.1
607	7-6	61.0	60.94	1.3667	4.4	10.9	8.0	18.5	19.5	12.3
607	7-6	69.0	61.02	1.3688	6.2	9.2	9.2	27.8	21.5	13.4
607	7-6	78.0	61.11	1.3711	5.2	8.7	11.7	23.6	20.1	12.2
607	7-6	91.0	61.24	1.3756	2.0	8.2	14.1	19.7	18.2	10.4
607	7-6	106.0	61.40	1.3807	4.1	11.1	19.0	22.2	17.2	10.0
607	7-6	114.0	61.47	1.3832	8.7	13.0	9.4	18.7	20.3	13.3
607	7-6	121.0	61.54	1.3852	12.2	14.1	8.0	19.2	21.7	14.8

TABLE A2. (continued)

DSDP Sample Identification										
Hole	Core-section	Depth, cm	Composite Depth, m	Age, Ma*	Species 1	Species 2	Species 3	Species 4	SSTs, °C	SSTw, °C
607	7-6	136.0	61.69	1.3893	15.7	12.3	1.4	17.2	24.4	17.5
607	7-7	1.0	61.84	1.3935	14.3	16.0	1.4	13.3	23.5	16.5
607	7-7	16.0	61.99	1.3976	18.0	16.1	0.9	20.2	25.8	18.6
607	7-7	24.0	62.07	1.3998	16.6	14.5	1.1	23.1	25.6	18.6
607A	8-5	1.0	62.23	1.4040	6.6	8.9	9.1	11.6	20.1	13.0
607	8-1	5.0	62.38	1.4078	3.1	11.3	6.8	31.3	20.6	12.7
607	8-1	16.0	62.48	1.4104	2.8	8.8	7.7	30.3	21.0	12.5
607	8-1	31.0	62.63	1.4140	1.0	9.9	13.4	36.7	19.7	10.3
607	8-1	38.0	62.70	1.4157	1.7	7.9	12.7	41.1	21.7	11.6
607	8-1	53.0	62.85	1.4172	1.2	11.7	12.8	36.4	19.2	10.4
607	8-1	61.0	62.93	1.4181	3.6	8.9	13.9	23.8	19.0	11.0
607	8-1	78.0	63.10	1.4199	4.1	10.8	13.2	24.9	19.0	11.2
607	8-1	89.0	63.22	1.4212	6.9	8.0	7.2	33.1	23.5	14.7
607	8-1	106.0	63.38	1.4228	4.0	10.3	25.8	16.2	15.2	9.2
607	8-1	113.0	63.45	1.4235	3.3	12.1	26.9	13.8	14.4	8.7
607	8-1	121.0	63.53	1.4242	4.9	8.6	8.6	13.8	19.9	12.6
607	8-1	129.0	63.61	1.4251	5.6	5.6	4.0	24.6	22.8	14.7
607	8-1	136.0	63.68	1.4260	5.1	10.6	4.0	27.0	21.6	14.1
607	8-2	3.0	63.85	1.4281	14.6	15.7	3.0	20.6	24.0	16.9
607	8-2	16.0	63.98	1.4335	11.0	13.0	2.7	15.0	22.4	15.6
607	8-2	29.0	64.11	1.4391	6.7	10.7	5.4	17.4	20.9	13.8
607	8-2	38.0	64.21	1.4421	4.1	7.9	7.2	22.6	20.8	12.9
607	8-2	53.0	64.35	1.4470	11.3	3.3	7.6	17.6	22.9	15.4
607	8-2	61.0	64.43	1.4495	5.4	8.3	8.0	17.4	20.5	13.0
607	8-2	78.0	64.60	1.4552	5.6	13.5	6.9	16.5	19.4	12.6
607	8-2	91.0	64.74	1.4587	6.6	11.0	6.6	12.1	20.2	13.3
607	8-2	106.0	64.89	1.4606	6.3	7.8	8.1	22.7	21.4	13.5
607	8-2	119.0	65.01	1.4615	4.8	7.5	9.2	29.0	21.6	13.0
607	8-2	136.0	65.18	1.4628	9.0	4.1	8.2	23.2	22.9	14.8
607	8-3	1.0	65.33	1.4639	8.4	10.0	14.1	18.4	19.4	12.6
607	8-3	16.0	65.49	1.4654	4.0	8.3	19.9	19.9	17.4	10.1
607	8-3	21.0	65.53	1.4659	3.2	8.6	15.2	21.8	18.4	10.6
607	8-3	31.0	65.64	1.4669	4.0	9.4	5.4	16.4	20.1	13.0
607	8-3	38.0	65.71	1.4677	4.4	8.2	5.1	20.8	21.0	13.5
607	8-3	53.0	65.85	1.4693	8.9	9.9	2.4	13.4	22.1	15.2
607	8-3	63.0	65.96	1.4704	12.3	11.0	1.7	11.3	23.1	16.3
607	8-3	78.0	66.10	1.4746	13.3	10.7	2.6	16.5	23.5	16.6
607	8-3	89.0	66.21	1.4778	9.9	7.4	3.4	12.3	22.6	15.5
607	8-3	106.0	66.39	1.4857	11.8	5.6	2.8	22.0	24.4	16.9
607	8-3	119.0	66.51	1.4917	8.1	7.1	4.2	21.8	22.8	15.2
607	8-3	136.0	66.68	1.4988	11.7	4.5	2.6	19.9	24.4	16.8
607	8-4	1.0	66.83	1.5038	11.6	6.4	3.5	14.2	23.3	16.1
607	8-4	16.0	66.99	1.5088	7.9	12.9	11.4	14.5	19.3	12.5
607	8-4	21.0	67.03	1.5104	6.0	13.8	18.0	13.8	16.9	10.7
607	8-4	31.0	67.14	1.5136	6.8	6.8	2.7	19.5	22.5	15.1
607	8-4	37.0	67.19	1.5153	9.5	6.1	1.4	22.0	24.1	16.5
607	8-4	53.0	67.35	1.5181	20.6	9.8	0.0	19.3	26.1	19.4
607	8-4	61.0	67.43	1.5196	16.1	8.9	1.1	21.8	25.4	18.4
607	8-4	78.0	67.60	1.5222	14.5	8.0	2.1	17.3	24.3	17.3
607	8-4	91.0	67.74	1.5241	9.2	7.5	2.9	11.3	22.5	15.4
607	8-4	106.0	67.89	1.5264	10.3	8.8	11.9	16.5	20.5	13.7
607	8-4	121.0	68.03	1.5287	9.5	8.9	3.9	20.3	22.8	15.5
607	8-4	136.0	68.18	1.5309	9.3	6.9	1.2	19.8	23.6	16.3
607	8-5	1.0	68.33	1.5338	10.5	8.6	2.8	19.8	23.3	16.1
607	8-5	15.0	68.49	1.5367	10.5	6.8	8.4	24.0	22.7	15.0
607	8-5	20.0	68.53	1.5375	8.8	4.6	17.3	24.0	20.1	12.5
607	8-5	31.0	68.64	1.5398	11.2	4.1	9.5	15.6	22.1	14.8

TABLE A2. (continued)

DSDP Sample Identification										
Hole	Core-section	Depth, cm	Composite Depth, m	Age, Ma*	Species 1	Species 2	Species 3	Species 4	SSTs, °C	SSTw, °C
607	8-5	53.0	68.85	1.5444	14.2	8.2	0.7	17.5	24.6	17.6
607	8-5	61.0	68.93	1.5461	13.7	9.7	4.3	21.3	23.7	16.7
607	8-5	78.0	69.10	1.5497	10.7	11.0	1.1	23.5	23.8	16.7
607	8-5	91.0	69.24	1.5525	15.9	15.2	0.0	29.1	27.1	19.9
607	8-5	106.0	69.39	1.5560	17.0	19.5	0.4	23.8	26.7	19.2
607	8-5	121.0	69.53	1.5597	13.7	12.3	1.4	21.6	24.4	17.4
607	8-5	136.0	69.68	1.5634	15.4	4.1	1.5	22.9	25.7	18.4
607	8-6	1.0	69.83	1.5671	4.9	8.5	16.1	16.1	18.3	11.1
607	8-6	16.0	69.99	1.5707	9.4	8.3	14.4	16.3	19.7	13.0
607	8-6	29.0	70.11	1.5739	1.0	14.5	17.7	13.8	14.9	8.4
607	8-6	37.0	70.19	1.5756	0.9	5.9	20.1	22.0	17.5	9.1
607	8-6	53.0	70.35	1.5790	6.2	9.3	14.1	20.3	19.2	11.9
607	8-6	61.0	70.43	1.5806	18.3	7.3	6.4	16.2	23.1	16.8
607	8-6	78.0	70.60	1.5874	5.4	11.7	9.5	15.6	19.1	12.2
607	8-6	89.0	70.71	1.5860	10.6	8.3	13.1	19.6	20.4	13.6
607	8-6	106.0	70.89	1.5892	4.9	7.2	9.2	21.3	20.7	12.8
607	8-6	121.0	71.03	1.5921	4.8	7.9	12.0	23.4	20.1	12.0
607	8-6	136.0	71.18	1.5950	6.5	10.5	7.8	13.1	20.1	13.1
607	8-7	1.0	71.33	1.5979	10.6	11.0	11.0	13.5	20.3	13.7
607	8-7	5.0	71.38	1.5987	8.7	11.6	9.4	14.2	20.2	13.4
607A	9-4	67.0	71.46	1.6004	3.2	12.9	14.5	18.3	17.1	10.2
607A	9-4	75.0	71.54	1.6020	5.4	13.5	24.0	13.1	15.3	9.8
607A	9-4	91.0	71.71	1.6051	5.2	15.1	21.2	9.3	15.8	9.9
607A	9-4	105.0	71.85	1.6078	7.0	12.8	14.4	17.3	18.4	11.7
607A	9-4	121.0	72.00	1.6108	5.0	12.6	10.7	22.6	19.1	11.8
607A	9-4	135.0	72.14	1.6144	4.5	12.9	10.1	20.4	18.7	11.6
607A	9-5	1.0	72.31	1.6185	5.2	19.3	8.8	11.4	17.4	11.0
607A	9-5	15.0	72.44	1.6223	5.2	10.5	8.3	14.9	19.6	12.6
607A	9-5	30.0	72.60	1.6264	6.5	10.1	6.5	20.1	20.9	13.6
607	9-1	1.0	72.71	1.6295	20.5	10.1	1.4	16.9	25.3	18.7
607	9-1	16.0	72.85	1.6338	25.2	8.3	1.1	16.5	25.6	19.4
607	9-1	31.0	73.00	1.6375	24.1	13.3	1.8	20.8	26.6	19.7
607	9-1	53.0	73.22	1.6426	23.4	6.1	2.4	14.9	24.8	18.7

Column identifications for species percentages are as follows: species 1, *Globigerinoides ruber* (white); species 2, *Globigerina bulloides*; species 3, *Neogloboquadrina pachyderma* (sinistral); and species 4, *Globorotalia inflata*.

* Ages based on TP607 time scale.

TABLE A3. Percent $CaCO_3$ Data from Site 609

DSDP Sample Identification					
Hole	Core-section	Depth, cm	Composite Depth, m	Age, Ma*	$CaCO_3$, %
609	1-1	6.0	0.06	0.0000	79.1
609	1-1	31.0	0.31	0.0040	71.4
609	1-1	61.0	0.61	0.0087	40.6
609	1-1	91.0	0.91	0.0134	32.7
609	1-1	121.0	1.21	0.0178	22.7
609	1-2	1.0	1.51	0.0219	10.5
609	1-2	31.0	1.81	0.0261	16.2
609	1-2	61.0	2.11	0.0307	29.0
609	1-2	91.0	2.41	0.0351	23.2
609	1-2	121.0	2.71	0.0395	35.5

TABLE A3. (continued)

DSDP Sample Identification					
Hole	Core-section	Depth, cm	Composite Depth, m	Age, Ma*	$CaCO_3$, %
609	1-3	1.0	3.01	0.0438	31.4
609	1-3	31.0	3.31	0.0485	56.1
609	1-3	61.0	3.61	0.0539	43.1
609	1-3	91.0	3.91	0.0595	19.8
609	1-3	121.0	4.21	0.0660	37.1
609	1-4	1.0	4.51	0.0724	64.2
609	1-4	31.0	4.81	0.0786	78.8
609	1-4	61.0	5.11	0.0845	54.8
609	1-4	91.0	5.41	0.0889	76.1
609	1-4	121.0	5.71	0.0932.	79.3

TABLE A3. (continued)

DSDP Sample Identification			Composite	Age,	$CaCO_3$,
Hole	Core-section	Depth, cm	Depth, m	Ma*	%
609	1-5	1.0	6.01	0.0974	66.2
609	1-5	31.0	6.31	0.1017	61.2
609	1-5	61.0	6.61	0.1056	66.8
609	1-5	79.0	6.79	0.1081	78.6
609B	2-3	60.5	7.09	0.1125	78.3
609B	2-3	90.5	7.39	0.1173	68.8
609B	2-3	120.5	7.69	0.1228	70.1
609B	2-4	1.0	7.99	0.1291	38.4
609B	2-4	31.0	8.30	0.1360	31.8
609B	2-4	61.0	8.60	0.1430	13.9
609	2-1	31.0	8.89	0.1537	15.8
609	2-1	61.0	9.19	0.1649	36.5
609	2-1	91.0	9.49	0.1729	58.0
609	2-1	121.0	9.80	0.1795	28.4
609	2-2	1.0	10.09	0.1842	34.7
609	2-2	31.0	10.39	0.1877	47.8
609	2-2	61.0	10.69	0.1914	64.6
609	2-2	91.0	10.99	0.1956	72.1
609	2-2	121.0	11.30	0.2006	66.6
609	2-3	1.0	11.59	0.2064	75.1
609	2-3	31.0	11.89	0.2133	61.0
609	2-3	61.0	12.19	0.2209	12.9
609	2-3	91.0	12.49	0.2262	35.5
609	2-3	121.0	12.80	0.2314	68.8
609	2-4	1.0	13.09	0.2362	80.1
609	2-4	31.0	13.39	0.2405	43.2
609	2-4	61.0	13.69	0.2444	23.6
609	2-4	91.0	13.99	0.2479	39.4
609	2-4	121.0	14.30	0.2507	23.6
609	2-5	1.0	14.59	0.2533	52.0
609	2-5	31.0	14.89	0.2558	38.7
609	2-5	61.0	15.19	0.2582	43.0
609	2-5	91.0	15.49	0.2605	17.1
609	2-5	121.0	15.80	0.2649	13.1
609	2-6	1.0	16.09	0.2716	67.7
609	2-6	31.0	16.40	0.2794	77.4
609	2-6	61.0	16.69	0.2889	58.9
609	2-6	91.0	16.99	0.3003	53.8
609	2-6	121.0	17.30	0.3039	78.5
609	2-7	1.0	17.59	0.3076	54.3
609B	3-3	31.0	17.90	0.3111	75.3
609B	3-3	61.0	18.19	0.3146	66.2
609B	3-3	91.0	18.49	0.3208	83.3
609B	3-3	121.0	18.80	0.3262	69.6
609B	3-3	135.5	18.94	0.3287	68.1
609B	3-4	0.5	19.09	0.3311	49.6
609B	3-4	15.5	19.24	0.3334	41.6
609B	3-4	31.0	19.40	0.3356	4.6
609B	3-4	45.5	19.54	0.3379	7.0
609B	3-4	61.5	19.70	0.3404	24.1
609B	3-4	75.5	19.84	0.3424	35.9
609B	3-4	91.0	19.99	0.3447	43.2
609B	3-4	105.5	20.14	0.3468	16.4
609B	3-4	121.0	20.30	0.3490	8.9
609B	3-4	135.5	20.44	0.3511	22.6
609B	3-5	1.0	20.59	0.3533	38.8
609B	3-5	15.5	20.74	0.3555	39.9
609B	3-5	31.0	20.90	0.3579	59.0

TABLE A3. (continued)

DSDP Sample Identification			Composite	Age,	$CaCO_3$,
Hole	Core-section	Depth, cm	Depth, m	Ma*	%
609B	3-5	45.5	21.04	0.3603	68.3
609B	3-5	61.0	21.19	0.3629	50.8
609B	3-5	75.5	21.34	0.3655	80.9
609B	3-5	91.0	21.49	0.3685	83.9
609B	3-5	105.5	21.64	0.3716	65.7
609B	3-5	135.5	21.94	0.3785	57.4
609	3-3	91.0	22.24	0.3867	81.0
609	3-3	121.0	22.55	0.3952	85.5
609	3-4	1.0	22.84	0.4034	85.8
609	3-4	31.0	23.14	0.4106	84.3
609	3-4	61.0	23.44	0.4165	81.8
609	3-4	91.0	23.74	0.4215	80.2
609	3-4	121.0	24.05	0.4257	15.4
609	3-5	1.0	24.34	0.4295	31.6
609	3-5	31.0	24.64	0.4333	33.4
609	3-5	45.5	24.79	0.4350	14.0
609	3-5	61.0	24.94	0.4369	12.6
609	3-5	75.5	25.09	0.4390	17.7
609	3-5	91.0	25.24	0.4413	37.5
609	3-5	105.5	25.39	0.4434	28.0
609	3-5	121.0	25.55	0.4459	46.4
609	3-5	135.5	25.69	0.4483	11.9
609	3-6	1.0	25.84	0.4505	16.6
609	3-6	15.5	25.99	0.4520	45.9
609	3-6	31.0	26.14	0.4539	46.6
609	3-6	45.5	26.29	0.4556	31.5
609	3-6	61.0	26.44	0.4577	17.8
609	3-6	75.5	26.59	0.4597	24.3
609B	4-2	15.5	26.73	0.4620	65.1
609B	4-2	31.0	26.89	0.4646	83.5
609B	4-2	45.5	27.03	0.4673	46.6
609B	4-2	61.0	27.19	0.4703	37.7
609B	4-2	75.5	27.33	0.4769	91.3
609B	4-2	91.0	27.49	0.4858	79.2
609B	4-2	121.0	27.79	0.5091	71.5
609B	4-3	1.0	28.09	0.5162	71.7
609B	4-3	31.0	28.39	0.5195	79.4
609B	4-3	61.0	28.69	0.5222	84.8
609B	4-3	91.0	28.99	0.5247	76.4
609B	4-3	121.0	29.29	0.5269	83.3
609B	4-4	1.0	29.59	0.5291	73.7
609B	4-4	31.0	29.89	0.5305	85.1
609B	4-4	61.0	30.19	0.5320	83.1
609B	4-4	91.0	30.49	0.5336	82.3
609B	4-4	121.0	30.79	0.5354	87.3
609B	4-5	1.0	31.09	0.5374	75.4
609B	4-5	31.0	31.39	0.5398	78.5
609	4-3	1.0	31.69	0.5427	34.4
609	4-3	15.5	31.83	0.5439	74.7
609	4-3	31.0	31.99	0.5455	56.2
609	4-3	61.0	32.29	0.5495	57.5
609	4-3	91.0	32.59	0.5548	44.9
609	4-3	121.0	32.89	0.5604	70.6
609	4-4	1.0	33.19	0.5713	73.6
609	4-4	31.0	33.49	0.5848	40.5
609	4-4	61.0	33.79	0.5907	63.4
609	4-4	91.0	34.09	0.5954	56.1
609	4-4	121.0	34.39	0.5992	65.0

TABLE A3. (continued)

DSDP Sample Identification					
Hole	Core-section	Depth, cm	Composite Depth, m	Age, Ma*	$CaCO_3$, %
609	4-5	1.0	34.69	0.6042	65.9
609	4-5	31.0	34.99	0.6091	64.9
609	4-5	61.0	35.29	0.6142	72.7
609	4-5	91.0	35.59	0.6169	51.5
609	4-5	121.0	35.89	0.6199	39.9
609	4-6	1.0	36.19	0.6238	15.6
609B	5-2	121.0	36.49	0.6290	31.8
609B	5-3	1.0	36.79	0.6356	30.9
609B	5-3	31.0	37.09	0.6420	20.1
609B	5-3	61.0	37.39	0.6466	27.5
609B	5-3	91.0	37.69	0.6502	29.4
609B	5-3	121.0	37.99	0.6529	30.3
609B	5-4	1.0	38.29	0.6552	29.8
609B	5-4	31.0	38.59	0.6619	47.2
609B	5-4	61.5	38.90	0.6764	29.4
609B	5-4	91.0	39.19	0.6813	63.1
609B	5-4	121.0	39.49	0.6848	77.9
609	5-3	1.0	39.79	0.6875	71.0
609	5-3	31.0	40.09	0.6892	59.8
609	5-3	61.0	40.39	0.6909	67.3
609	5-3	91.0	40.69	0.6927	63.9
609	5-3	121.0	40.99	0.6945	51.8
609	5-4	1.0	41.29	0.6961	3.8
609	5-4	31.0	41.59	0.6976	4.6
609	5-4	61.0	41.89	0.6997	36.5
609	5-4	91.0	42.19	0.7018	57.4
609	5-4	121.0	42.49	0.7040	42.0
609	5-5	1.0	42.79	0.7066	70.5
609	5-5	31.0	43.09	0.7104	71.5
609	5-5	61.0	43.39	0.7152	29.3
609	5-5	91.0	43.69	0.7186	15.1
609	5-5	105.5	43.83	0.7226	58.8
609	5-5	121.0	43.99	0.7264	67.4
609	5-6	1.0	44.29	0.7328	77.7
609	5-6	31.0	44.59	0.7387	56.5
609	5-6	61.0	44.89	0.7446	16.9
609	5-6	91.0	45.19	0.7485	22.0
609B	6-2	61.0	45.49	0.7502	39.9
609B	6-2	91.0	45.79	0.7521	51.0
609B	6-2	121.0	46.09	0.7540	31.6
609B	6-3	1.0	46.39	0.7561	78.2
609B	6-3	31.0	46.69	0.7583	83.8
609	6-1	31.0	46.99	0.7607	76.7
609	6-1	61.0	47.29	0.7633	62.5
609	6-1	91.0	47.59	0.7661	57.7
609	6-1	121.0	47.89	0.7691	63.9
609	6-2	1.0	48.19	0.7723	65.0
609	6-2	31.0	48.49	0.7757	55.5
609	6-2	61.0	48.79	0.7792	76.4
609	6-2	91.0	49.09	0.7828	63.7
609	6-2	121.0	49.39	0.7863	39.8
609	6-3	1.0	49.69	0.7896	28.9
609	6-3	31.0	49.99	0.7928	18.7
609	6-3	61.0	50.29	0.7959	11.2
609	6-3	91.0	50.59	0.7987	6.0
609	6-3	121.0	50.89	0.8025	6.2
609	6-4	1.0	51.19	0.8069	10.1
609	6-4	31.0	51.49	0.8108	35.3

TABLE A3. (continued)

DSDP Sample Identification					
Hole	Core-section	Depth, cm	Composite Depth, m	Age, Ma*	$CaCO_3$, %
609	6-4	61.0	51.79	0.8144	51.9
609	6-4	91.0	52.09	0.8179	56.5
609	6-4	121.0	52.39	0.8212	45.5
609	6-5	1.0	52.69	0.8245	50.5
609	6-5	31.0	52.99	0.8278	11.4
609	6-5	61.0	53.29	0.8313	33.8
609	6-5	91.0	53.59	0.8354	24.2
609	6-5	121.0	53.89	0.8402	8.1
609	6-6	1.0	54.19	0.8440	48.4
609	6-6	31.0	54.49	0.8479	55.8
609	6-6	61.0	54.79	0.8520	74.5
609	6-6	91.0	55.09	0.8562	78.5
609	6-6	121.0	55.39	0.8598	75.5
609	6-7	1.0	55.69	0.8632	61.5
609	6-7	31.0	55.99	0.8665	45.0
609	6-7	51.0	56.19	0.8688	34.0
609B	7-3	1.0	56.49	0.8722	15.4
609	7-1	31.0	56.79	0.8743	54.3
609	7-1	61.0	57.09	0.8763	60.0
609	7-1	91.0	57.39	0.8782	62.0
609	7-1	121.0	57.69	0.8801	56.0
609	7-2	1.0	57.99	0.8820	59.1
609	7-2	31.0	58.29	0.8839	38.9
609	7-2	61.0	58.59	0.8859	41.9
609	7-2	91.0	58.89	0.8891	15.4
609	7-2	121.0	59.19	0.8958	70.5
609	7-3	1.0	59.49	0.9037	71.5
609	7-3	31.0	59.79	0.9151	53.7
609	7-3	61.0	60.09	0.9237	23.1
609	7-3	91.0	60.39	0.9292	59.2
609	7-3	121.0	60.69	0.9347	15.6
609	7-4	1.0	60.99	0.9381	58.7
609	7-4	31.0	61.29	0.9415	48.3
609	7-4	58.5	61.56	0.9445	71.0
609	7-4	61.0	61.59	0.9448	76.0
609	7-4	91.0	61.89	0.9481	58.1
609	7-4	121.0	62.19	0.9513	62.9
609	7-5	1.0	62.49	0.9544	55.2
609	7-5	31.0	62.79	0.9575	64.4
609	7-5	61.0	63.09	0.9605	48.2
609	7-5	91.0	63.39	0.9634	61.8
609	7-5	121.0	63.69	0.9664	59.6
609	7-6	1.0	63.99	0.9696	25.9
609	7-6	15.5	64.14	0.9716	21.5
609	7-6	31.0	64.29	0.9731	32.4
609	7-6	61.0	64.59	0.9760	72.2
609	7-6	91.0	64.89	0.9789	86.3
609	7-6	121.0	65.19	0.9817	81.1
609	7-7	1.0	65.49	0.9846	61.7
609B	8-3	1.0	65.79	0.9875	60.7
609B	8-3	31.0	66.09	0.9903	62.3
609	8-1	61.0	66.39	0.9930	59.4
609	8-1	91.0	66.69	0.9957	60.3
609	8-1	121.0	66.99	0.9983	62.9
609	8-2	1.0	67.29	1.0008	62.4
609	8-2	31.0	67.59	1.0033	58.6
609	8-2	61.0	67.89	1.0056	64.6
609	8-2	91.0	68.19	1.0079	61.5

TABLE A3. (continued)

DSDP Sample Identification			Composite	Age,	$CaCO_3$,
Hole	Core-section	Depth, cm	Depth, m	Ma*	%
609	8-2	121.0	68.49	1.0102	50.7
609	8-3	1.0	68.79	1.0123	7.2
609	8-3	31.0	69.09	1.0157	18.0
609	8-3	61.0	69.39	1.0190	39.0
609	8-3	91.5	69.69	1.0223	63.3
609	8-3	121.0	69.99	1.0254	45.8
609	8-4	1.0	70.29	1.0286	49.2
609	8-4	31.0	70.59	1.0319	55.9
609	8-4	61.0	70.89	1.0352	49.7
609	8-4	91.0	71.19	1.0386	47.7
609	8-4	121.0	71.49	1.0422	17.8
609	8-5	1.0	71.79	1.0458	10.0
609	8-5	31.0	72.09	1.0478	35.2
609	8-5	61.0	72.39	1.0498	40.1
609	8-5	90.3	72.68	1.0518	16.1
609	8-5	121.0	72.99	1.0539	35.7
609	8-6	1.0	73.29	1.0560	42.0
609	8-6	31.0	73.59	1.0581	56.6
609	8-6	61.0	73.89	1.0602	63.4
609	8-6	91.0	74.19	1.0624	72.2
609B	9-2	0.5	74.49	1.0645	62.7
609B	9-2	30.5	74.79	1.0667	57.0
609B	9-2	60.5	75.09	1.0688	65.2
609B	9-2	91.0	75.39	1.0710	50.4
609B	9-2	121.0	75.69	1.0731	59.7
609B	9-3	1.0	75.99	1.0752	65.2
609B	9-3	31.0	76.29	1.0779	72.4
609	9-1	31.0	76.43	1.0782	71.8
609	9-1	61.0	76.74	1.0802	56.9
609	9-1	91.0	77.03	1.0822	39.8
609	9-1	121.0	77.33	1.0842	24.3
609	9-2	0.8	77.63	1.0861	55.5
609	9-2	31.0	77.93	1.0880	28.0
609	9-2	61.0	78.24	1.0922	42.5
609	9-2	91.0	78.53	1.0963	27.5
609	9-2	121.0	78.83	1.1004	48.3
609	9-3	1.0	79.13	1.1045	77.0
609	9-3	31.0	79.43	1.1087	74.8
609	9-3	61.0	79.74	1.1129	69.0
609	9-3	91.0	80.03	1.1173	45.3
609	9-3	121.0	80.33	1.1218	22.9
609	9-4	1.0	80.63	1.1265	28.9
609	9-4	31.0	80.93	1.1317	31.6
609	9-4	61.0	81.24	1.1369	18.7
609	9-4	91.0	81.53	1.1423	45.3
609	9-4	121.0	81.83	1.1477	82.6
609	9-5	1.0	82.13	1.1532	70.5
609	9-5	32.0	82.44	1.1587	73.4
609	9-5	61.0	82.74	1.1639	23.1
609	9-5	91.0	83.03	1.1691	34.2
609	9-5	121.0	83.33	1.1737	19.5
609	9-6	1.0	83.63	1.1762	22.7
609	9-6	31.0	83.93	1.1786	63.0
609	9-6	61.0	84.24	1.1810	46.0
609	9-6	91.0	84.53	1.1834	72.8
609	9-6	121.0	84.83	1.1857	67.4
609B	10-2	91.0	85.13	1.1880	68.2
609B	10-2	121.0	85.43	1.1903	66.4

TABLE A3. (continued)

DSDP Sample Identification			Composite	Age,	$CaCO_3$,
Hole	Core-section	Depth, cm	Depth, m	Ma*	%
609	10-1	61.0	85.74	1.1926	58.1
609	10-1	91.0	86.03	1.1949	62.3
609	10-1	121.0	86.33	1.1972	62.1
609	10-2	1.0	86.63	1.2000	48.1
609	10-2	15.5	86.78	1.2026	35.2
609	10-2	31.0	86.93	1.2055	23.4
609	10-2	45.5	87.08	1.2099	19.6
609	10-2	61.0	87.24	1.2161	64.4
609	10-2	91.3	87.54	1.2270	88.1
609	10-2	121.0	87.83	1.2319	58.1
609	10-3	1.0	88.13	1.2348	61.4
609	10-3	31.0	88.43	1.2380	61.1
609	10-3	61.0	88.74	1.2413	59.0
609	10-3	91.0	89.03	1.2447	55.0
609	10-3	121.0	89.33	1.2480	52.5
609	10-4	1.0	89.63	1.2510	59.5
609	10-4	31.0	89.93	1.2538	52.6
609	10-4	61.0	90.24	1.2574	40.0
609	10-4	76.5	90.39	1.2602	54.8
609	10-4	91.0	90.53	1.2627	55.4
609	10-4	121.0	90.83	1.2675	49.4
609	10-5	1.0	91.13	1.2719	71.3
609	10-5	31.0	91.43	1.2754	74.1
609	10-5	61.0	91.74	1.2782	79.6
609	10-5	91.0	92.03	1.2803	71.1
609	10-5	121.0	92.33	1.2823	69.3
609	10-6	1.0	92.63	1.2843	72.8
609	10-6	31.0	92.93	1.2862	67.3
609	10-6	61.0	93.24	1.2882	60.8
609B	11-2	31.0	93.54	1.2901	20.3
609B	11-2	61.0	93.84	1.2921	50.0
609B	11-2	91.0	94.14	1.2952	11.4
609B	11-2	121.0	94.44	1.2987	50.6
609B	11-3	1.0	94.74	1.3025	84.4
609B	11-3	31.0	95.04	1.3071	82.0
609B	11-3	61.0	95.34	1.3126	76.3
609B	11-3	91.0	95.64	1.3192	79.9
609B	11-3	121.3	95.94	1.3267	62.5
608B	11-4	0.8	96.24	1.3344	12.2
609B	11-4	31.0	96.54	1.3426	50.1
609B	11-4	61.0	96.84	1.3495	79.7
609B	11-4	91.0	97.14	1.3552	78.2
609	11-2	61.0	97.44	1.3600	74.1
609	11-2	91.0	97.74	1.3643	72.6
609	11-2	121.0	98.04	1.3683	42.0
609	11-2	135.5	98.18	1.3702	27.0
609	11-3	1.0	98.34	1.3722	21.7
609	11-3	15.5	98.49	1.3741	47.7
609	11-3	31.0	98.64	1.3754	50.3
609	11-3	61.0	98.94	1.3778	49.5
609	11-3	91.0	99.24	1.3804	45.9
609	11-3	121.0	99.54	1.3832	69.2
609	11-4	1.0	99.84	1.3860	72.6
609	11-4	31.0	100.14	1.3891	70.3
609	11-4	61.0	100.44	1.3924	67.0
609	11-4	91.0	100.74	1.3959	71.8
609	11-4	121.0	101.04	1.3997	66.7
609	11-5	1.0	101.34	1.4037	74.8

TABLE A3. (continued)

DSDP Sample Identification					
Hole	Core-section	Depth, cm	Composite Depth, m	Age, Ma*	$CaCO_3$, %
609	11-5	31.0	101.64	1.4078	36.5
609	11-5	45.5	101.78	1.4099	41.1
609	11-5	61.0	101.94	1.4120	32.8
609	11-5	91.0	102.24	1.4161	67.8
609	11-5	121.0	102.54	1.4202	58.4
609	11-6	1.0	102.84	1.4242	80.4
609	11-6	24.0	103.07	1.4272	51.4
609B	12-2	31.0	103.37	1.4311	77.0
609B	12-2	61.0	103.67	1.4348	81.6
609B	12-2	91.0	103.97	1.4384	80.5
609B	12-2	121.0	104.27	1.4419	77.6
609	12-1	11.0	104.57	1.4455	66.2
609	12-1	31.0	104.77	1.4478	58.4
609	12-1	61.0	105.07	1.4512	59.9
609	12-1	91.0	105.37	1.4547	59.2
609	12-1	121.0	105.67	1.4582	69.0
609	12-2	1.0	105.97	1.4627	68.5
609	12-2	31.3	106.27	1.4672	35.4
609	12-2	61.0	106.57	1.4715	85.6
609	12-2	91.0	106.87	1.4758	84.9
609	12-2	121.0	107.17	1.4800	71.5
609	12-3	1.0	107.47	1.4841	76.2
609	12-3	31.0	107.77	1.4881	63.2
609	12-3	61.0	108.07	1.4919	72.2
609	12-3	91.0	108.37	1.4958	65.0
609	12-3	105.5	108.51	1.4976	59.2
609	12-3	121.0	108.67	1.4996	47.3
609	12-3	135.5	108.81	1.5012	60.8
609	12-4	1.0	108.97	1.5030	65.5
609	12-4	31.0	109.27	1.5064	71.6
609	12-4	61.0	109.57	1.5099	85.8
609	12-4	91.0	109.87	1.5134	69.9
609	12-4	121.0	110.17	1.5170	73.9
609	12-5	1.0	110.47	1.5207	76.7
609	12-5	31.0	110.77	1.5245	70.9
609	12-5	61.0	111.07	1.5284	73.6
609	12-5	91.0	111.37	1.5323	50.8
609	12-5	105.5	111.51	1.5342	40.0
609	12-5	121.0	111.67	1.5363	30.9
609	12-5	135.5	111.81	1.5376	49.5
609	12-6	1.0	111.97	1.5391	54.8
609	12-6	31.0	112.27	1.5419	52.3
609	12-6	61.0	112.57	1.5445	52.2
609B	13-2	31.0	112.87	1.5471	53.4
609B	13-2	61.0	113.17	1.5496	57.8
609B	13-2	91.0	113.47	1.5521	54.8
609B	13-2	121.0	113.77	1.5544	49.1
609B	13-3	1.0	114.07	1.5567	50.1
609B	13-3	31.0	114.37	1.5589	55.0
609B	13-3	61.0	114.67	1.5610	44.4
609B	13-3	91.0	114.97	1.5630	57.1
609B	13-3	121.0	115.27	1.5651	54.0
609B	13-4	1.0	115.57	1.5671	55.9
609B	13-4	31.0	115.87	1.5691	44.4
609B	13-4	61.0	116.17	1.5711	54.3
609B	13-4	90.8	116.47	1.5742	5.7
609B	13-4	121.0	116.77	1.5774	27.4

TABLE A3. (continued)

DSDP Sample Identification					
Hole	Core-section	Depth, cm	Composite Depth, m	Age, Ma*	$CaCO_3$, %
609	13-2	61.0	117.07	1.5807	29.0
609	13-2	75.5	117.21	1.5824	44.1
609	13-2	91.0	117.37	1.5842	44.9
609	13-2	121.0	117.67	1.5888	36.6
609	13-3	1.0	117.97	1.5939	58.2
609	13-3	31.0	118.27	1.5952	79.0
609	13-3	45.5	118.42	1.5966	55.3
609	13-3	61.0	118.57	1.6024	27.1
609	13-3	91.0	118.87	1.6043	38.0
609	13-3	121.0	119.17	1.6054	48.8
609	13-4	1.0	119.47	1.6071	38.2
609	13-4	15.5	119.61	1.6086	8.7
609	13-4	31.0	119.77	1.6101	65.4
609	13-4	61.0	120.07	1.6120	67.4
609	13-4	91.0	120.37	1.6144	62.9
609	13-4	121.0	120.67	1.6177	62.9
609	13-5	1.0	120.97	1.6210	58.5
609	13-5	31.0	121.27	1.6251	60.6
609	13-5	61.0	121.57	1.6292	69.7
609	13-5	91.0	121.87	1.6354	66.9
609	13-5	121.0	122.17	1.6419	68.7
609	13-6	1.0	122.47	1.6495	67.6

* Ages generated by correlation to tuned site 607 record (as described in this paper).

TABLE A4. Adjusted $\delta^{18}O$ and $\delta^{13}C$ Values for V30-97/CHN82-24-4 Stack

Age, Ma	$\delta^{18}O$, ‰	$\delta^{13}C$, ‰
0.0000	3.28	0.88
0.0029	3.16	0.96
0.0058	3.33	0.88
0.0087	3.66	0.70
0.0119	4.35	0.55
0.0152	5.07	0.15
0.0186	4.99	0.17
0.0230	4.82	0.22
0.0277	4.65	0.59
0.0309	4.80	0.76
0.0338	4.67	0.76
0.0369	4.59	0.72
0.0411	4.53	0.84
0.0454	4.45	0.74
0.0492	4.58	0.97
0.0521	4.45	0.85
0.0551	4.19	0.77
0.0581	4.23	0.32
0.0609	4.55	0.03
0.0637	4.66	-0.01
0.0665	4.37	0.40
0.0713	3.96	1.09

TABLE A4. (continued)

Age, Ma	$\delta^{18}O$, ‰	$\delta^{13}C$, ‰
0.0742	3.99	1.19
0.0766	3.89	1.07
0.0791	3.77	0.91
0.0816	4.04	0.67
0.0844	4.29	0.93
0.0874	4.07	1.01
0.0905	4.02	0.98
0.0936	3.81	1.01
0.0976	3.62	0.83
0.1041	3.97	0.71
0.1104	4.00	0.70
0.1143	3.69	0.91
0.1179	3.62	0.81
0.1209	3.19	0.78
0.1239	3.05	0.92
0.1265	3.84	0.29
0.1315	4.64	0.12
0.1409	4.89	-0.17
0.1465	4.93	-0.25
0.1488	4.97	-0.03
0.1507	4.83	-0.02
0.1525	4.74	0.07
0.1551	4.58	0.14
0.1582	4.59	-0.13
0.1612	4.60	0.09
0.1643	4.38	0.14
0.1670	4.35	0.21

TABLE A4. (continued)

Age, Ma	$\delta^{18}O$, ‰	$\delta^{13}C$, ‰
0.1695	4.30	0.28
0.1713	4.36	0.38
0.1738	4.50	0.17
0.1766	4.42	0.08
0.1793	4.52	0.04
0.1812	4.61	-0.18
0.1839	4.33	0.02
0.1880	4.06	0.61
0.1933	3.73	0.86
0.1965	3.48	0.85
0.2012	3.69	0.84
0.2045	3.80	1.09
0.2071	3.63	0.92
0.2095	3.55	0.97
0.2119	3.56	0.86
0.2151	3.61	0.80
0.2196	3.53	0.38
0.2224	3.56	0.26
0.2250	4.67	0.44
0.2277	4.33	0.53
0.2304	3.99	0.62
0.2332	4.28	0.83
0.2360	3.64	0.79
0.2387	3.45	0.70
0.2399	3.40	0.72
0.2412	3.91	0.56

TABLE A5. Percentages of Species Used in Transfer Function F13x5, and Summer and Winter Temperature Estimates for Core V30-97

Depth, m	Age, Ma	Species 1	Species 2	Species 3	Species 4	SSTs, °C	SSTw, °C
0.02	0.0003	9.9	15.9	1.1	11.9	21.7	15.1
0.05	0.0008	12.8	12.5	2.6	10.6	22.8	16.0
0.10	0.0015	12.2	13.1	2.6	11.0	22.6	15.8
0.12	0.0018	11.5	18.5	1.2	11.8	22.1	15.3
0.15	0.0023	11.6	10.7	1.4	13.3	23.1	16.2
0.20	0.0031	12.2	13.2	2.6	12.9	22.7	15.8
0.25	0.0038	10.4	23.8	2.6	10.1	20.8	13.9
0.30	0.0046	20.8	13.7	4.6	10.3	24.1	17.2
0.35	0.0053	25.6	14.1	6.6	6.9	24.1	17.0
0.38	0.0058	8.7	22.6	5.4	11.7	19.5	12.7
0.40	0.0061	9.0	20.8	10.0	8.7	19.0	12.1
0.43	0.0065	6.0	23.2	12.5	9.4	16.7	10.0
0.45	0.0068	5.5	22.1	20.1	11.2	15.4	9.1
0.50	0.0076	5.2	22.0	13.2	12.3	16.2	9.8
0.55	0.0084	3.4	24.7	35.1	6.0	12.9	6.9
0.60	0.0091	1.4	23.1	30.5	11.2	11.5	6.0
0.62	0.0094	0.8	29.9	19.9	7.8	11.3	5.3
0.65	0.0099	4.1	15.5	35.1	6.6	12.9	8.3
0.70	0.0106	0.6	22.0	28.4	8.0	11.5	6.1
0.75	0.0114	4.7	19.3	32.9	8.6	13.3	8.3
0.76	0.0115	0.7	20.3	9.3	17.0	14.4	8.7
0.80	0.0121	1.9	21.5	16.7	13.1	13.7	7.7
0.85	0.0128	4.0	20.9	8.1	19.6	16.7	10.5
0.90	0.0136	2.9	29.8	13.1	15.1	13.4	7.3
0.95	0.0143	4.2	20.8	8.7	20.2	16.8	10.5

TABLE A5. (continued)

Depth, m	Age, Ma	Species 1	Species 2	Species 3	Species 4	SSTs, °C	SSTw, °C
1.00	0.0151	3.1	24.6	8.7	25.7	15.6	9.9
1.05	0.0158	1.9	42.2	4.1	15.9	10.9	7.7
1.10	0.0166	4.5	20.4	8.4	18.2	17.0	10.7
1.15	0.0173	5.2	17.6	8.3	20.7	18.3	11.6
1.20	0.0180	7.2	17.1	4.5	24.3	20.6	13.9
1.25	0.0188	3.2	21.1	11.4	18.8	15.6	9.4
1.30	0.0195	2.8	21.7	7.5	17.1	15.6	9.8
1.35	0.0203	3.4	25.9	5.9	21.3	15.4	10.1
1.40	0.0210	5.3	21.6	7.8	20.6	17.5	11.2
1.45	0.0218	1.7	25.7	20.1	5.0	12.8	6.7
1.50	0.0226	2.9	20.8	15.8	13.7	14.6	8.5
1.55	0.0233	1.4	19.7	29.9	15.5	11.8	6.3
1.60	0.0241	1.4	26.9	26.2	16.1	11.6	5.5
1.65	0.0249	1.1	18.6	26.0	19.4	12.5	6.5
1.70	0.0256	2.1	23.0	25.8	9.3	12.5	6.8
1.75	0.0264	1.0	21.6	25.4	19.9	12.0	6.1
1.80	0.0272	1.2	24.3	18.9	8.4	12.5	6.7
1.85	0.0280	1.9	29.4	23.9	7.1	12.2	5.8
1.90	0.0288	0.3	28.1	30.9	7.7	10.6	4.8
1.95	0.0296	1.7	38.8	22.7	5.2	12.2	4.6
2.00	0.0304	0.9	38.8	15.9	5.8	10.8	4.5
2.05	0.0313	1.2	33.9	17.0	11.6	11.1	5.1
2.10	0.0321	1.8	36.7	14.3	10.7	11.6	5.5
2.15	0.0329	2.7	27.3	14.5	5.8	13.7	7.5
2.20	0.0338	1.9	42.4	15.5	7.0	11.9	5.0
2.25	0.0347	3.0	23.1	12.7	8.0	14.8	8.7
2.30	0.0355	0.7	25.3	16.2	6.1	12.4	6.7
2.35	0.0364	2.1	26.1	19.5	5.4	13.0	6.9
2.40	0.0373	2.8	25.7	9.6	11.1	14.4	8.6
2.45	0.0382	2.1	23.4	8.6	10.3	14.6	8.9
2.50	0.0392	3.0	22.7	10.5	13.0	15.0	9.1
2.55	0.0401	3.0	15.5	11.6	10.4	16.7	10.3
2.60	0.0410	3.1	17.1	12.0	12.6	16.2	9.9
2.65	0.0420	2.4	15.7	9.8	8.4	16.7	10.4
2.70	0.0429	4.0	23.6	6.7	11.1	16.1	10.2
2.75	0.0439	3.6	21.1	10.8	6.3	15.9	9.7
2.80	0.0449	2.8	23.3	10.7	8.8	14.8	8.9
2.85	0.0458	1.9	34.0	15.7	5.1	12.3	5.8
2.90	0.0468	4.0	18.4	4.8	11.5	17.6	11.6
2.95	0.0478	4.1	14.0	3.2	13.3	19.1	12.8
3.00	0.0489	4.4	19.6	3.0	5.1	17.9	12.1
3.05	0.0499	3.4	18.7	2.9	4.9	17.6	11.9
3.10	0.0509	4.6	13.7	2.0	10.0	19.5	13.3
3.15	0.0519	4.8	11.9	4.5	7.1	19.6	13.1
3.20	0.0530	2.5	31.3	17.0	4.6	13.1	6.4
3.25	0.0540	3.4	26.7	11.9	5.5	14.6	8.4
3.30	0.0551	3.0	22.5	16.0	6.5	14.5	8.4
3.35	0.0562	1.5	33.7	18.3	3.7	12.0	5.4
3.40	0.0572	0.9	32.0	21.6	1.5	11.7	5.2
3.45	0.0583	1.4	32.7	24.6	7.4	11.6	5.0
3.50	0.0594	1.7	28.0	18.9	3.1	12.7	6.5
3.55	0.0605	3.1	30.8	21.7	6.6	13.4	6.4
3.60	0.0616	1.7	29.7	11.1	5.2	12.9	7.2
3.65	0.0628	2.1	22.7	17.9	11.6	13.4	7.5
3.70	0.0639	1.1	20.9	7.3	9.5	14.9	9.4
3.75	0.0651	2.6	10.2	6.3	18.1	19.3	12.1
3.80	0.0662	3.2	17.7	5.3	17.0	17.4	11.3
3.85	0.0674	5.4	27.2	3.5	20.2	17.1	11.6
3.90	0.0686	4.8	21.0	5.2	15.0	17.4	11.4
3.95	0.0698	5.0	31.3	2.1	13.8	16.0	10.7

TABLE A5. (continued)

Depth, m	Age, Ma	Species 1	Species 2	Species 3	Species 4	SSTs, °C	SSTw, °C
4.00	0.0710	5.0	20.8	5.2	13.6	17.5	11.5
4.05	0.0723	6.0	30.6	3.0	15.5	17.0	11.2
4.10	0.0735	2.2	26.2	6.6	11.4	14.2	8.9
4.15	0.0748	3.4	27.7	2.3	14.2	15.2	10.3
4.20	0.0760	2.8	24.3	2.2	12.5	15.7	10.7
4.25	0.0773	4.5	29.4	1.4	11.9	15.9	10.8
4.30	0.0786	4.7	26.8	3.7	12.6	16.3	10.7
4.35	0.0799	5.2	29.7	3.4	9.2	16.3	10.5
4.40	0.0812	3.9	24.4	7.4	9.8	15.8	9.8
4.45	0.0825	4.8	33.1	6.1	7.7	15.4	9.1
4.50	0.0838	3.9	31.7	7.4	6.5	14.7	8.6
4.55	0.0851	4.6	21.0	2.3	15.1	17.7	12.1
4.60	0.0864	5.0	15.0	2.1	10.3	19.4	13.2
4.65	0.0877	4.9	9.4	1.6	13.6	20.9	14.2
4.70	0.0890	5.2	9.8	1.3	15.5	21.1	14.4
4.75	0.0903	4.0	12.6	1.2	15.0	19.8	13.5
4.80	0.0916	8.1	8.7	1.7	13.9	22.3	15.3
4.85	0.0929	6.5	11.0	1.6	14.9	21.3	14.6
4.90	0.0943	5.4	9.5	0.0	18.9	21.8	14.9
4.95	0.0959	9.1	8.5	0.0	19.1	23.4	16.4
5.00	0.0976	6.1	23.9	3.7	14.4	17.9	11.9
5.05	0.0993	8.9	25.0	1.7	14.4	20.0	13.6
5.09	0.1007	5.1	30.4	2.4	11.0	16.2	10.6
5.13	0.1021	2.8	27.4	5.2	10.2	14.6	9.3
5.17	0.1035	3.5	26.5	6.8	11.5	15.1	9.4
5.21	0.1049	4.5	21.4	8.6	9.8	16.6	10.4
5.25	0.1062	5.6	24.4	4.5	11.5	17.3	11.3
5.29	0.1076	7.3	21.1	5.4	12.5	18.8	12.4
5.34	0.1093	2.8	23.8	7.6	12.8	15.1	9.4
5.38	0.1106	2.3	18.5	5.7	15.7	16.5	10.6
5.42	0.1120	5.4	0.0	1.5	23.6	24.5	15.9
5.46	0.1133	3.6	18.4	2.7	25.2	18.5	12.6
5.50	0.1147	4.7	19.3	5.7	18.3	17.8	11.6
5.54	0.1160	5.6	15.5	2.0	28.8	21.2	14.6
5.58	0.1173	9.0	26.0	1.6	19.0	20.5	14.0
5.62	0.1187	11.5	20.7	1.3	22.7	23.1	16.3
5.66	0.1200	9.1	19.7	4.3	22.2	21.1	14.3
5.70	0.1213	18.8	19.7	2.2	5.3	25.0	16.9
5.74	0.1227	14.9	24.2	3.7	20.9	25.1	16.8
5.78	0.1240	16.4	20.0	2.7	19.3	25.0	17.4
5.82	0.1253	9.8	26.4	6.1	19.6	20.8	13.4
5.86	0.1266	6.3	32.1	8.0	17.1	17.1	10.3
5.90	0.1279	5.0	39.6	11.7	7.5	15.6	7.6
5.94	0.1293	0.0	55.5	7.9	3.9	8.5	5.5
5.98	0.1306	1.7	44.7	17.3	4.3	12.0	4.7
6.02	0.1318	2.5	44.8	10.5	9.4	12.1	6.2
6.06	0.1330	2.5	39.3	5.0	10.0	12.2	7.4
6.10	0.1342	4.0	21.5	5.2	16.9	16.8	11.0
6.20	0.1373	1.6	23.6	1.6	15.5	15.1	10.4
6.25	0.1388	1.4	21.3	0.6	25.0	16.3	11.6
6.35	0.1419	5.6	16.2	6.9	22.6	19.3	12.5
6.40	0.1435	3.4	31.0	2.9	13.0	14.5	9.6
6.45	0.1452	4.2	18.6	2.0	14.7	18.1	12.4
6.50	0.1469	3.1	22.7	1.0	20.3	16.7	11.7
6.55	0.1485	6.1	15.7	4.1	16.3	19.6	13.1
6.60	0.1502	3.3	24.8	3.6	11.9	15.7	10.4
6.65	0.1518	2.9	41.1	3.8	4.1	12.9	7.8
6.70	0.1534	1.4	33.1	6.3	4.3	12.5	7.5
6.75	0.1551	1.5	33.5	9.2	4.8	12.2	6.8
6.80	0.1566	1.8	35.7	12.4	4.2	12.1	6.0

TABLE A5. (continued)

Depth, m	Age, Ma	Species 1	Species 2	Species 3	Species 4	SSTs, °C	SSTw, °C
6.85	0.1582	2.7	26.3	15.6	2.5	14.0	7.8
6.90	0.1598	1.4	26.3	15.7	3.1	13.1	7.1
6.95	0.1614	1.2	22.1	15.1	4.6	13.8	7.9
7.00	0.1629	2.9	23.5	10.4	5.3	15.1	9.1
7.05	0.1645	3.4	23.1	7.5	7.1	15.8	9.9
7.10	0.1659	4.0	31.0	5.5	5.9	15.0	9.2
7.15	0.1673	6.0	20.4	4.5	14.1	18.4	12.2
7.20	0.1687	4.8	19.3	2.8	13.9	18.2	12.3
7.25	0.1700	3.1	22.0	2.5	14.9	16.5	11.2
7.30	0.1712	3.5	19.4	7.8	11.6	16.6	10.5
7.35	0.1728	1.1	28.9	8.5	9.3	12.5	7.4
7.40	0.1744	3.0	20.9	8.6	10.7	15.8	9.8
7.45	0.1762	1.4	20.0	15.7	9.4	14.0	8.0
7.50	0.1780	1.3	21.5	7.7	11.2	14.7	9.2
7.55	0.1796	1.6	21.6	12.9	10.9	14.1	8.2
7.60	0.1808	1.0	15.3	4.4	22.0	17.4	11.1
7.65	0.1818	1.2	11.7	2.4	20.4	18.9	12.4
7.70	0.1826	1.5	13.2	5.3	16.6	17.9	11.4
7.75	0.1835	2.5	17.5	5.8	17.0	17.0	10.9
7.80	0.1844	1.9	20.3	3.5	25.7	16.6	11.2
7.85	0.1853	1.7	21.2	3.5	24.6	16.1	10.8
7.90	0.1861	2.6	20.1	0.7	25.8	17.6	12.5
7.95	0.1870	2.1	26.3	3.4	16.4	14.4	9.7
8.00	0.1879	3.3	27.7	2.1	17.5	15.2	10.5
8.05	0.1890	3.4	32.0	4.8	14.3	14.1	9.0
8.10	0.1902	7.2	25.2	1.4	14.5	18.8	12.8
8.15	0.1913	8.6	20.7	1.8	13.5	20.3	13.9
8.20	0.1925	5.3	26.5	2.1	18.8	17.2	11.9
8.25	0.1940	9.3	11.4	4.6	16.5	21.7	14.8
8.30	0.1969	5.8	11.2	5.5	20.7	20.6	13.5
8.35	0.2014	7.3	10.6	4.2	28.0	22.7	15.0
8.40	0.2046	3.6	14.1	4.5	23.4	19.3	12.6
8.45	0.2072	4.1	13.1	4.1	26.0	20.2	13.2
8.50	0.2096	5.4	13.7	4.8	20.5	20.0	13.1
8.55	0.2120	3.9	19.3	9.8	13.4	16.5	10.3
8.60	0.2144	3.1	27.1	9.7	9.4	14.4	8.5
8.65	0.2171	2.3	32.6	11.5	7.3	12.8	6.8
8.70	0.2197	4.1	21.1	5.0	16.8	17.0	11.2
8.75	0.2224	3.5	23.0	4.4	15.0	16.2	10.6
8.80	0.2250	3.8	15.1	4.5	16.4	18.6	12.2
8.85	0.2277	5.8	14.8	4.4	20.1	19.9	13.2
8.90	0.2304	4.4	15.3	2.7	22.0	19.5	13.1
8.95	0.2332	6.1	12.8	3.4	18.0	20.5	13.8
9.00	0.2360	7.5	22.6	2.2	12.6	19.2	13.0
9.05	0.2387	8.5	21.4	4.7	11.1	19.6	12.9
9.10	0.2399	9.1	23.1	2.9	10.4	20.0	13.4
9.15	0.2412	3.8	27.7	7.6	5.8	15.2	9.2

Column identifications for species percentages are as follows: species 1, *Globigerinoides ruber* (white); species 2, *Globigerina bulloides*; species 3, *Neogloboquadrina pachyderma* (sinistral); and species 4, *Globorotalia inflata*.

TABLE A6. Percent $CaCO_3$ for Core V30-97

Depth, m	Age, Ma	$CaCO_3$, %
0.00	0.0000	82.8
0.02	0.0003	85.0
0.04	0.0006	83.7
0.06	0.0009	85.2
0.08	0.0012	84.4
0.10	0.0015	84.6
0.12	0.0018	83.9
0.14	0.0021	84.7
0.16	0.0024	82.6
0.18	0.0027	81.8
0.20	0.0031	83.0
0.22	0.0034	81.7
0.24	0.0037	81.4
0.26	0.0040	81.0
0.28	0.0043	78.8
0.30	0.0046	78.3
0.32	0.0049	77.7
0.34	0.0052	73.7
0.36	0.0055	70.3
0.38	0.0058	68.7
0.40	0.0061	65.9
0.42	0.0064	69.0
0.44	0.0067	64.2
0.46	0.0070	67.1
0.48	0.0073	63.2
0.50	0.0076	58.7
0.52	0.0079	63.1
0.54	0.0082	57.3
0.56	0.0085	62.6
0.59	0.0090	55.8
0.62	0.0094	56.1
0.64	0.0097	53.4
0.66	0.0100	52.2
0.68	0.0103	55.2
0.70	0.0106	52.1
0.72	0.0109	53.1
0.74	0.0112	57.5
0.76	0.0115	49.5
0.78	0.0118	57.0
0.80	0.0121	57.8
0.82	0.0124	58.4
0.84	0.0127	58.0
0.86	0.0130	58.6
0.88	0.0133	59.4
0.96	0.0145	60.4
0.98	0.0148	60.7
1.00	0.0151	59.4
1.02	0.0154	60.0
1.04	0.0157	59.8
1.06	0.0160	58.5
1.08	0.0163	56.4
1.10	0.0166	53.7
1.12	0.0169	53.2
1.14	0.0172	54.0
1.16	0.0175	51.4
1.18	0.0177	50.7
1.20	0.0180	53.5
1.22	0.0183	52.4
1.24	0.0186	51.5

TABLE A6. (continued)

Depth, m	Age, Ma	$CaCO_3$, %
1.26	0.0189	51.3
1.28	0.0192	54.2
1.30	0.0195	53.3
1.32	0.0198	52.8
1.40	0.0210	45.0
1.42	0.0213	47.4
1.44	0.0216	47.0
1.46	0.0220	48.4
1.48	0.0223	49.1
1.50	0.0226	50.5
1.52	0.0229	45.9
1.54	0.0232	47.7
1.56	0.0235	49.4
1.58	0.0238	44.1
1.60	0.0241	53.0
1.62	0.0244	56.0
1.64	0.0247	54.9
1.66	0.0250	54.5
1.68	0.0253	54.9
1.70	0.0256	58.7
1.72	0.0260	66.5
1.74	0.0263	55.3
1.76	0.0266	56.3
1.78	0.0269	56.3
1.80	0.0272	51.7
1.82	0.0275	44.9
1.84	0.0278	54.3
1.86	0.0282	54.1
1.88	0.0285	53.0
1.90	0.0288	54.4
1.92	0.0291	55.5
1.94	0.0295	55.3
1.96	0.0298	56.9
1.98	0.0301	58.6
2.00	0.0304	58.9
2.02	0.0308	63.0
2.04	0.0311	62.1
2.06	0.0314	65.2
2.08	0.0318	65.3
2.10	0.0321	64.1
2.12	0.0324	61.0
2.14	0.0328	62.6
2.16	0.0331	62.2
2.18	0.0334	62.1
2.20	0.0338	63.0
2.22	0.0341	61.1
2.24	0.0345	64.4
2.26	0.0348	65.4
2.28	0.0352	62.8
2.30	0.0355	63.8
2.32	0.0359	61.4
2.34	0.0362	61.9
2.36	0.0366	61.4
2.38	0.0369	58.5
2.40	0.0373	63.1
2.42	0.0377	69.4
2.44	0.0381	67.2
2.46	0.0384	62.1
2.48	0.0388	68.9

TABLE A6. (continued)

Depth, m	Age, Ma	$CaCO_3$, %
2.50	0.0392	75.4
2.52	0.0395	59.8
2.54	0.0399	68.3
2.56	0.0403	66.7
2.58	0.0406	65.3
2.60	0.0410	66.1
2.62	0.0414	66.6
2.64	0.0418	64.8
2.66	0.0422	65.4
2.68	0.0425	65.8
2.72	0.0433	65.7
2.74	0.0437	64.9
2.76	0.0441	63.5
2.78	0.0445	67.1
2.80	0.0449	65.0
2.84	0.0456	57.6
2.86	0.0460	59.2
2.88	0.0464	71.8
2.90	0.0468	73.1
2.92	0.0472	74.0
2.94	0.0476	74.7
2.96	0.0480	76.7
2.98	0.0485	77.9
3.00	0.0489	76.1
3.02	0.0493	76.3
3.04	0.0497	76.0
3.06	0.0501	76.9
3.08	0.0505	76.0
3.10	0.0509	76.4
3.12	0.0513	75.9
3.14	0.0517	76.4
3.16	0.0521	75.3
3.18	0.0526	73.6
3.20	0.0530	67.0
3.22	0.0534	63.7
3.24	0.0538	66.8
3.26	0.0542	70.3
3.28	0.0547	69.3
3.30	0.0551	66.3
3.32	0.0555	66.2
3.34	0.0559	58.7
3.36	0.0564	57.3
3.38	0.0568	54.4
3.40	0.0572	55.5
3.42	0.0577	53.3
3.44	0.0581	54.5
3.46	0.0585	56.1
3.48	0.0590	58.2
3.50	0.0594	55.6
3.52	0.0599	56.6
3.54	0.0603	57.0
3.56	0.0607	57.1
3.58	0.0612	62.1
3.60	0.0616	62.8
3.62	0.0621	58.8
3.64	0.0625	59.1
3.66	0.0630	59.6
3.68	0.0634	61.5
3.70	0.0639	66.5
3.72	0.0644	65.2

TABLE A6. (continued)

Depth, m	Age, Ma	$CaCO_3$, %
3.74	0.0648	67.1
3.76	0.0653	69.5
3.78	0.0658	69.7
3.80	0.0662	71.5
3.82	0.0667	70.6
3.84	0.0672	74.4
3.86	0.0676	77.9
3.88	0.0681	77.1
3.90	0.0686	77.5
3.92	0.0691	77.5
3.94	0.0696	77.1
3.96	0.0701	77.5
3.98	0.0705	79.6
4.00	0.0710	80.7
4.02	0.0715	82.0
4.04	0.0720	81.2
4.06	0.0725	80.6
4.08	0.0730	79.8
4.10	0.0735	82.7
4.12	0.0740	86.9
4.14	0.0745	86.2
4.16	0.0750	86.4
4.18	0.0755	88.3
4.20	0.0760	87.0
4.22	0.0765	88.3
4.24	0.0771	88.4
4.26	0.0776	88.1
4.28	0.0781	88.5
4.30	0.0786	86.8
4.32	0.0791	86.7
4.34	0.0796	86.8
4.36	0.0802	85.9
4.38	0.0807	86.1
4.40	0.0812	85.8
4.42	0.0817	82.3
4.44	0.0823	81.9
4.46	0.0828	82.4
4.48	0.0833	78.8
4.50	0.0838	78.1
4.52	0.0844	84.6
4.54	0.0849	87.5
4.56	0.0854	85.4
4.58	0.0859	86.9
4.60	0.0864	89.1
4.62	0.0870	89.1
4.64	0.0875	88.5
4.66	0.0880	89.2
4.68	0.0885	89.2
4.70	0.0890	88.3
4.72	0.0895	88.6
4.74	0.0901	87.8
4.76	0.0906	88.6
4.78	0.0911	87.8
4.80	0.0916	87.6
4.82	0.0921	88.1
4.84	0.0926	84.8
4.86	0.0931	88.3
4.88	0.0936	89.1
4.92	0.0949	88.2
4.94	0.0956	89.3
4.96	0.0963	89.6

TABLE A6. (continued)

Depth, m	Age, Ma	$CaCO_3$, %
4.98	0.0969	89.1
5.00	0.0976	88.8
5.02	0.0983	88.1
5.04	0.0990	88.2
5.06	0.0997	88.0
5.08	0.1004	87.4
5.10	0.1011	87.3
5.12	0.1018	85.7
5.14	0.1025	83.5
5.16	0.1032	83.1
5.18	0.1039	83.5
5.20	0.1045	84.5
5.22	0.1052	84.6
5.24	0.1059	85.5
5.26	0.1066	84.0
5.28	0.1073	83.6
5.30	0.1079	84.1
5.32	0.1086	82.7
5.34	0.1093	81.0
5.36	0.1100	83.0
5.38	0.1106	86.2
5.40	0.1113	85.8
5.42	0.1120	86.8
5.44	0.1126	88.4
5.46	0.1133	87.7
5.48	0.1140	87.6
5.50	0.1147	86.1
5.52	0.1153	81.1
5.54	0.1160	87.2
5.56	0.1167	88.1
5.58	0.1173	87.1
5.60	0.1180	88.5
5.62	0.1187	88.1
5.64	0.1193	88.3
5.66	0.1200	87.9
5.68	0.1207	88.4
5.70	0.1213	87.8
5.72	0.1220	88.6
5.74	0.1227	88.8
5.76	0.1233	88.1
5.78	0.1240	87.2
5.80	0.1247	87.1
5.82	0.1253	83.2
5.84	0.1260	85.7
5.86	0.1266	76.2
5.88	0.1273	73.3
5.90	0.1279	72.7
5.92	0.1286	67.2
5.94	0.1293	65.2
5.96	0.1299	63.8
5.98	0.1306	62.2
6.00	0.1312	62.4
6.02	0.1318	66.2
6.04	0.1324	67.5
6.06	0.1330	66.9
6.08	0.1336	66.7
6.10	0.1342	67.3
6.12	0.1349	65.0
6.14	0.1355	66.8
6.16	0.1361	66.6

TABLE A6. (continued)

Depth, m	Age, Ma	$CaCO_3$, %
6.18	0.1367	68.7
6.20	0.1373	68.6
6.22	0.1379	67.4
6.24	0.1385	66.5
6.26	0.1391	64.9
6.28	0.1397	64.6
6.30	0.1403	64.7
6.32	0.1409	64.4
6.34	0.1415	68.8
6.36	0.1422	66.3
6.38	0.1429	65.8
6.40	0.1435	65.0
6.42	0.1442	67.0
6.44	0.1449	72.8
6.46	0.1455	74.4
6.48	0.1462	72.0
6.50	0.1469	72.9
6.52	0.1475	73.9
6.54	0.1482	72.0
6.56	0.1489	73.3
6.58	0.1495	64.6
6.60	0.1502	72.9
6.62	0.1509	71.0
6.64	0.1515	72.0
6.66	0.1522	71.2
6.68	0.1528	76.6
6.70	0.1534	70.4
6.72	0.1541	69.4
6.74	0.1547	68.8
6.76	0.1554	66.1
6.78	0.1560	62.1
6.80	0.1566	63.7
6.82	0.1573	58.5
6.84	0.1579	58.3
6.86	0.1586	59.6
6.88	0.1592	62.3
6.90	0.1598	58.1
6.92	0.1604	59.3
6.94	0.1611	55.7
6.96	0.1617	64.4
6.98	0.1623	67.0
7.00	0.1629	66.0
7.02	0.1636	64.4
7.04	0.1642	65.7
7.06	0.1648	68.9
7.08	0.1653	69.0
7.10	0.1659	68.6
7.12	0.1665	71.0
7.14	0.1671	69.5
7.16	0.1676	73.7
7.18	0.1681	74.5
7.20	0.1687	78.4
7.22	0.1692	79.2
7.24	0.1697	80.8
7.26	0.1702	80.8
7.28	0.1707	79.2
7.30	0.1712	78.4
7.32	0.1718	79.5
7.34	0.1724	73.5
7.36	0.1731	72.7

TABLE A6. (continued)

Depth, m	Age, Ma	$CaCO_3$, %
7.38	0.1737	71.1
7.40	0.1744	68.8
7.42	0.1751	68.2
7.44	0.1758	65.9
7.46	0.1766	68.4
7.48	0.1773	68.0
7.50	0.1780	67.4
7.52	0.1787	67.6
7.54	0.1793	67.6
7.56	0.1798	64.1
7.58	0.1803	66.5
7.60	0.1808	67.5
7.62	0.1813	67.3
7.64	0.1816	68.1
7.66	0.1820	70.0
7.68	0.1823	71.3
7.70	0.1826	70.8
7.72	0.1830	67.8
7.74	0.1833	67.8
7.76	0.1837	64.6
7.78	0.1840	65.9
7.80	0.1844	67.6
7.82	0.1847	63.4
7.84	0.1851	64.0
7.86	0.1854	66.5
7.88	0.1858	67.0
7.90	0.1861	70.9
7.92	0.1865	72.6
7.94	0.1868	72.8
7.96	0.1872	74.4
7.98	0.1875	74.8
8.00	0.1879	77.3
8.02	0.1883	76.8
8.04	0.1888	75.8
8.06	0.1892	73.1
8.08	0.1897	75.8
8.10	0.1902	81.6
8.12	0.1906	82.5
8.14	0.1911	83.3
8.16	0.1915	85.4
8.18	0.1920	88.1
8.20	0.1925	86.0
8.22	0.1929	86.6
8.24	0.1935	86.7
8.26	0.1946	84.5
8.28	0.1956	82.5
8.30	0.1969	80.3
8.32	0.1987	82.1
8.34	0.2006	80.6
8.36	0.2021	86.1
8.38	0.2034	87.5
8.40	0.2046	86.3
8.42	0.2057	86.1
8.44	0.2067	86.9
8.46	0.2077	86.3
8.48	0.2086	86.6
8.50	0.2096	85.9
8.52	0.2106	85.4
8.54	0.2115	84.8
8.56	0.2125	83.7

TABLE A6. (continued)

Depth, m	Age, Ma	$CaCO_3$, %
8.58	0.2135	79.8
8.60	0.2144	75.7
8.62	0.2154	72.6
8.64	0.2165	67.5
8.66	0.2176	63.5
8.68	0.2187	65.8
8.70	0.2197	64.7
8.72	0.2208	72.7
8.74	0.2218	72.0
8.76	0.2229	70.5
8.78	0.2240	70.9
8.80	0.2250	71.6
8.82	0.2261	70.5
8.84	0.2271	71.7
8.86	0.2282	73.3
8.88	0.2293	75.4
8.90	0.2304	72.1
8.92	0.2315	80.5
8.94	0.2326	82.4
8.96	0.2338	82.5
8.98	0.2349	82.0
9.00	0.2360	82.7
9.02	0.2371	82.8
9.04	0.2382	80.2
9.06	0.2389	82.9
9.08	0.2394	80.7
9.10	0.2399	82.5
9.12	0.2404	80.8
9.14	0.2409	78.2
9.16	0.2414	76.5
9.18	0.2419	73.9

Acknowledgments. We thank J. Munkelt, C. Hardy, and K. McIntyre for efforts in the laboratory, B. Rasmussen for help assembling the manuscript, and especially A. Esmay for data processing and figure production. We thank George Kukla and Alan Mix for critical comments. This research was funded by National Science Foundation grants OCE-8219862 and OCE-8521514 from the Marine Geology and Geophysics Program in the Ocean Sciences Section. We also acknowledge the support of Lamont-Doherty through the Doherty Scientist Program. Lamont-Doherty Geological Observatory contribution # 4454.

REFERENCES

Backman, J., Pliocene biostratigraphy of DSDP sites 111 and 116 from the North Atlantic Ocean and the age of the northern hemisphere glaciation, *Geology, 32,* 115-137, 1979.

Backman, J., and N. J. Shackleton, Quantitative biochronology of Pliocene and Early Pleistocene - calcareous nannofossils from the Atlantic, Indian and Pacific Oceans, *Mar. Micropal., 8,* 141-170, 1983.

Berger, A. L., Long-term variations of caloric solar radiation resulting from the Earth's orbital elements, *Quat. Res., 9,* 139-167, 1978.

Black, K. P., C. S. Nelson, and C. H. Hendy, A spectral analysis procedure for dating Quaternary deep-sea cores and its application to a high-resolution Brunhes record from the southwest Pacific, *Mar. Geol., 83,* 21-30, 1988.

Boyle, E. A., and L. D. Keigwin, Comparison of Atlantic and Pacific paleochemical records for the last 215,000 years: Changes in deep ocean circulation and chemical inventories, *Earth Planet. Sci. Lett., 76,* 135-150, 1985.

Broccoli, A. J., and S. Manabe, The influence of continental ice, atmospheric CO_2, and land albedo on the climate of the last glacial maximum, *Clim. Dyn., 1,* 87-99, 1987.

Clement, B. M., and D. V. Kent, Geomagnetic polarity transition records from five hydraulic piston core sites in the North Atlantic, *Initial Rep. Deep Sea Drill. Proj., 94,* 831-852, 1986.

Clement, B. M., and D. V. Kent, Short polarity intervals within the Matuyama: Transitional field records from hydraulic piston cored sediments from the North Atlantic, *Earth Planet. Sci. Lett., 81,* 253-264, 1987.

Clement, B. M., and F. Robinson, The magnetostratigraphy of leg 94 sediments, *Initial Rep. Deep Sea Drill. Proj., 94,* 635-650, 1986.

Hays, J. D., J. Imbrie, and N. J. Shackleton, Variations in the Earth's orbit: Pacemaker of the ice ages, *Science, 194,* 1121-1132, 1976.

Hulsemann, J., Notes: On the routine analysis of carbonates in unconsolidated sediments, *J. Sediment. Petrol., 2,* 622-625, 1966.

Imbrie, J., A theoretical framework for the Pleistocene ice ages, *J. Geol. Soc. London, 142,*417-432, 1985.

Imbrie, J., and J. Z. Imbrie, Modeling the climatic response to orbital variations, *Science, 207,* 943-953, 1980.

Imbrie, J., J. Hays, D. Martinson, A. McIntyre, A. Mix, J. Morley, N. Pisias, W. Prell, and N. J. Shackleton, The orbital theory of Pleistocene climate: Support from a revised chronology of the marine $\delta^{18}O$ record, in *Milankovitch and Climate,* Part I, edited by A. Berger et al., pp. 269-305, D. Reidel, Hingham, Mass., 1984.

Keffer, T., D. G. Martinson, and B. H. Corliss, The position of the Gulf Stream during Quaternary glaciations, *Science, 241,* 440-442, 1988.

Kent, D. V., Post-depositional remanent magnetization in deep-sea sediment, *Nature, 246,* 32-34, 1973.

Kukla, G. J., Correlation between loesses and deep-sea sediments, *Geol. Foeren. Stockholm Foerh., 92,* 148-180, 1970.

Kukla, G. J., Loess stratigraphy in Central China and correlation with an extended oxygen isotope stage scale, *Quat. Sci. Rev., 6,* 191-219, 1987.

Kutzbach, J. E., Monsoon climate of the early Holocene: Climatic experiment using the Earth's orbital parameters for 9000 years ago, *Science, 214,* 59-61, 1981.

Kutzbach, J. E., and P. J. Guetter, The influence of changing orbital parameters and surface boundary conditions on climate simulations for the past 18,000 years, *J. Atmos. Sci., 43,* 1726-1759, 1984.

Maasch, K. A., Statistical detection of the mid-Pleistocene transition, *Clim. Dyn., 2,* 133-143, 1988.

Manabe, S., and A. J. Broccoli, The influence of continental ice sheets on the climate of an ice age, *J. Geophys, Res., 90,* 2167-2190, 1985.

Mankinen, E. A., and G. B. Dalrymple, Revised geomagnetic polarity time scale for the interval 0-5 m.y. B.P., *J. Geophys. Res., 84,* 615-626, 1979.

Mankinen, E. A., and C. S. Grommé, Paleomagnetic data from the Coso Range, California, and current status of the Cobb Mountain normal Geomagnetic Polarity Event, *Geophys. Res. Lett., 9,* 1279-1282, 1982.

Mankinen, E. A., J. M. Donnelly-Nolan, C. S. Grommé, and B. C. Hearn, Jr., Paleomagnetism of the Clear Lake volcanics and new limits on the age of the Jaramillo normal-polarity event, *U.S. Geol. Surv. Prof. Pap. 1141,* 67-82, 1980.

Martinson, D. G., W. Menke, and P. Stoffa, An inverse approach to signal correlation, *J. Geophys. Res., 87,* 4807-4818, 1982.

Martinson, D. G., N. G. Pisias, J. D. Hays, J. Imbrie, T. C. Moore, and N. J. Shackleton, Age dating and the orbital theory of the ice ages: development of a high-resolution 0 to 300,000-year chronostratigraphy, *Quat. Res., 27,* 1-29, 1987.

Milankovitch, M., Kanon der Erdbestrahlung und seine Andwendung auf das Eiszeitenproblem, *Royal Serb. Acad., Sp. Publ. 133,* Belgrade, p. 1-633, 1941. English translation published in 1969 by Israel Program for Scientific Translations; available from U.S. Department of Commerce.

Mix, A. C., and R. F. Fairbanks, North Atlantic surface-ocean control of Pleistocene deep-ocean circulation, *Earth Planet. Sci. Lett., 73,* 231-243, 1985.

Peltier, W. R., Dynamics of the ice-age Earth, *Adv. Geophys., 24,* 2-146, 1982.

Pisias, N. G., and T. C. Moore, The evolution of Pleistocene climate: A time series approach, *Earth Planet. Sci. Lett., 52,* 450-458, 1981.

Prell, W. L., Oxygen and carbon isotopic stratigraphy for the Quaternary of hole 502B: Evidence for two modes of isotopic variability, *Initial Rep. Deep Sea Drill. Proj., 68,* 455-464, 1982.

Raymo, M. E., W. F. Ruddiman, J. Backman, B. M. Clement, and D. G. Martinson, Late Pliocene variation in northern hemisphere ice sheets and North Atlantic Deep Water circulation, *Paleoceanography,* this issue.

Rossignol-Strick, M., African monsoons, an immediate climatic response to orbital insolation, *Nature, 303,* 46-49, 1983.

Ruddiman, W. F., Late Quaternary deposition of ice-rafted sand in the subpolar North Atlantic (lat 40° to 63°N), *Geol. Soc. Am. Bull., 88,* 1813-1827, 1977.

Ruddiman, W. F., and A. Esmay, A streamlined foraminiferal transfer function for the subpolar North Atlantic, *Initial Rep. Deep Sea Drill. Proj., 94,* 1045-1057, 1986.

Ruddiman, W. F., and A. McIntyre, Oceanic mechanism for amplification of the 23,000-year ice-volume cycle, *Science, 212,* 617-627, 1981.

Ruddiman, W. F., and A. McIntyre, Ice-age thermal response and climatic role of the surface North Atlantic Ocean, 40° to 63°N, *Geol. Soc. Am. Bull., 95,* 381-396, 1984.

Ruddiman, W. F., and M. E. Raymo, Northern hemisphere climatic regimes during the past 3 Ma: Possible tectonic connections, *Philos. Trans. R. Soc. London, Ser. B, 318,* 411-430, 1988.

Ruddiman, W. F., N. J. Shackleton, and A. McIntyre, North Atlantic sea-surface temperatures for the last 1.1 million years, North Atlantic Paleoceanography, edited by C. P. Summerhayes and N. J. Shackleton, *Spec. Publ. Geol. Soc., 21,* 155-173, 1986a.

Ruddiman, W. F., A. McIntyre, and M. Raymo, Matuyama 41,000-year cycles: North Atlantic Ocean and northern hemisphere ice sheets, *Earth Planet. Sci. Lett., 80,* 117-129, 1986b.

Ruddiman, W. F., A. McIntyre, and M. Raymo, Paleoenvironmental results from North Atlantic sites 607 and 609, *Initial Rep. Deep Sea Drill. Proj., 94,* 855-878, 1986c.

Ruddiman, W. F., D. Cameron, and B. M. Clement, Sediment

disturbance and correlation of offset holes drilled with the hydraulic piston corer: Leg 94, *Initial Rep. Deep Sea Drill. Proj., 94*, 615-634, 1986d.

Saltzman, B., Modeling the $\delta^{18}O$-derived record of Quaternary climatic change with low-order dynamical systems, in *Irreversible Phenomena and Dynamical Systems Analysis in Geosciences*, edited by C. Nicolis and G. Nicolis, pp. 355-380, D. Reidel, Hingham, Mass., 1987.

Shackleton, N. J., and M. A. Hall, Stable isotope record of the hole 504 sediments: High resolution record of the Pleistocene, *Initial Rep. Deep Sea Drill. Proj., 69*, 431-441, 1983.

Shackleton, N. J., and N. D. Opdyke, Oxygen isotope and paleomagnetic stratigraphy of equatorial Pacific core V28-238: Oxygen isotope temperatures and ice volume on a 10^5 and 10^6 year scale, *Quat. Res., 3*, 39-55, 1973.

Shackleton, N. J., and N. D. Opdyke, Oxygen isotope and paleomagnetic stratigraphy of Pacific core V28-239: Late Pliocene to latest Pleistocene, Investigations of Late Quaternary Paleoceanography and Paleoclimatology, edited by R. M. Cline and J. D. Hays, *Mem. Geol. Soc. Am., 145*, 449-464, 1976.

Shackleton, N. J., J. Backman, H. Zimmerman, D. V. Kent, M. A. Hall, D. G. Roberts, D. Schnitker, J. G. Baldauf, A. Desprairies, R. Homrighausen, P. Huddleston, J. B. Keene, A. J. Kaltenback, K. A. O. Krumsiek, A. C. Morton, J. W. Murray, and J. Westberg-Smith, Oxygen isotope calibration of the onset of ice-rafting and history of glaciation in the North Atlantic region, *Nature, 307*, 620-623, 1984.

Start, G. G. and W. L. Prell, Evidence for two Pleistocene climatic modes: Data from DSDP site 502, in *New Perspectives in Climate Modeling*, edited by A. L. Berger and C. Nicolis, pp. 3-22, Elsevier, New York, 1984.

Thierstein, H. R., K. R. Geitzenauer, B. Molfino, and N. J. Shackleton, Global synchroneity of late Quaternary coccolith datum levels: Validation by oxygen isotopes, *Geology, 5*, 400-404, 1977.

Williams, D. F., R. C. Thunell, E. Tappa, D. Rio, and I. Raft, Chronology of the Pleistocene oxygen isotope record: 0-1.88 m.y. B.P., *Palaeogeogr. Palaeoclimatol. Palaeoecol., 64*, 221-240, 1988.

Zahn, R., K. Winn, and M. Sarnthein, Benthic foraminiferal $\delta^{13}C$ and accumulation rates of organic carbon: *Uvigerina peregrina* group and *Cibicidoides wuellerstorfi*, *Paleoceanography, 1*, 27-42, 1986.

J. Backman, Department of Geology, University of Stockholm, Stockholm, Sweden, S-106 91.

B. M. Clement, Department of Geology, Florida International University, Tamiami Trail, Miami, FL 33199.

D. G. Martinson and W. F. Ruddiman, Lamont-Doherty Geological Observatory, Columbia University, Palisades, NY, 10964.

M. E. Raymo, Department of Geology, Monash University, Clayton, Victoria, 3168, Australia.

(Received October 11, 1988;
revised February 23, 1989;
accepted February 24, 1989.)